Characterization
of the ground state
Pluripotency in Planarian

Dissertation

zur Erlangung des Grades

des Doktors der Naturwissenschaften

der Naturwissenschaftlich-Technischen Fakultäten

der Universität des Saarlandes

von

Thao Anh Tran

M.Sc.

Saarbrücken 2019

Tag des Kolloquiums:	30.07.2019
Dekan:	Prof. Dr. Gregor Jung
Berichterstatter:	Prof. Dr. Heiko Zimmermann
	Prof. Dr. Jörn Walter
Vorsitz:	Prof. Dr. Uwe Walldorf
Akad. Mitarbeiter:	Dr. Judith Becker

ACKNOWLEDGEMENTS

ABSTRACT

Planarian is an excellent model for regenerative studies due to its ability to regenerate the entire body from a tiny fragment. Thanks to a large number of adult stem cells, the mechanism of stem cell compartment could be studied in vivo, in the context of an adult organism. How pluripotent stem cells commit to prime states to regenerate new tissues without tumor formation? To answer this fundamental question, it is essential to characterize the ground state of the stem cell compartment. In this project, we proposed a novel surface antibody 6-9.2 that isolated pluripotent cells from a heterogeneous stem cell population. We concluded that the 6-9.2 antigen is a new biomarker for stem cell commitment and 6-9.2 antibody could be a useful tool for a live cell tracking method. Mass spectrometry and RNAi data showed a high relation of the 6-9.2 antibody with the transmembrane protein TMEM215/128. Knocking down of TMEM128/215 significantly affected the stem cell population and impaired the planarian regeneration and homeostasis. Our data contributed to defining the fluidic identity of stem cell transition. The gained knowledge will lead to a better understanding of regeneration and stem cell biology.

ZUSAMMENFASSUNG

Planarier gelten als Meister der Regeneration. Aufgrund eines großen Vorrats pluripotenter Stammzellen können sie ihren gesamten Körper aus einem winzigen Fragment regenerieren. Planarien sind derzeit die einzigen Bilateria, bei denen pluripotente Stammzellen in vivo im Kontext zu einem erwachsenen Organismus untersucht werden können. Wie erneuern oder differenzieren sich pluripotente Zellen, ohne dass sich ein Tumor bildet? Um diese grundlegenden Frage zu beantworten, ist es wichtig, den Grundzustand der Stammzellen zu charakterisieren. Hierzu wird in der vorliegenden Arbeit ein neuartiger Oberflächenantikörper mit der Bezeichnung 6-9.2 vorgeschlagen. Wir konnten zeigen, dass das 6-9.2-Antigen ein neuartiger Biomarker für das Stammzellkompartiment ist und der 6-9.2-Antikörper ein nützliches Werkzeug für die Beobachtung lebender Zellen sein könnte. Daten aus massenspektrometrischen Analysen zeigten den engen Bezug dieses Antikörpers zum Transmembranprotein TMEM128/215. Zusammenfassend lässt sich sagen, dass die Daten aus diesem Projekt zur Entwicklung eines Modells zur Beobachtung lebender Zellen verwendet werden können, was zu einem besseren Verständnis der Regeneration und der Stammzellbiologie führt.

Project Scope

The main objective of my Ph.D project is to unravel the complex biology behind planarian of pluripotent stem cells. Tracing the fate of individual stem cells during homeostasis and regeneration in the only animal that posses pluripotent stem cells in the adult will help identifying conserved mechanisms of pluripotency-based cell turnover and regeneration.

Project objectives

To achieve this goal, we need to find a novel way to characterize stem cell sub-populations and developing an *in vivo* tracking method via non-genetic labeling (e.g. FluoSpheres). The project included three major steps:
- The development of surface antibody to recognize stem cell sub-populations.
- A cell labeling system to transplant into planarians.
- An immobilization method to trace fluorescent cells *in vivo*.

Project achievement

- We successfully developed a surface antibody 6-9.2 that can recognize sub-populations of stem cells: naive and committed stem cells.
- We found the putative name for 6-9.2 antigen, the transmembrane protein TMEM215/128 by Mass Spec and RNAi methods.
- We developed a labeling system using fluospheres that are biocompatible for planarians.
- We showed the possibility to immobilize planarian in alginate hydrogels for at least five days and did not affect the animal's homeostasis and regeneration.
- Our data provided an ability to trace the fluorescent signals of different stem cell sub-groups in planarians.
- For applied researches, planarians can be used as a model system for tumorigenesis. We found that MMPB plays an essential role in controlling tumor formation in planariran.
- Planarians were also used for environmental toxicity assessment of iron oxide nanoparticles (IOPs). Our data showed the non-toxic effect of IOPs and encourage the use of these particles in medical applications.

Contents

List of Figures

List of Abbreviations

α	anti
°C	degree Celsius
γ	gamma
μg	microgram
μl	microliter
μm	micrometer
μM	micromolar
%	percent
AP	Alkaline Phosphatase
pASCs	planarian adult stem cells
BCIP	5-bromo-4-chloro-3'–indolyphosphate
Bp	base pair
BSA	Bovine Serum albumin
CB	chromatid bodies
C.elegans	*Caenorhabdis elegans*
cDNA	complementary DNA
cNeoblast	Clonogenic neoblast
Ct	Cycle threshold
D.japonica	*Dugesia japonica*
D.melanogaster	*Drosophila melanogaster*
ddH2O	double-distilled water
DIG	digoxigenin
DNA	Deoxyribonucleic acid
dNTP	deoxyribonucleotide triphosphate
ds	double stranded
ESCs	Embryonic stem cells
EpiSCs	Epiblast stem cells
FA	formaldehyde
FACS	Fluorescence activated cell sortings
g	gram
hr	hour
HSCs	Hematopoietic stem cells

hPSCs	human pluripotent stem cells
ICM	Inner cell mass
IgM	Immunoglobulin
iPSCs	induced pluripotent stem cells
MaSCs	Mammary gland stem cells
mg	milligram
min	minute
ml	milliliter
mM	millimolar
mm	millimeter
NAC	N-Acetyl-L-cysteine
NBT	Nitro blue tetrazolium
ns	not significant
PBS	Phosphate buffered saline
PCA	Principal Component Analysis
PCR	Polymerase chain reaction
PFA	paraformaldehyde
qRT-PCR	quantitative Real-Time Polymerase Chain Reaction
RNA	Ribonucleic acid
RNAi	RNA interference
RNP	Ribonucleoprotein granules
rRNA	ribosomal RNA
rNTP	ribonucleotide triphosphate
RT	Room temperature
S. Mediterranea	*Schmidtea mediterranea*
SD	Standard deviation
SEM	Standard error of mean
SDS	Sodium dodecyl sulfate
Ss	single stranded
TEA	triethanolamine
Tm	melting temperature
U	units
WISH	Whole mount *in situ* hybridizaAon
FISH	Fluorescent *in situ* hybridization
WT	Wild type
Irr	Irradiation
RNAseq	RNA sequencing

Chapter 1

INTRODUCTION AND MOTIVATION

1.1 Planarian: An excellent model for regenerative medicine research

Over one billion people are estimated to live with significant disabilities; and this number is increasing due to population ageing and an increase in chronic health conditions. It leads to an urgent need to find a process for replacing or regenerating human cells, tissues, and organs. To circumvent the problem of organ transplant rejection and reliance, the regenerated organs derived from human stem cells became the major approach. Regenerative medicine has been one of the most challenging medical treatment due to the complex process of regeneration involves stem cell technology and tissue engineering. Human embryonic stem cells (hESCs) are known as totipotent stem cells that could be expanded indefinitely while retaining the potential to make any cell of the body. Twenty years ago, hESCs were isolated for the first time from the inner cell mass of embryos and became the ideal source for tissue regeneration (Thomson AJ et al., 1998). However, many obstacles such as ethical issues, potential immune rejection and the possibility of tumor formation from residual pluripotent cells blocked the road to use hESCs in therapy. Amazingly, in 2006, Takahashi and Yamanaka successfully induced adult mouse fibroblasts to an embryonic-like cells by simply added some transcription factors in the culture media (Takahashi and Yamanaka, 2006). One and two years later, human pluripotent stem cells were successfully induced from human fibroblasts (Yu et

al., 2007; Park et al., 2008). This finding attracted scientists attention and became a revolution. Different cell lineages have been reported to be reprogrammed to produce human induced pluripotent stem cells (hiPSCs) by using different transcription factor sets (Sareen and Svendsen, 2010; Clive N. Svendsen, 2013). However, we are still facing many problems to trigger and control these pluripotent stem cells and their harmonization inside the tissues. How the stem cells decide to differentiate instead of self-renewing and vice versa? What is the internal and external cues that regulate the outcome of stem cell division? Many fundamental questions about this complex process is far from understood. Therefore, we are seeking for a paradigm to study the pluripotency-based regeneration to uncover the black box of stem cell decision.

Regeneration is a multiple-step process of renewal, restoration and regrowth of lost genomes, cells, and organs in response to damage. In nature, many animals have the remarkable ability to regenerate their body parts throughout life such as: salamander and fog can regenerate tail and limb, zebrafish regenerates their fin and heart, etc. However, the best-known model in regenerative capacity is planarian, a small flat worm whose entire body can be regenerated over and over again from a very small fragments. The fascinating regenerative ability of planarian thanks to a unique pluripotent stem cell population that spread throughout their body. Pluripotent cells are the cells have indefinite capacity to renew and differentiate into all cell types to build up every adult organisms. In mammals, fish, flies, pluripotent cells are derived from the early stages of embryonic development and become fate-restricted. Pluripotent stem cells are gradually quiescent in the adult, generally become multipotent or unipotent cells reside in a specific microenvironment called niches to maintain their stemness and repair the correlative tissues upon injury. In planarian, however, they contain a large number of adult stem cells that survive for the life time, and are ready to transform into any specific cell types that the body needs to replace the lost tissues (Reddien and Sanchez Alvarado, 2004). The stem cell compartment, the pattern and polarity controls, all together harmonize and directly regulate the regeneration. When planarian is amputated, the wound closes immediately, the stem cells start to proliferate and form a non-pigmented tissue, called blastema. In blastema, different types of cells are well patterned in a way that any missing part (e.g. head, tail) can be regenerated correctly without any abnormal cell proliferation, tissue overgrowth or cancer formation (Reddien and Sanchez Alvarado, 2004; Tran and Gentile., 2018). Therefore,

1.1 Planarian: An excellent model for regenerative medicine research

planarians are an excellent guide for induced pluripotent stem cell (iPSC) research and an ideal model for pluripotent stem cell-based regeneration study.

In 2011, Wagner et al have shown that a single planarian adult stem cell (pASC) can rescue a stem cell-depleted animal (Wagner et al., 2011). This single pASC gives rise to the entire range of cell types and organs in the planarian body including both somatic and germ cells to regenerate a new brain, digestive-, excretory-, sensory-, and reproductive systems (Jochen C. Rink, 2012; Baguna, 2012: Baguna, 1989). Do the new cells directly come from pASCs or there are dedifferentiation and transdifferentiation processes in planarian? Do they strictly follow a hierarchical tree where naive stem cells undergo pluri- oligo- and uni-potent progenitors (Tran and Gentile., 2018)? Finding the source of stem cells that are able to renew and commit to mature stages is a central focus in understanding regenerative process. Recently, the compartment of stem cells and new stem cell-involved genetic components are partially elucidated by single cell analysis, and comparing transcript sets during planarian homeostasis and regeneration (Josien C. van Wolfswinkel et al., 2014). They indicated that pASCs are divided into multiple prominent classes with distinct properties. These studies shed light on isolating unique naïve and primed pASCs in a heterogenous stem cell population. However, this mechanistic analysis is unable to provide a direct evidence of downstream of pluripotent stem cells, and the molecular changes upon regenerative signals. The pluripotent stem cells undergo different intermediate stages where they share many features in common so it is difficult to describe one stem cell population in absolute terms. To precisely identify the source of pluripotent cells and accurately understand the complex stem cell decisions of individual pASC, the new strategies with more straight forward methods are required (Tran and Gentile., 2018).

The use of surface antigens to characterize specific cell types has been applied in a long history, for example in embryonic stem cells (ESC), human hematopoietic stem cells (Landsteiner 1901, Race and Sanger 1975, Notta et al., 2010). These early studies marked the potential value of surface antigens in isolating heterogenous cell population. Unlike other model organisms, the available antibodies in planarians have been appeared in a few reports so far and directly against intracellular epitopes (Bueno et al., 1997). The lack of surface antibody against specific markers prevent us from developing a live cell tracing method

and leave us without a molecular insight of stem cell commitment and patterning in *in vivo*. For this reason, our previous group generated a library of mouse monoclonal antibodies against the planarian membrane proteome with a focus on antibodies specific to pASCs or subpopulations (Moritz et al., 2012). Moritz and colleagues purified plasma membrane proteins and immunized with the mice and did ELISA screening to obtain a list of surface antibodies. Among them, the antibody called 6-9.2 identified subfractions of stem cells, in which the cells recognized by this antibody express both early and late progeny, while the negative one express only stem cell markers (Tran and Gentile., 2018). This finding shed light on using this antibody as a biomaker for pluripotent stem cell commitment. However, to substantiate this hypothesis, we need to examine further the profile of sub-populations isolated from this 6-9.2 antibody. In this thesis, we characterized these stem cell sub-groups, connected their profiles with the updated sub-populations from the literature and at the same time elucidating the 6-9.2 antigen characteristics and its role in planarian regeneration and homeostasis.

In the direction of translational research, we tried to converge the planarian model from basic science into the scale of applied studies. The application of invertebrate models in toxicology reduces the maintenance cost and the difficulty of the experimental manipulation but also provide a high-through put screening tool (Kustov L et al., 2014; Haji Bahadar et al., 2016). With a complex body structure (including center nervous system, gastrovascular cavity, excretory system, etc.) and a high sensitivity to environmental exposure, planarian emerges as an ideal model to study toxicology, in both food safety and environmental manners (Alessandra Savetti et al., 2015, Hagstrom D et al., 2016, Kustov L et al., 2014, Roten et al., 2018). Thanks to the populations of adult stem cells pASCs that readily differentiate into any cell types, planarian can regenerate the entire body within one or two weeks. This short time scale of full regeneration enables us to examine the effect of toxicants on the highly sensitive cells – the stem cell population. The way to evaluate the stem cell compartment from the functional perspective, is to assess the regenerative capacity. In this study, we investigate the toxicity of Iron Oxide Fe3O4 (IOPs), the common particles used in industry, medical devices and therapy. The particles change their chemical activities, surface charge, and size due to the aggregation or disaggregation after releasing from the industries (Gualtieri M et al., 2012; Haji Bahadar et al., 2016; Lei C et al., 2016; Mirco Bundschuh et al.,

2018). These processes ultimately determine their toxicity in the environment. Therefore, we incubated planarian in IOPs media (environmental exposure) or injected IOPs directly into the gastrovascular system (food exposure) with the range of IOPs concentrations and particle sizes to test their effect in planarian regeneration and homeostasis. The data in this study provide an important information for the examination of iron oxide particles at environmental releasing fates. Especially, we highlighted the use of planarian system to push forward the adoption of 3R (Reduction, Refinement, Replacement) approaches in toxicological studies (Russell and Burch, 1959), where the invertebrate or *in vitro* models is encouraged.

Planarians show the remarkable ability to regenerate thanks to the population of adult stem cells. These hyper-proliferating cells are prone to replication error so they are very sensitive to environmental toxicants. Therefore, planarians can be used to investigate the effect of tumor suppressor genes (TSGs). One of the top human carcinogen agents is cadmium (Cd), which can cause different types of cancer in human (Akesson et al., 2008; IARC, 1993, McElroy et al., 2006; Waalkes, 2003). In planarian *Schmidtea mediterranea*, the effect of Cd in inducing tumor has never been observed (Plusquin et al., 2012), implying the ability to escape the carcinogenic initiation of planarian *S.mediterranea*. However, it has been reported the Cd can induce tumorigenesis in Planarian *Dugesia dorotocephala* (Hall et al., 1986). The recent study in *Dugesia tigrina* pointed out the role of matrix metalloproteinases (MMPs) in Cd tumorigenic effects (Voura et al., 2017). The tumor invasion is mainly regulated by MMP enzymes via proteolytic activities and the extracellular matrix degradation (Kim and Hwang, 2011, Merdad et al., 2014; Yamada et al., 2010). Therefore, most of MMPs function as tumor inducer genes, except a few members of MMP family that have been shown as tumor suppressor genes, like MMP19 (Chan et al., 2011; Hynes, 2009). In planarian, MMPs play an important role in regeneration process. To investigate the effect of MMPs in the tumor formation of planarians *S. mediterranea*, we exposed animals with human carcinogen Cd and performed *in silico* screening and a proteomic screening to find which MMP genes that is significantly affected. Gene knockdown experiments were performed to examine the role of MMP gene. The changes in different stem cell sub-populations isolated from 6-9.2 antibody were also tested to have a broader view of MMP function in planarian stem cells and regeneration. Our data reveals a potential therapeutic target for cancer treatment based on tumor suppressor genes.

In summary, our project indicates the possibility to isolate live stem cells and their committed states by using a novel surface antibody 6-9.2. Characterizing the 6-9.2 antigen, we found two putative transmembrane proteins TMEM128 and TMEM215 that are more likely to be 6-9.2 protein. Knocking down of this protein significantly affected the stem cell viability as well as the regeneration and homeostasis of planarians. The utility of this 6-9.2 antibody is a potential tool for developing live cell tracking methods, which could help us understanding the stem cell commitment and fate decision. Additionally, the planarian stem cell compartment can also be studied in a functional perspective in toxicological research by testing the capacity of stem cells to generate new tissues without tumor formation. Therefore, planarian is a great model to test the toxicity of nanoparticles to the environment and food safety. We profoundly investigated the effect of iron oxide particles with the wide range of size and concentration in the planarian homeostasis and regeneration. Furthermore, planarian can also be a relevant model to study tumorigenesis due to the presence of hyper-proliferating cells in the adult animal. Altogether, we highlight the multiple approaches using planarian from basic research to applied science.

1.2 Planarian overview

1.2.1 What planarians are?

Planarian is a free living flat worm, can be found in fresh water and marine. Some species are terrestrial and are found under logs or soils. They are known as cannibalism and their foods are living or dead small animals. Planarian is in the Phylum Platyhelminthes and the Class Turbellaria. The common species found in planarians are: *Girardia tigrina, Planaria maculata, Girardia dorotocephala,* and *Schmidtea mediterranea.* Among them, *Schmidtea mediterranea* has been widely studied in stem cell and molecular research due to its diploid chromosomes (Newmark PA, Sánchez Alvarado A, 2002). Thanks to the RNAi technology using double-stranded RNA, the genomic data of planarian has been screened and uncovered more than 240 genes that affect regeneration in *S. mediterranea.* Many of these genes have orthologs in the human genome (Petersen and Reddien, 2008; Yazawa et al., 2009; Felix and Aboobaker, 2010; Gavino and Reddien, 2011; Molina et al, 2011).

1.2.2   Planarian structures

Planarian are bilaterial animals with a soft body and three germ layers (ectoderm, mesoderm, and endoderm). They have a complex internal anatomy with central nervous system, intestine, epidermis, photoreceptor, musculature, and excretory system (Baguna et al., 1989). A single opening digestive tract consists of a pharynx (both mouth and anus) and a gastrovascular cavity (Campbell NA and Reece JB., 2005). The excretory system is made of many tubes with flame cells which function like a kidney that releasing waste products through filtration via pores located along the sides of the body. Planarian are photophobic; the worms move away quickly when exposed to the light. They move by the ventral ciliated epithelial cells or by the contraction of mucus layer around the body in some species navigate obstacles by muscles (Rompolas P et al., 2009). They receive oxygen and release carbon dioxide by diffusion.

Planarians is also a model to study neurodegenerative disease in human due to their complex central nervous system (CNS) and its structure and function are more similar to the vertebrate brain than to other invertebrate animals (Buttarelli et al., 2008). The CNS consists of a bi-lobed cephalic ganglion (brain) and ventral nerve cords (Claire G. Stevenson and Wendy Scott Beane., 2010). It contains approximately 10.000 neurons and share the same neuronal sub-populations and neurotransmitters as the mammalian brain (Buttarelli et al., 2008; Cebrià, 2007; Cebrià et al., 2002; Hagstrom D et al., 2015).

Planarian *S. mediterranea* have both sexual and asexual strains. They also have "sexual conversion" ability which means they can convert from asexual to a sexual state upon sexualizing substance inducing or the changing of feeding conditions (Shibata N et al., 1999; Kobayashi K et al., 2002a; Kobayashi K et al., 2002b; Agata K et al., 2006). Sexual planarians are hermaphroditic, meaning that they have both male and female sex organs. The ovaries are located in a rostral direction, near the eyespots. Testes are located laterally, along the sides of the body, along with seminal ducts. Both sperm and eggs can be produced in a same body. While asexual planarian reproduce by fission, sexual animals create eggs by cross-fertilizing hermaphrodites. The eggs are packed into a cocoon containing specialized yolk glands and then transferred into the environment. A thin mucous filament around the egg capsule helps it attaches to the surface. New born planarians hatch and grow into adult worm
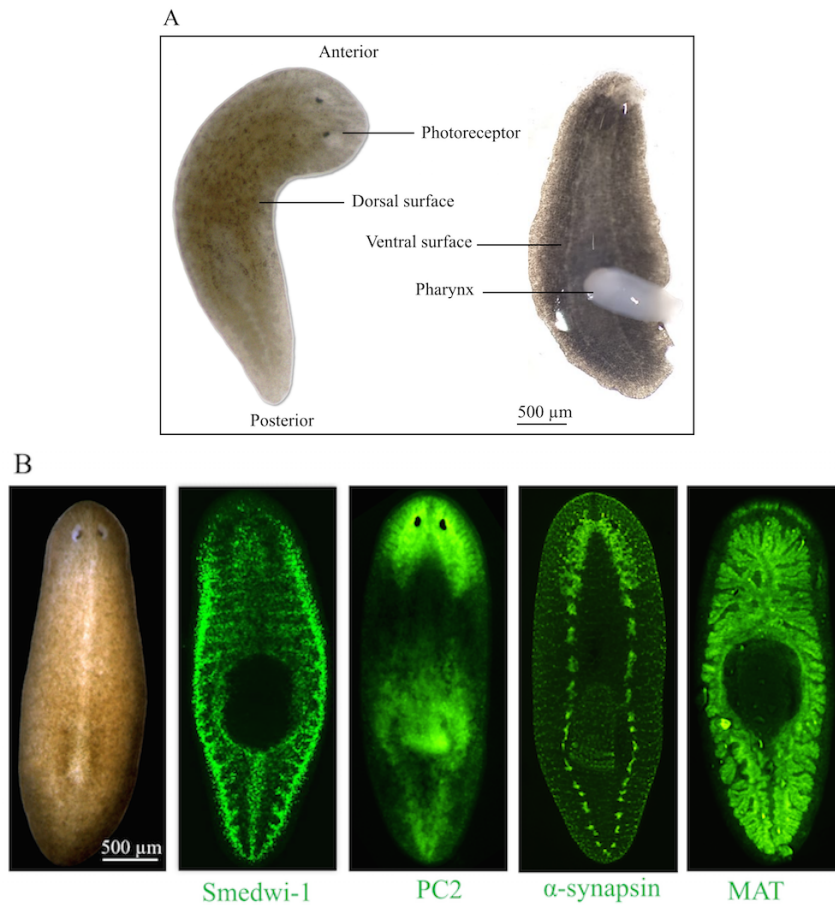
Figure 1.1: Planarian *Schmidtea mediterranea* anatomy. A. Live animal. B. Whole-mount fluorescent *in situ* hybridization with stem cell marker Smedwi-1, neuronal marker PC2, whole-mount immuno staining with synapsin antibody, and gastrovascular marker MAT. Scale bar 500 μ m. Images were taken under the stereo microscope (ZM25 Nikon).

without a larval stage. Planarian asexual reproduction, or regeneration, occurs when the flatworm experiences an injury that splits the worm. Planarian worms can be cut into as many as 1/279th of the original body plan and regenerate into fully formed genetic copies. The adult sexual animal can regenerate as robust as an asexual one.

1.2.3 Planarian neoblasts

The information of this part and section 1.3 was published in my review paper: **Thao Tran**, Luca Gentile. **A lineage CLOUD for neoblasts**. Seminars in Cell and Developmental Biology. **2018**. DOI: 10.1016/j.semcdb.2018.04.012.

Planarian has remarkable regenerative ability due to a large resident population
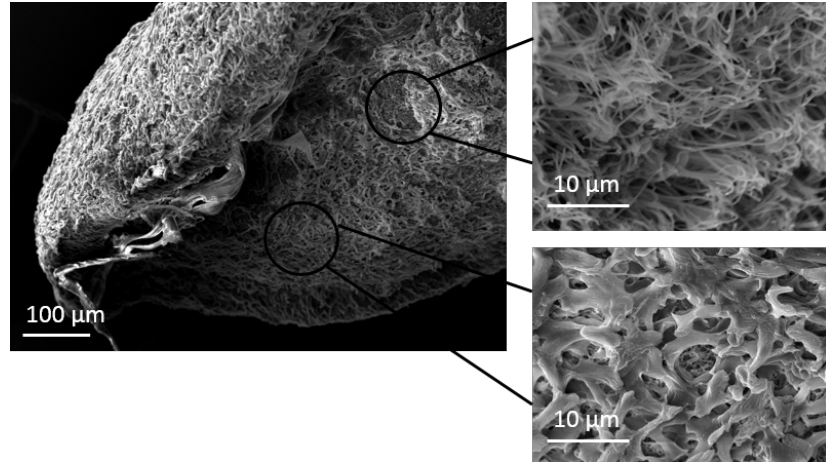
Figure 1.2: Planarian mucus and cilia under the Scanning electron microscope (SEM). Head fragment was fixed and subjected to SEM. Upper right, planarian cilia; bottom right, planarian mucus layer.
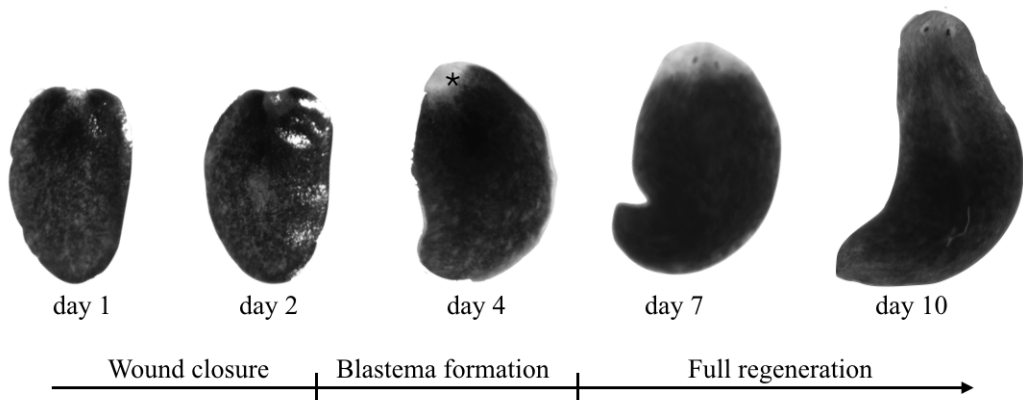
Figure 1.3: Planarian regeneration. Planarian was amputated and the tail fragment was observed during 10 days of regeneration under the stereo microscope. (*) blastema.

of pluripotent stem cells (Reddien and Sanchez Alvarado, 2004). The whole adult planarian contains 10-15% of stem cells, called "neoblast" that found abundantly in the parenchyma, except for the pharynx and the area in front of the photoreceptors (which are the only areas incapable of regeneration) (Reddien and Alvarado, 2004; Jochen C. Rink, 2013). Neoblasts are small roundish or ovoid cells (ranging from 5-10 μm) with a large nucleus and a thin rim of cytosol, and lots of free ribosome and few round mitochondria (Pedersen 1959: Hori 1982: Hay and Coward 1975: Coward 1974; Tran and Gentile., 2018). With the successful development of molecular tools, the molecular and cellular characteristics of neoblasts is established in the last decade. The common feature of neoblast is cell division: neoblasts are the only dividing cells in planarian. Once neoblasts differentiate, they no longer maintain proliferative activity. Bardeen and Baetjer, 1904 showed the first evidence of neoblast role in the forming of new tissue (blastema) by irradiation experiments (Bardeen and Baetjier, 1904). Proliferative cells are the most sensitive cells affected by irradiation. Therefore, the high dose of X-ray 1750 rad exposed neoblasts failed to regenerate (Tran and Gentile., 2018). Different techniques have also been used to define neoblast division such as BrdU visualization, the detection and visualization of cell cycle marker genes by in situ hybridization, qPCR, and immune histo/cyto chemistry (Newmark and Sanchez Alvarado, 2000; Shibata et al., 2010). RNA-mediated genetic interference (RNAi) was also successfully developed (Alejandro Sánchez Alvarado and Phillip A. Newmark, 1999), which helped identifying many key players that regulate both neoblast maintenance and differentiation. The effect of RNAi in the knockout of Histone variant H2B has been shown more specific to eliminate neoblasts in planarian (Solana et al. 2012). The expression of *Smedwi-1* – the gene encodes a PIWI-like protein is also a canonical neoblast marker gene (Reddien et al., 2005). *Smedwi-1* express in all dividing cells and cells that will divide, and the *Smedwi-1*^{+} cells rapidly depleted within 1 day following irradiation (Reddien et al., 2005; Eisenhoffer et al., 2008). Neoblasts can be isolated by fluorescence-activated cell sorting (FACS), based on their cellular features (DNA content and cytoplasm) and their sensitivity to irradiation (Reddien et al., 2005; Hayashi et al., 2006; Tran and Gentile., 2018). X ray-sensitive cells were defined by two populations 1 and 2 (X1 and X2) and one X ray-insensitive population (Xin) which contains large and heterogeneous cells (S. Moritz et al., 2012; P.W. Reddien et al., 2005; Hayashi T et al., 2006). The cells in G0/G1 are also considered stem cells as they will enter mitotic process. Therefore, neoblasts populate both the X1 (cells

in S-G2/M phase of the cell cycle) and partial X2 cells. Many studies have shown the heterogeneity of X1 gated cells, based on their cellular morphology and ultrastructure, the expression of specific markers (D.E. Wagner et al., 2010; S. Moritz et al., 2012; S. Higuchi et al., 2007; Hayashi T et al., 2006) and, more recently, based on single-cell transcriptomics signatures (S.W. Lapan et al., 2012; O. Wurtzel et al., 2017; J.C. van Wolfswinkel et al., 2014). Hence, the term "neoblast" defines a mixed population of pluri-, oligo- and uni-potent mitotic cells (Elly M. Tanaka and Peter W. Redden, 2011; Jochen C. Rink, 2013; Tran and Gentile., 2018).

1.2.4 Planarian germ cells

Germ cells are very similar to neoblasts in terms of morphology and irradiation sensitivity (Jochen C. Rink, 2013). Whether neoblast is an origin that differentiate into germ cells in sexualizing process? To determine the germ cells, earlier studies have suggested that the germ line is segregated from totipotent neoblasts by the involvement of epigenetic mechanism (Morgan, 1902; Zayas et al., 2005; Emili Salo et al., 2009). The expression of *nanos* are highly conserved in germ cells and play a vital role in gonad regeneration but not fundamentally express in neoblasts (Wang et al., 2007; Sato et al., 2006; Handberg-Thorsager and Salo, 2007; Nakagawa et al., 2012a). Therefore, with the increasing of *nanos* expression, neoblast could transit into germ line fate (Jochen C. Rink., 2013). Most recently, it has been reported that neoblasts anarchically arise from an early *smedwi-1*[+] cell population that express a unique set of early embryo enriched transcripts and distinct from neoblasts in cell transplantation assay. They revealed that neoblasts emerge from embryonic stem cells as the major organs start to form (Alejandro S. Alvarado et al., 2017). The link between adult asexual neoblast and germ line stem cells is strongly related to the pluripotency of neoblast.

1.3 Planarian stem cell compartment - State of the Art-

1.3.1 The heterogeneity of neoblast

Neoblast isolated by FACS using nuclear content and cytoplasmic size staining is an evidence of a heterogenous population in terms of morphology,

ultrastructure and the transcript levels (Higuchi et al., 2007; Morris et al., 2006; Eisenhoffer et al., 2008; Hayashi et al., 2010; Pearson and Sanchez Alvarado, 2010; Scimone et al., 2010: Moritz et al., 2012; Tran and Gentile., 2018). Wagner et al created the term "cNeoblast" (clonogenic neoblast) to specialize the planarian pluripotent stem cells. The demonstration of cNeoblast as a pluripotent cells was performed by a single cell transplantation. All the dividing cells were depleted in the animal after exposed to 6000 rad irradiation. Transplantation of a single cNeoblast could form multiple colonies and restore the homeostasis and regenerative capacity (Wagner et al., 2011). However, the first evidence of a committed neoblast derived from pluripotent state was shown in the frame of eye regeneration (Tran and Gentile., 2018). The cells were found posterior to the eyes in intact animals, expressed the pan-eye marker *ovo* together with $Smedwi1^+/H2B^+$ markers (S.W. Lapan et al., 2012). The evidences of lineage restricted progenitors in neoblast during homeostasis and regeneration have been shown further in many studies (Currie and Pearson., 2013; Lapan and Redden., 2011; Scimone et al., 2011; Hayashi et al., 2010). For examples, nine bHLH (basic helix-loop helix) genes expressed in specific neural and stem cell subpopulations that required for regeneration (Cowles et al., 2013), and a novel spliced leader (SL) SL3 which is highly enriched in a subset of neoblast (Rossi et al., 2014) have been identified (Tran and Gentile., 2018). Additionally, our group introduced a large portion of X1 cells co-express the epidermal lineage (*Prog-1, Agat-1*) together with an uncharacterized surface antigen 6/9.2 (Moritz et al., 2012). Recently, the functionally three distinct classes of neoblast were defined from a group of Peter Reddien (Josien C. Wolfswinkel et al., 2014). They directly compared gene expression of a thousand individual neoblasts using high-dimensional single cell transcriptional profiling and suggest two prominent major classes of neoblast, named σ (sigma) ζ (zeta), and at least one subclass γ (gamma) within σ class. They proposed the transcript sets remarkably express in sigma class (*Smed-soxP-1, Smed-soxP-2, Smed-soxB-1, Smed-smad-6/7, Smed-inx-13, Smed-pbx-1, Smed-fgfr-4,* and *Smed-nlk-1*) and zeta class (e.g., *Smed-zfp-1, Smed-g6pd, Smed-fgfr-1, Smed-p53, Smed-soxP-3*, and *Smed-egr-1*) that largely overlap with *smedwi-1* but do not overlap between classes (Table 1). They also found that both sigma and zeta classes are cell-cycle-independent classes, which remain prominent in all cell cycle stages: G2-M, S, G0 and G1. In responding to regeneration, sigma and zeta classes are stably present in the regions of anterior and posterior of the regenerated tissues or repopulation of the neoblast

compartment. However, the early cellular response to wounds are dominantly controlled by sigma class (Tran and Gentile., 2018). At 0 hr postamputation, both neoblast sub-classes equally presented across the fragments. At 6 to 48 hr while zeta-neoblast maintained the same distribution, sigma-neoblast dramatically overrepresented among the mitotic cells and were enriched near the wound site. The study found that sigma-class mediates the proliferation and migration of the early response upon injury. Sigma-neoblasts maintain the long-term self-renewal capacity and normally form a broad range of new tissues independent of zeta-blast contribution. Moreover, the RNAi experiments of zfp-1 - a pool marker for zeta class showed the new tissue is derived from zeta-class-depleted cells, and sigma-neoblast could reestablish a zeta-class. Therefore, the conclusion is that sigma-neoblasts represent actual pluripotent cells and can give rise to zeta-neoblasts. Their data also suggested that the cNeoblast is likely contained within sigma-class (Tran and Gentile., 2018). In parallel, zeta class is required for the maintenance of epidermal cells and highly contribute in regeneration. In normal condition, zeta-class are generated from the 2N-DNA content sigma-class population, the cells derived from zeta-class (largely related to epidermal cells) exit the cell cycle permanently. Gamma-neoblasts - the subclass within sigma cells, express the transcript set of *prox-1, hnf4, gata4/5/6*, and *nkx2.2*, which is previously linked to the planarian intestine. Altogether, sigma-neoblasts likely represent as a naïve stem cell subpopulation, whereas zeta-neoblasts are defined as progenitors to restricted lineages, and gamma neoblasts are intestinal progenitor cells (Table 1) (Tran and Gentile., 2018). Interestingly, the expression of the 6/9.2 antigen, and therefore the expression of the epidermal lineage markers in X1 cells, are also cell-cycle-independent (Moritz S et al., 2012). So possibly, zeta-neoblasts behave as safeguards in planarian system, at some special conditions, they might acquire pluripotency and transit into sigma-neoblasts. In 2016, the group of Bret Pearson identified the planarian neural stem cell νeoblast using single-cell transcriptomics. They proved that σNeoblasts give rise to νNeoblasts and these cells co-express the neoblast markers *smedwi1* and *smedwi2* with neuron-specific genes (Table 1) and give rise to $pc\text{-}2^+/synapsin^+$ neurons (A.M. Molinaro and B.J. Pearson., 2016). Neoblasts had also been identified into two more subclasses with pharyngeal (C.E. Adler et al., 2014) and protonephridial (M.L. Scimone et al., 2011), as defined by specific transcript sets (Table1). There are no direct evidences showing these pharynx and excretory progenitors derived directly from σNeoblasts or from additional populations. However, it is

more likely that one sub-group of σNeoblasts which highly express *MCM7, RuvB, cyclinD1, SAE-2, CPSF3,* and *zmym-1* will derive to pharynx progenitors with the high expressions of *FoxA* and some specific genes such as *PABP-2, COP9, WDR, SART-3* (C.E. Adler et al., 2014). In case of protonephridia, one σNeoblast sub-group that co-express *Six1/2-2* and *pou2/3* will produce protonephridial progeny which enriches the transcript set of *Six1/2-2, pou2/3, eya, Sall, Osr* (M.L. Scimone et al., 2011). These subpopulations are likely equivalent to ζ, γ and νNeoblasts because of the co-expression with pan-neoblast marker *smedwi-1*, the ability to self-renew, and the distinct transcript set from ζ, γ and νNeoblasts (Tran and Gentile., 2018). Recently, the group of Bret Pearson provided the first insight into the pigment cell lineage. They suggested that a still unknown pigment cell progenitor, distinct from the ζ cells, may stem from the endodermal γNeoblasts and give rise to both dendritic and punctate cells (X. He et al., 2017).

Neoblast subclasses	Molecular marker(s)	Give rise to	References
c-Neoblasts	uncharacterized	all cell types	Wagner et al., 2011
δ-Neoblasts	*SoxP-1, SoxP-2, smad-6/7*	brain, eyes, protonephridia, pharynx, muscles, ζ, γ, ν Neoblasts	Van Wolfswinkel et al., 2014
ζ-Neoblasts	*zfp-1, SoxP-3, egr-1*	epidermal lineage	Van Wolfswinkel et al., 2014
γ-Neoblasts	*hnf-4, gata456, nkx2.2*	intestinal cells	Van Wolfswinkel et al., 2014
ν-Neoblasts	*ston-2, elav-2, ptprd-9, msi-1*	neurons	Molinaro et al., 2016
Pigment progenitor	*foxF-1, albino, fgfr-1, ets-1*	pigment cells	Xinwen He et al., 2017
Pharynx neoblasts	*foxA*	pharynx cells	Adler et al., 2014
Protonephridia neoblasts	*pou2/3, six1/2, eya, Osr, Sall*	excretory system	Scimone et al., 2011
Eye progenitor	*ovo, eya, six1/2, sp6/9*	photoreceptors and optic cup cells	Lapan and Reddien, 2011

Table 1: Subclasses of Neoblasts and progenitors in *S. mediterranea.*

1.3.2   Pathway underlying pluripotent state transition

The specialized function of one cell type depends on their location (Lavin et al., 2014), which requires additional control over their differentiation (Baxendale et al., 2004; Gautier et al., 2012). For examples, eye-specialized neoblasts are only found in the anterior part of planarian (Lapan and Reddien, 2012), and intestinal neoblasts are often near to the gut system (Wagner et al., 2011). Previous studies have shown that patterning molecules such as BMP (Reddien et al., 2007) and Wnt5 (Adell et al., 2009) are constitutively expressed in planarian and play an essential role in patterning in intact and regenerating animals (Reddien, 2011; Tran and Gentile., 2018). A pluripotent stem cell undergoes different stages of stem cell compartment following the positional signals. How the progenitors from particular lineage acquire appropriate functions based on their location has been elegantly elucidated by using epidermal stem cells (Omri Wurtzel et al., 2017) and *Hofstenia* muscle cells (Amelie A. Raz et al., 2017). Upon regeneration process, the epidermal mitotic zeta-neoblasts, normally distribute along the mesenchyme, exit the cell cycle and start differentiating. During differentiation, they migrate from the mesenchyme to the preexisting epidermis and form a single epithelial layer integrated into the mature epidermis (Eisenhoffer et al., 2008; Tu et al., 2015). Omri et al., found that patterning signals come from muscle cells at distinct location. The levels of these signals regulate the regional identity of epidermal neoblast. The zeta-neoblasts can read the gradient signal from BMP (patterning factor produced by dorsal muscle cells), and activate a transcript set related to Dorsal-Ventral positional identity, which ultimately derive the right epidermal cells. Strikingly, two genes *PRDM1-1* and *kal1* are sufficient for identifying the dorsal and ventral locations respectively of early stage progenitors. Another positional cue, bmp4, is also found to regulate the identity of dorsal tissues, and its RNAi causes progressive ventralization in animal regeneration. Hence, the cell fate decision is mediated by a set of patterning signals (Reddien 2011; Forsthoefel and Newmark 2009; Jochen Rink 2013; Tran and Gentile., 2018). Recently, the experiments on planarian eye removing showed a surprising fact that the absence of the eye did not trigger a regenerative response (Samuel A. LoCascio et al., 2017). The producing of eye progenitor cells are increased following the regeneration signal from head amputation or flank resection (with the presence of eyes). However, eye removal alone is not sufficient to induce stem cells to generate eye progenitor cells. In normal condition, eye progenitors

derived from neoblasts will differentiate to eye cells, which ultimately undergo cell death. In the eye-specific resection condition, eye progenitor cells maintain the same, the less cell death occurred in regenerating eyes facilitate the growth of new eyes in net size. In large injuries such as head amputation or flank resection, planarian non-specifically induced uninjured pre-pharyngeal region cells and neuron cells. It is suggested that upon injury, neoblast generate diverse cell types depends on positional information and general wounding signals to create more opportunities for cell fate decision to occur. Hence, the planarian regeneration seems to follow a "target-blind" model where regeneration is triggered despite the presence or absence of the specific tissue to be regenerated (Tran and Gentile., 2018). It is tempting to think that it is not the stem cell per se, or the pluripotency that makes the differences in regenerative ability among animals, it is the way these cells are controlled in the environment of the whole body (Tran and Gentile., 2018).

Many mechanisms underlying the stem cell compartment have also been recovered to understand how the complex structure is accurately regenerated and maintained during tissue turnover. Rebuilding new tissue in planarian requires an important component: the source of stem cells to differentiate into many cell types. Homeostatic and post-injury states also requires a large population of stem cells to compensate the loss of cells after remodeling process. It has been reported that epidermal growth factor (*Egf*) signaling regulates neoblast expansion by asymmetric cell division (Kai Lei et al., 2016). Sublethal irradiation experiments were performed to remarkably reduce stem cell numbers in the animals. During homeostasis, stem cells display both symmetric and asymmetric division. However, when stem cells are diminished, the EGF receptor-3 (*egfr-3*) protein is found to localize asymmetrically on the cytoplasmic membrane of neoblasts. The RNAi of *egfr-3* dramatically decreased the asymmetric but not symmetric cell division in stem cell depletion condition but had no effect under homeostatic condition, indicating that *egfr-3* mediates asymmetric cell division during neoblast repopulation and is not required for neoblast maintenance. Another study also proposed the role of EGFR signaling in controlling cell differentiation and neoblast stability. They identified that *egfr-1* and *ngr-1* (a new putative EGF ligand) promote the differentiation of gastrodermal cells (Sara Barberan et al., 2016). Silencing of *egfr-1* and the putative ligand *nrg-1* impaired the differentiation of gut progenitor cells into mature gut cells but did not affect the commitment of neoblasts to this cell

lineage.

1.3.3   A lineage CLOUD for neoblast

Classically, neoblast sub-classes are defined by discrete gene sets and their progenitors are related to distinct cell types such as neuron, epidermis, and gastrovascular. As proposed by Waddington in 1942, the difference between neoblast and committed cells was based strictly on a tree-like structure where stem cell gradually lose their potency throughout discrete intermediate stages where each cell has a precise function and molecular and epigenetic signature (C.H. Waddington., 1942; Tran and Gentile., 2018). However, this model can no longer explain the "fluidic" identity that planarian stem/progenitor cells acquire, as shown in many recent studies (Josien C. Wolfswinkel et al., 2014; C.E. Adler et al., 2014; A.M. Molinaro and B.J. Pearson., 2016; X. He et al., 2017). One prominent example is the eye regeneration. $Smedwi1^+/h2b^+$ neoblasts express the early eye lineage markers *six-1/2 eya* and *ovo* during head regeneration. The expression of *sp-6/9* and *dlx* are induced later and ultimately induce the forming of the optic cup by $tyro^+$ cells, where *otxA* specifies the retinal cell fate (S.W. Lapan and P.W. Reddien., 2011 and 2012; Tran and Gentile., 2018). According to the t-distributed stochastic neighbour embedding (t-SNE) (O. Wurtzel et al., 2015), tyrosinase-positive cells localize almost exclusively in the epidermal lineage (figure 1.4A), while mature retinal cells expressing the Transient Receptor Potential Cation family genes (*TRPC4, 5, 6*) locate almost exclusively in the neural lineage (figure 1.4B) (Tran and Gentile., 2018). This raises the question about the relationship among the eye neoblast (which generates cells of both the epidermal and the neuronal clusters), the νNeoblast (which supposedly generates only neuronal cells) and the ζNeoblasts (which supposedly only generates epidermal cells (Tran and Gentile., 2018). The study from Josien C. Wolfswinkel also considered that neither the sigma-class nor the zeta-class can be considered homogeneous cell populations. The potential sub-classes within sigma and zeta-class are suggested. For example, one subset of the zeta-class cells co-expressed higher levels of both *AbdBb* and a *six6*-related transcript whereas another subset expressed high levels of *AbdBa*, *meis-2*, and a *gata1/2/3*-related transcript (Josien C. Wolfswinkel et al., 2014; Tran and Gentile., 2018). Another study in νNeoblast showed that the planarian neural stem cell, which originate from σNeoblasts, have a distinct set of transcript (Table 1) (A.M. Molinaro and B.J. Pearson., 2016). In case of the

gamma subclass, the cells derived from σNeoblasts start to express *hnf4* and *gata4/5/6* together with *egfr-1* which is required for the differentiation of gut system (S. Barberan et al., 2016). However, some common themes also present among these progenitors. The study from Bret Pearson's group shown the critical role of *mex3-1* acts as a stem cell lineage mediator of multiple neoblast progeny. The inhibition of *mex3-1* could significantly decrease the commitment of new cells into brain, intestine, and pharynx (A.W. Neff et al., 2011). It indicates that there are some factors that express in the general stem cell pool and control the differentiation of post-mitotic lineages at the upstream level (Tran and Gentile., 2018). Even though there are no evidences prove that zeta-neoblasts can reversely turn into pluripotent cells, it has been reported in mammals and other animal models that stem cell function is not strictly cell autonomous and there is a potential for some cells to gain stemness (Nakagawa et al., 2007; Tran and Gentile., 2018). For example, progenitor cells can take on stem cell functions when stem cells are lost in Drosophila germ line (Brawley and Matunis., 2004; Kai and Spradling., 2004) or the transient-amplifying progenitor represent potential stem cells in the mouse testis (Nakagawa et al, 2007; Tran and Gentile., 2018).
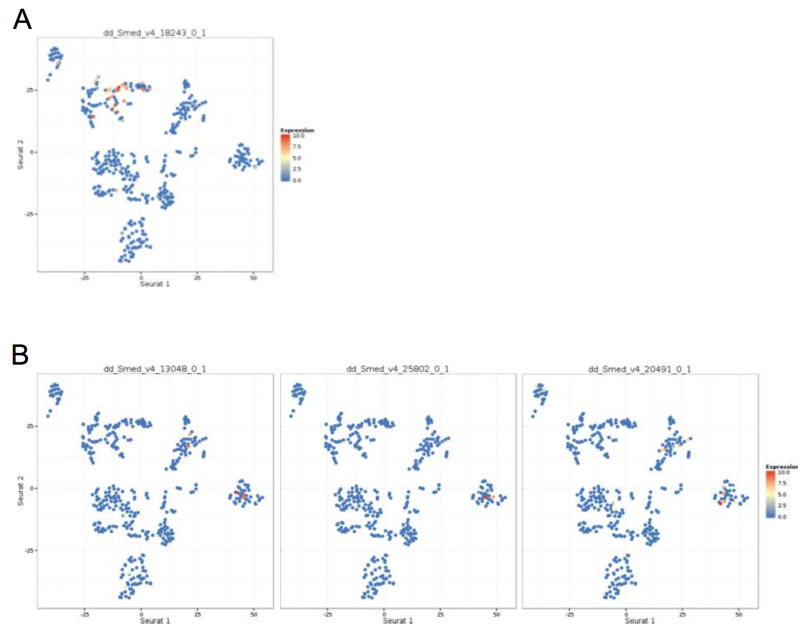
Figure 1.4: t-distributed stochastic neighbor embedding (t-SNE) for eye markers. Different planarian cell types are identified by the expression of a specific set of genes that represented by the different clusters depicted. Localization of the tyosinase-positive cells of the optic cup (A) and the TRPC4, 5, 6-positive cells of the retina (B) according to the whole-transcriptome landscape generated on single planarian cells (Omri Wurtzel et al., 2015) using the tool from radiant.wi.mit.edu/app/. Figure from my review Tran and Gentile, 2018

Based on these findings and the study in human hematopoiesis (Velten et al., 2017), we proposed a novel way to see the compartment of planarian cells and their relationship with different potency. Instead of a discrete lineage tree, the "Continuum of LOw-primed UnDifferentiated (CLOUD) stem/progenitor cells model could explain better the generation of multiple-direction lineages. As described in the study of Velten, this CLOUD model is similar to a badlands landscape, where the pluripotent stem cells have multiple directions to commit into different lineages and the barriers between them gradually deepen (Tran and Gentile., 2018). In the upper part of the mountain (figure 1.5 and 1.6), the gene expression of difference lineages may be very small, at the point that two cells with similar molecular profile may virtually locate in two different portions on the landscape. Downstream, differences in the molecular signature and potential increase, so that the border between lineages becomes impassable. Therefore, rather than being fully characterized by the expression of a set of markers, they are clouds of likelihood for the commitment/fate restriction of each cell (Tran and Gentile, 2018).
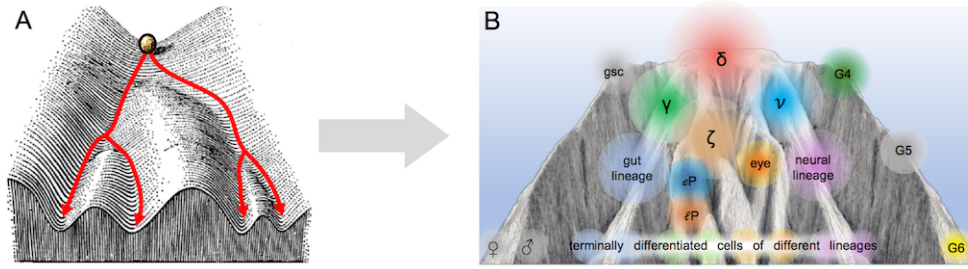
Figure 1.5: Planarian stem cell commitment models. A. The Waddington's landscape model. B. The bad land landscape model, where the pluripotent stem cells (σ class) are in the upper part of the mountain and have multiple directions to commit into different lineages. (Tran and Gentile, 2018)
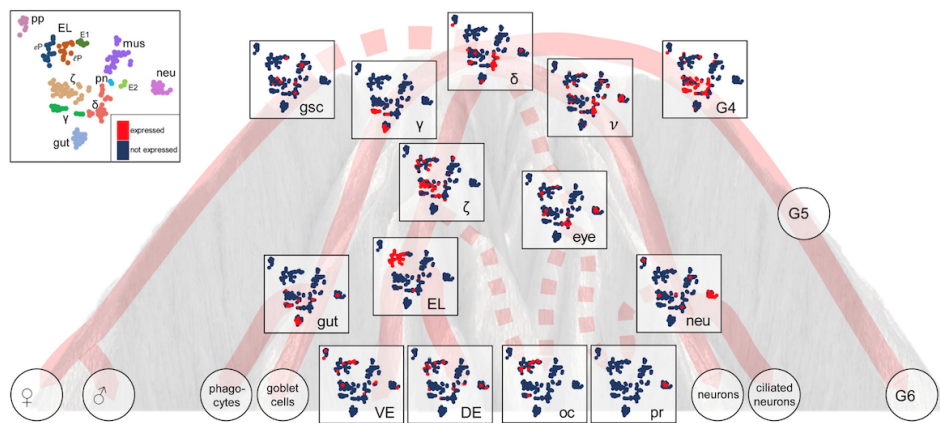
Figure 1.6: A lineage CLOUD for neoblasts on the badlands landscape. Four subclasses of neoblasts have been described so far, each identified by the expression of a specific set of genes and by the commitment towards one or more cell lineage. Additional stem/progenitor cells have been proposed so far, like the eye-Neoblast and the Group 4 neoblasts; A germ stem cell population is also postulated. Instead of by a discrete set of markers, planarian stem/progenitor cells are depicted as cloud of likelihood within the t-SNE plot generated via single-cell whole transcriptomics. Individual plots are idealized based on the expression of the proper set of specific markers, as follows: σ (σNeoblast): *soxP-2, smad-6/7, inx-13*; γ (γNeoblast): *nkx-2.2, hnf-4, gata- 4/5/6, prox-1*; ζ (ζNeoblast): *egr-1, soxP-3, zfp-1*; ν (νNeoblast): *elav-2, msi-1*; eye (eye neoblast): *ovo-1, eya, six-1/2*; gsc (germ stem cell): *nanos*; EL (epidermal lineage, early+late): *prog-1, prog-2, agat-1, agat-3*; gut (gut lineage): *gata-4/5/6*; neu (neural lineage): *pc-2, synapsin*; DE (dorsal epidermis): *ovo-2, prdm-1*; VE (ventral epidermis): *kal-1, foxJ-1*; oc (optic cup cells): *tyrosinase*; pr (photoreceptors): *TRPC4, 5, 6*. Other abbreviation used in the figure: G4/5/6: Group 4/5/6 [39]; ♀/♂: female/male gametes. (Tran and Gentile, 2018)

1.3.4   Tissue remodeling in planarian

During both homeostasis and regeneration, planarian turnover their tissues throughout life to restore a proper scale and proportion and integrate the new structures into preexisting tissues (Pellettieri and Sánchez Alvarado, 2007). The remodeling process is also triggered under prolonged starvation, resulting in decreasing up to 20 fold of their size (Baguna and Romero 1981, Reddien and Sánchez Alvarado, 2004). This cell turnover requires a stable rate of cell death in differentiated cells.   Autophagy (including cell survival and cell death autophagy) and apoptosis are known as key mechanisms regulate tissue remodeling in planarian (Pellettieri et al., 2010; González-Estévez, 2009). It is unclear whether cell death mechanisms only occur in differentiated cells or some neoblast sub-populations also undergo these processes. Pellettieri et al., sought to examine whether the cell competition exists in planarian during regeneration, as similar to Drosophila, the dividing cells induce the death of the postmitotic surrounding cells (Senoo-Matsuda and Johnston, 2007; Pellettieri et al., 2010). Based on the change in apoptotic cells following the amputation of irradiated and unirradiated animals, they proposed that both localized and systemic regenerative cell deaths primarily or exclusively occurs in differentiated cells, and the neoblasts are not necessary for this response. Conversely, the hypothesis that cell death might trigger neoblast division is considered. The significant increasing of apoptotic cell death concomitantly appeared with the enhancing of dividing neoblasts at 4-12 hr and 2-4 days postamputation (Baguna, 1984; Pellettieri et al., 2010), implied the possibility that neoblast division might be stimulated by the cell death signals.   Other model systems also proposed the term "apoptosis-induced proliferation" to describe the phenomena of apoptotic cells release mitogen to trigger the proliferation of neighbor stem cells (Martin et al., 2009; Chera et al., 2009; Mollereau et al., 2013). Oppositely, the recent study indicated that JNK, one wound signal translator, initiates apoptosis and attenuates the commencement of stem cell division, and apoptosis-induced proliferation might not occur during planarian regeneration (Almeudo-Castillo et al., 2014).   However, it is worth noting that the apoptosis-induced proliferation may be independent on JNK signals and the two mitotic peaks observed in the mentioned studies (Baguna, 1984 and Pellettieri et al., 2010) depending on the degree of the injury (Wenemoser and Reddien, 2010). Altogether, the examinations on the mechanism underlying stem cell compartment require the consideration of a time window during animal

regeneration, sub-classes of neoblasts, and the scale of tissue recovery events.

1.3.5 Planarian stem cell compartment is more and more similar to other models

Planarian is unique in the metazoans and differ from other model systems due to their extreme plasticity and the remarkable regenerative ability along with the presence of pluripotent stem cell population in the adult. However, gathering the studies archived over the last decades, planarian stem cell compartment is revealed to be more and more similar to other models in terms of the molecular mechanisms that govern them, from both cell autonomous and non-cell autonomous perspectives (Onal et al., 2012; Rouhana et al., 2010; Shibata et al., 2010; Scimone et al., 2010, Tran and Gentile., 2018). The pluripotency network of planarian share remarkable similarities with mammalian such as mouse and human (Onal et al., 2012). For example, genes *six-1/2* and *eya*, which are involved in the early state of eye precursor cells in planarian, are also found in the eye development of vertebrates and other animals (Lapan and Reddien., 2012; Pineda et al., 2000; Mannini et al., 2004; Tran and Gentile., 2018). Moreover, numerous of mutual molecules have been identified widely express in planarian and other model systems. A vasa-family gene (*DjvlgA*) from planarian *Dugesia japonica*, which is reported as a marker for neoblasts, also found in Drosophila as a vital gene for germ cell formation (Shibata et al., 1999); or the co-expression of stem cell marker genes (*smedwi-1, vasa, nanos*) in both planarian and cnidarians (Rebscher et al., 2008; Denker et al., 2008), and the human antiapoptotic gene Bcl2 is also play a key role in regulating planarian apoptotic cell death and stem cell maintenance (Pellettieri et al., 2010; Tran and Gentile., 2018). Especially, recent studies have found that non-cell autonomous mechanisms are also conserved (Tran and Gentile., 2018). They have identified that muscle cells are the conserved source of the patterning signals in planarians. This cell secrets positional control molecules such as WNT, BMP, notum, frizzled, ndk, sFRP, netrin-1 (Raz et al., 2017) to control the cell fate. Interestingly, such a positional control mechanism also exists in acoels, a flatworm that has a similar morphology with planarian but has been separated from planarian by at least 550 million years of evolution (Goldstein and King, 2016; Raz et al., 2017; Tran and Gentile., 2018). We still do not know whether the downstream response of stem cells according to the positional control genes is similar by homology or convergence (Gehrke et al., 2016).

However, the remarkable similarity between planarians and acoels in positional control indicated that the regeneration process have been preserved from the ancient to bilaterians (Srivastava et al., 2014; Goldstein and King, 2016; Raz et al., 2017; Tran and Gentile., 2018). From insects to mammals, Wnt signaling mediates axial polarity during embryo- and organogenesis (Hikasa et al., 2013; Nusse., 2005) and during heart regeneration in zebrafish (Ozhan and Weidinger., 2015). Additionally, other conventional mechanism pathways involved in mammalian cell death and proliferation were also found to play important roles in tissue maintenance and the regeneration of planarian (Tran and Gentile., 2018), such as: ERK signaling (Tasaki et al., 2011), Akt (Harshani-Peiris et al., 2016), and JNK pathway (Almuedo-Castillo et al., 2014).

The surprising common features of planarian with list of animal models indicates that stem cell systems across the animal kingdom are potentially preserved in the context of evolution (Tran and Gentile., 2018). As a stem cell *in vivo* system, planarian emerges as an ideal paradigm to define the cellular mechanisms of natural regenerative process which information could be ultimately applied in human organs to develop the treatments for clinical goal.

Chapter 2

MATERIALS AND METHODS

2.1 Materials

2.1.1 Chemicals and reagents

Reagent	Supplier
Acetic acid glacial (C2H4O2)	Sigma Aldrich (Munich, Germany)
Acetic anhydride (C4H6O3)	Sigma Aldrich (Munich, Germany)
Agarose Neeo Ultra	Carl Roth (Karlsruhe, Germany)
Ampli-Tag 360 Polymerase	Thermo Fisher (Dreieich, Germany)
Aqua-Poly/Mount	Polysciences (Bergstrasse, Germany)
Bovine Serum Albumine (BSA)	Sigma Aldrich (Munich, Germany)
Bromophenol Blue	Sigma Aldrich (Munich, Germany)
Calcein AM	Sigma Aldrich (Munich, Germany)
Calcium Chloride (CaCl2)	Sigma Aldrich (Munich, Germany)
Chloroform (CHCl3)	Sigma Aldrich (Munich, Germany)
D-Glucose anhydrous (C6H12O6)	AppliChem (Darmstadt, Germany)
Deoxynucleotide triphosphate (dNTPs)	Promega (Wisconsin, United States)
Dextran sulfate	Sigma Aldrich (Munich, Germany)
DIG RNA Labeling Mix (10x)	Roche (Mannheim, Germany)
Dithiothreitol (DTT)	Sigma Aldrich (Munich, Germany)
DNA Ladder Mix	Invitrogen (Carlsbad, United States)
DNase I (DN25)	Sigma Aldrich (Munich, Germany)
Ethanol absolute (EtOH)	Sigma Aldrich (Munich, Germany)
Ethylenediaminetetraacetic Acid (EDTA)	Sigma Aldrich (Munich, Germany)

Fluorescent Microsphere	Thermo Fisher (Dreieich, Germany)
Ficoll 400	Promega (Wisconsin, United States)
Formaldehyde (FA) 36%	Sigma Aldrich (Munich, Germany)
Formamide (CH3NO)	Sigma Aldrich (Munich, Germany)
Gentamicin	Life Technologies (Darmstadt, Germany)
Heparin	AppliChem (Darmstadt, Germany)
HEPES	Carl Roth (Karlsruhe, Germany)
High-Capacity cDNA Reverse Transcription Kit	Life Technologies (Darmstadt, Germany)
Glutaraldehyde 25%	Sigma Aldrich (Munich, Germany)
Glycogen	Sigma Aldrich (Munich, Germany)
Hoechst 33342	Thermo Fisher (Dreieich, Germany)
Horse serum	Thermo Fisher (Dreieich, Germany)
Hydrochloric acid (HCl)	Sigma Aldrich (Munich, Germany)
Hydrogen peroxide (H2O2) 36%	Sigma Aldrich (Munich, Germany)
Label IT DNP Kit	VWR GmbH (Darmstadt, Germany)
L-cysteine hydrochloride	Sigma Aldrich (Munich, Germany)
Lithium chloride (LiCl) 8M	Sigma Aldrich (Munich, Germany)
Magnesium chloride (MgCl2)	Sigma Aldrich (Munich, Germany)
Magnesium sulfate (MgSO4)	Sigma Aldrich (Munich, Germany)
Maleic acid (C4H4O4)	Sigma Aldrich (Munich, Germany)
Methanol, absolute (MetOH)	AppliChem (Darmstadt, Germany)
Mineral oil	Sigma Aldrich (Munich, Germany)
Monosodium phosphate dehydrate (NaH2PO4 – 2H2O)	Sigma Aldrich (Munich, Germany)
N-Acetyl-L-cysteine (NAC)	Sigma Aldrich (Munich, Germany)
NBT/BCIP	Roche (Mannheim, Germany)
Non-fat Dried Milk	Sigma Aldrich (Munich, Germany)
Nonidet P-40 (NP-40)	Carl Roth (Karlsruhe, Germany)
Nuclease free water (ddH2O)	Millipore (Schwalbach, Germany)
NucleoSpin RNA XS	Macherey-Nagel (Düren, Germany)
Papain suspension	Worthington (New Jersey, United States)
Paraformaldehyde (PFA)	Sigma Aldrich (Munich, Germany)
Phosphate buffered saline (PBS)	Biochrom Millipore (Berlin, Germany)
Poly-L-Lysine	Sigma-Aldrich (Taufkirchen, Germany)
Poly-L-Ornithine hydrochloride	Sigma Aldrich (Munich, Germany)

Polyoxyethylenesorbitan Tween 20   AppliChem (Darmstadt, Germany)

Polyoxyethylenesorbitan Tween 20	AppliChem (Darmstadt, Germany)
Polyvinyl alcohol (PVA)	Sigma Aldrich (Munich, Germany)
Polyvinylpyrrrolidone (PVP)	Millipore (Schwalbach, Germany)
Potassium chloride (KCl)	Sigma Aldrich (Munich, Germany)
Pre-Amplification Master Mix (2X)	Fisher Scientific (Schwerte, Germany)
Propidium iodide (PI)	Sigma Aldrich (Munich, Germany)
Proteinase K	Life Technologies (Darmstadt, Germany)
QIAquick Gel Extraction Kit	QIAGEN (Hilden, Germany)
RNA 6000 Nano Reagents	Agilent Technologies (Santa Clara, USA)
RibonucleoKde triphosphate (rNTP)	Promega (Wisconsin, United States)
Sodium bicarbonate (NaHCO3)	Sigma Aldrich (Munich, Germany)
Sodium chloride (NaCl)	Sigma Aldrich (Munich, Germany)
Sodium hydroxide (NaOH)	Sigma Aldrich (Munich, Germany)
SP6 RNA Polymerase	Fermentas (St. Leon-Rot, Germany)
Surebead Protein G	BioRad (Munich, Germany)
T7 RNA Polymerase	Fermentas (St. Leon-Rot, Germany)
TaqMan® PCR Master Mix (2x)	ThermoFisher (Munich, Germany)
Tris base (C4H11NO3)	Sigma Aldrich (Munich, Germany)
Triton X-100	Sigma Aldrich (Munich, Germany)
Trypsin inhibitor ovomucoid	Sigma Aldrich (Munich, Germany)
TSA Plus System	Perkin Elmer (Shelton, United States)
TURBO DNase	Life Technologies (Darmstadt, Germany)
Yeast tRNA	Sigma Aldrich (Munich, Germany)

2.1.2 Antibodies

Antibody	Suplier
Surface antibody 6-9.2	(Moritz et al., 2012)
Alexa Luor 488 goat anti-mouse IgM	Life Technologies (Darmstadt, Germany)
Alexa Luor 555 goat anti-mouse IgM	Life Technologies (Darmstadt, Germany)
Alexa Luor 647 goat anti-mouse IgM	Life Technologies (Darmstadt, Germany)
Anti-DIG-AP Fab Fragment	Roche (Mannheim, Germany)
Anti-DIG-POD	Roche (Mannheim, Germany)
Anti-actin mouse monoclonal	Abcam (Cambridge, UK)
Anti-smedwi-1 rabbit monoclonal	Kerstin Bartscherer, Max Planck Münster
Goat anti mouse IgM	ThermoFisher (Dreieich, Germany)
Phospho Histon H3 (Ser 10)	New England Biolabs (Frankfurt, Germany)

2.1.3 Solutions and buffers

PAM (planarian artificial medium)
1.6 mM NaCl
1 mM CaCl2
0.1 mM MgSO4
1 mM MgCl2
0.1 mM KCl
1.2 mM NaHCO3
In ddH2O

TBE
89 mM Tris
89 mM boric acid
2 mM EDTA pH 8.0
In ddH2O

Cell dissociation solutions

CMFH
2.56 mM NaH2PO4–2H2O
14.28 mM NaCl
10.21 mM KCl
9.42 mM NaHCO3
0.1% BSA
0.5% Glucose
5 mM HEPES
pH 7.2 in ddH2O

2x Papain solution (1ml)
15 U/mL papain
1mM L-cystein
In CMFH, incubate 37°C to the clear solution, then add 0.2 M L-cystein

2% L-cystein
0.5 g L-cystein HCL in 25 ml H2O, dissolve, adjust pH to 7.2

3x Stop solution
1.5 mg/ml trypsin inhibitor ovomucoid
60 μg/ml DNase I
In CMFH

Whole-mount *in situ* hybridizations buffers

0.2x SSC Wash solution
0.2x SSC
0.1% Triton X—100
In ddH2O

2x SSC wash solution
2x SSC
0.1% Triton X—100
In ddH2O

50x Denhardt's solution
1% Ficoll 400
1% PVP
1% BSA
In ddH2O

AP buffer 0.1 M Tris HCl pH 9.5
0.1 M NaCl
0.1% Tween 20
In ddH2O

Carnoy's solution
60% ethanol
30% chloroform
10% Glacial acetic acid
In ddH2O

Development buffer
10% PVA
375 μg/ml NBT

188 μg/ml BCIP

In AP buffer

Hybridization buffer

50% Deionized formamide

5x SSC

1x Denhardt's solution

1 mg/ml yeast tRNA

0.1 mg/ml Heparin

1.0% Tween 20

10 mM DTT

10% Dextran sulfate

In ddH2O

MABTx buffer

100 mM maleic acid

150 mM NaCl

0.1% Triton X 100

In ddH2O

MABTxB buffer

10% horse serum in MABT buffer

PBTx:

0.3% Triton X 100 in 1x PBS

Prehybridization buffer

50% Deionized formamide

5x SSC

1x Denhardt's solution 1 mg/ml yeast tRNA

0.1 mg/ml Heparin

1.0% Tween 20

10 mM DTT

In ddH2O

Reduction solution

50 mM DTT

1% NP-40

0.5% SDS

In 1x PBS

Wash Hyb1 solution

50% formamide

5x SSC

1x Denhardt's solution

0.1% Triton X 100

In ddH2O

Wash Hyb2 solution

75% Wash Hyb1

25% 2x SSC

Wash Hyb3 solution

50% Wash Hyb1

50% 2x SSC

Wash Hyb4 solution

25% Wash Hyb1

75% 2x SSC

<u>**Western Blot buffers**</u>

Running buffer: Tris/Glycine/SDS 10X for 1L

250 mM Tris (30.3g)

1.92 M glycine (144g)

35 mM SDS (10.08g)

Ponceau S staining buffer

0.2% (w/v) Ponceau S

5% glacial acetic acid

Tris-buffered saline with Tween 20 (TBST) buffer

20 mM Tris pH 7.5

150 mM NaCl

0.1% Tween 20

Blocking buffer

3% bovine serum albumin (BSA) in TBST

Stripping buffer

20 ml 10% SDS

12.5 ml 0.5 M Tris HCl

67.5 ml D.W

0.8 ml ß-mercaptoethanol

4X protein sample buffer

4 ml 100% glycerol

2.4 ml Tris/HCl pH 8.0

0.8g SDS

4 mg Bromophenol blue

5. ml Mercaptoethanol

Lysis buffer (RIPA) for planarian

20 mM Tris HCl pH 8.0

150 mM NaCl

1 % NP-40

2 % Glycerol

2 mM EDTA

Add proteinase inhibitor: Complete, Mini, EDTA-free protease inhibitor
cocktail tablets

2.1.4   List of primers used in this study

2.1.4.1   List of primer sequences for qPCR

Smedwi-1

Forward AGTTCCTGTTCCAACGCATTATG

Probe CTGAACTCGTTGGCAAGA

Reverse CTGGAGGAGTAACACCACGATGA

Smed-gapdh

Forward GAGTTGGAATCAATGGCTTCG

Probe CGCGCAACACCAATCGTCCAATTC

Reverse TCAACTGTGCCTTTCTCCAG

Smed-pcna
Forward GTGATGGTTTTGAGACTTATCGATG
Probe TGTTAGGGAATCATTACTACCAAGCGCC
Reverse GTTTCACTTGAATCAGCGGC

Smed-inx13
Forward TTCTGTTTCTCAGGTCGATTTCT
Probe TCAAACAATCGGCAAACAACGCTCG
Reverse CCATGAACGTTGGCGATTTG

Smed-smad6/7
Forward GCCACAGTGAGTCAGGTTTA
Probe ACCAGTCATGCCCATCTATCACGAC
Reverse CACCAGCGATTTCCAGTTTG

Smed-soxP-1
Forward TCAACACCACTAAGCACCTATC
Probe CACACGTAAGCTGAGAACGCCTGA
Reverse CAGCTGCAATTTGGCCTATG

Smed-soxP-2
Forward GACTTTAACCATGAGCCGATTG
Probe CAACCGATTCCAGTTCAACGATTGCC
Reverse CCCGTTCCATCTATCAGAAACT

Smed-egr-1
Forward TCGGACAATTCGAACAGGTAAA
Probe CGGGTGGCAGTTGATTGGATTTGC
Reverse CGATCAGTACAATTTCGAGAGAGG

Smed-fgfr-1
Forward CTCCAGACGCTAGTTCCATTATAG
Probe CGATGGCGACCGATTTGTTGCAT
Reverse GGACAAGACATGCTGTTTGATG

Smed-soxP-3
Forward GAAGCTGCTTGGCCTCATTA
Probe CGGAGTCCGTTCTTCAGCTGACATT
Reverse GGCTAGCCAATATCCGAATTTCT

Smed-zfp-1
Forward TCCCGTGCCTGAACAATTT
Probe TGTCACATTTGCAACACCAGCTTCAC
Reverse CGCATGCCTCTGTAGATTTGA

Smed-p53
Forward ATCGTCGAGCCTGTTTCATC
Probe TCCGACGACATGCCAACATTGTCT
Reverse ATCAAATTCTCCGTTGGGAATAAAG

Smed-gata4/5/6
Forward GTGAACTGTGGAGCTAGCAATA
Probe TTGTGGTCCCGGGATAATTCTGGC
Reverse AGAGAACCTGTCGCATTCATC

Smed-hnf-4
Forward TTTGGAAGCGACTTGGTATAGG
Probe TGTCGTTGATCCGTCGCTTCTTGT
Reverse CTAATCCACCCAGCTCTTTCTG

Smed-nkx2.2
Forward CCGATTTCAAACAGTTCCACTTAC
Probe TGCCAGCAGACTCAAACATCCAGT
Reverse CAGTGATCCGTACGCTGAATTA

Smed-prox-1
Forward GATAAAGTCAGCCGGAATAGCA
Probe ACGTCCTCAATGTGCTGTAAAGTGCA
Reverse CGCCTTCTTGATTTAGCAAAGAC

Smed-Agat-1
Forward GGTTGGAAGATTGTGAAGGG

Probe TGTATGAAGGCATGAGTTACAAGTGGC
Reverse CCAACCTCTCGCTTTTCA

Smed-NB32.1.g
Forward GGCACTCATTTCTCGTTTCTGTATT
Probe TGTCGAGTCGCATTTTAAATCGGCG
Reverse GTTCTCGCTGTGTTATTTGTTTACGT

Smed-HB19.11.g
Forward CGAATGTCGTTATAGAGCTCG
Probe ACAAGCGTGAATTGAGTGCTGAATGC
Reverse GCGCCTCGTCCAATTTT

Smed-myhc-1
Forward TGAAGAGCGAGCTGATCAAGC
Probe AGCTCGGTATCTGTTAGTC
Reverse GCGGATTGATGTCGCAGTTATAG

Smed-ABCC2
Forward GATTCTTCGTTCTGCAACCTATTT
Probe TAACTTGGTTCTGTGCACCGTTCCT
Reverse CTGGATAAAGTGAATGCGGTAAAG

Smed-ABCB7
Forward TGATGGGCCTGATGACATTT
Probe AGTCAGATGGGCATTTCCAGTGGT
Reverse TGGAACAGGAGCCCATTTAC

Smed-TMEM128
Forward CGTATGCATTCATCTGGAAAGG
Probe TCCCAAAGTGCAACTCCTTACAAACGA
Reverse TTAACTTAAACCATCCAGGAATCG

Smed-TMEM215
Forward GCAGAAGTGGTGCTGTTAGA
Probe AAACCTCCCTGGACAAGCTATGGG
Reverse CTTGATGGGTAGAGCATAATACGA

Smed-ATP2B1
Forward TCAAGGTGTCATGGTTGGTATG
Probe TCGGAGATGAAGCACAATCCAAACGA
Reverse GGTAACAATGCCGTGTTCAATG

2.1.4.2 List of primers for RNAi

Smed-ABCC2 (dd_Smed_v6_6609_0_1)
Forward ATTTAGGTGACACTATAGTTAGCAAGGGCCGTATACCA
Reverse ATTTAGGTGACACTATAGTCTGCTTCAGCTTCCTCAGC

Smed-ABCB7 (dd_Smed_v6_6005_0_1)
Forward ATTTAGGTGACACTATAGTCGATATTGCCATCATGAACA
Reverse ATTTAGGTGACACTATAGTCCTCCCATTATTGCTAATCCA

Smed-TMEM128 (dd_Smed_v6_360_0_1)
Forward ATTTAGGTGACACTATAGGGTTCGTATGCATTCATCTGG
Reverse ATTTAGGTGACACTATAGTATGAAACTAAAGCTGATGCCG

Smed-TMEM215 (dd_Smed_v6_318_0_1)
Forward ATTTAGGTGACACTATAGCCAATTGGTCGTCTTTACGTT
Reverse ATTTAGGTGACACTATAGTTTCCCATAGCTTGTCCAGG

Smed-ATP2B1 (dd_Smed_v6_3_0_1)
Forward ATTTAGGTGACACTATAGTAGCCCCTGAAGAACATCCA
Reverse ATTTAGGTGACACTATAGATGACGAGGCTGAAGCTGTT

Smed-GFP
Forward ATTTAGGTGACACTATAGAGTGGAGAGGGTGAAGGTGA
Reverse ATTTAGGTGACACTATAGGGTAAAAGGACAGGGCCATC

Smed-β catenin
Forward ATTTAGGTGACACTATAGCAATCACTTGGAGTCGATTCAG
Reverse ATTTAGGTGACACTATAGTCGGCAGAAACCTCAACC

2.2 Methods

2.2.1 Planarian maintenance

Schmidtea mediterranea, asexual and sexual strains were used in this study. Planarians were maintained at 18-20°C in dark with planarian artificial media (PAM) in plastic Tupper boxes. Animals were fed with veal liver twice a week. Animals with a size ranging from 4-6 mm were used for experiments. Planarians were starved for at least one week before performing any experiments.

2.2.2 Planarian irradiation

Planarians were placed in a plastic petri dish with PAM media and exposed to 110 kVp X-ray radiation for 35 min to eliminate stem cells.

2.2.3 Alginate preparation

High molecular alginates extracted from the stipes of the brown algae Lessonia nigrescens (LN) and Lessonia trabeculata (LT) (Alginatec, Riedenheim, Germany). Both alginate types were dissolved separately as 0.65% (w/v%) solutions in isotonic, 0.9% sodium chloride solution (NaCl; B. Braun, Melsungen, Germany) and mixed afterwards in equal parts to adjust a defined M/G ratio (mannuronic acid (M) and guluronic acid (G)) (Schulz et al., 2018).

2.2.4 Cell dissociation and Flow cytometry

Animals were treated with 2% L-cystein HCL (pH 7.0) in ddH2O for 2 min at RT to remove the mucus. Rinse briefly in CMFH. Put the animals onto a glass slide, cut them into small pieces using a scalpel blade. The fragments were then transferred into a 1.5 ml tube using 250 μl CMFH (used wide bore hole 1000G tip, Eppendorf). 250 μl 2x Papain-digestion solution were added and incubated the samples for 60 min at 26°C without shaking. The enzymatic reaction was stopped by adding 250 μl of x stop solution. Single cell dissociation was obtained by up- and down-pipetting for about 20 times with a P1000 pipette. The suspension was filtered through a pre-wet 30 μm strainer (Partec Celltrics) and then centrifuged for 5 min at 350 g at RT. Discarded the supernatant, the pellets were then washed with CMFH and then centrifuged and resuspended again in CMFH. Cell counting was performed using Neubauer chamber under the microscope (SMZ745T). The

cell suspension was then adjusted to 0.5 x 106 cells/ml in CMFH. Cells were stained by adding 10 μM Hoechst 33342 and 0.05 μg/ml Calcein AM for 2hr at 26°C in dark. Pellets were centrifuged for 5 min at 350 g at RT and resuspend in 350 μl CMFH. 1 μg/ml Propidium Iodide was added at the end to label the dead cells, incubate for 5 min and proceeded to FACS analysis. Samples were acquired by FACS Aria III (DB, Germany). The stem cells (X1) are the proliferating cells that contain double DNA amount (4X), which gave the highest signals in Hoechst blue channel (DAPI channel) compare to progenitor and differentiated cells (X2, Xin, respectively) . The differentiated cells have relatively large cytosols which gave the stronger signals in Hoechst red channel (Qdot800 channel) or Calcein AM green channel (FITC channel) (Reddien P et al., 2005).

2.2.5 Live immune staining with 6-9.2 antibody and cell sorting by FACS

The cells were dissociated, adjusted to 0.5 x 106 cells/ml in CMFH and stained with 10 μM Hoechst 33342 for 90 min under the slow agitation (horizontal shaker) at RT in the dark. The primary antibody 6-9.2 supernatant was added into the samples (1:10 diluted) and incubated for 30 min. Cells were then centrifuged 5 min at 350 g and washed pellets with CMFH. Secondary antibody (Alexa Fluor 488 goat anti-mouse IgM, 1:1000 diluted) was added into the samples and incubated for 15 min. Pellets were washed again, centrifuged and then resuspended in 350 μl CMFH containing 1 μg/ml Propidium Iodide. Samples were then analyzed by flow cytometry. Different cell sub-populations were gated and 100.000 cells per fraction were sorted out in RNA-low binding tubes containing CMFH buffer. Cells were then centrifuged at 350 g for 5 min and the pellets were lyzed in RA1 lysis buffer for RNA extraction.

2.2.6 Immobilization using Alginate hydrogels

Polystyrene-based coverslips (PC; Thermanox^{TM}, 13 mm in diameter, Thermo Fisher Scientific, Dreieich, Germany) were coated with poly-L-Lysine as 1:5 dilution [v/v%] in phosphate buffered saline for 30 min at 37°C. We then discarded the solution and added 300 μL of alginate solution (LN/LT 1:1, 0.65% (w/v %)). Planarians were then carefully placed on the top of the alginate layer, waited for 2 min and added another layer of alginate onto the planarian. 200 μL of crosslinking solution containing 20 mM sodium chloride were added

and incubated for 20 min at RT. We then replaced the crosslinking solution with PAM and the immobilized animals were observed under the microscope.

2.2.7   RNA extraction

RNA isolation was performed following the standard protocol from NucleoSpin RNA kit, XS column, Macherey&Nagel.

2.2.8   Reverse Transcriptase PCR – cDNA synthesis

Reverse transcription of total RNA was performed using High-Capacity cDNA Reverse Transcription Kit (Thermo Fisher).

Master Mix: total RNA, 2 μl random hexamer primers 20X, 0.8 dNTPs, 2 μl Buffer 10X, 1 μl Reverse transciptase, ddH2O.

Synthesis reaction: 25°C in 10 min, 37°C in 2 hrs, 85°C in 5 min, 4°C in ∞

2.2.9   Polymerase chain reaction (PCR)

PCR was performed to amplify specific sequences using AmpliTaq®360 Kit (Thermo Fisher). Master Mix: cDNA, 400 μM forward primer, 400 μM reverse primer, 3 mM dNTPs, 1.5 mM MgCl2, 1X reaction buffer, 0.05 U/μl Taq-DNA polymerase.

Synthesis reaction:

95°C	5 min	
95°C	30 sec	
62°C	30 sec	37x
72°C	90 sec	
72°C	7 min	
4°C	∞	

2.2.10   Quantitative Real-Time PCR (qRT-PCR)

qRT-PCR was performed to quantify the expression level of genes using QuantStudio™ 7 Flex Real-Time PCR (Thermo Fisher) in Fast Optical 96-Well Reaction Plates in 10 μl.

Master Mix: 5 ng cDNA, 0.5 μl assay 20X (primers + probe), 5 μl Taqman 20X, dd H2O

Double or triple technical replicates were carried out for each sample. Gapdh was used for endogenous control for normalization.

95°C	20 sec	
95°C	1 sec	40x
60°C	20 sec	

2.2.11 RNAi synthesis

Amplify the desired target sequence from cDNA using PCR with SP6 sequence tagged primers and SP6 RNA polymerase. PCR reaction: 100 ng of cDNA; 2 μl of sense and antisense primers (10 picromole); 5 μl of 10x PCR buffer, 1 μl of 10 mM dNTP mix, 5 μl of 25 mM MgCl, 0.25 μl of Taq DNA Polymerase. Bring up to a final volume of 50 μl using ddH2O.

Analysis of dsRNA integrity

Load 1 μl of dsRNA solution mixed with 1 μl of formaldehyde load dye (Ambion, Austin, TX) in a nondenaturing 1% agarose gel containing ethidium bromide (See Agarose gel electrophoresis).

2.2.12 *In vitro* transcription

In vitro transcription of RNA probe for whole-mount in situ hybridization (WISH)

The PCR reaction used specific primers with SP6 polymerase binding site at the 5' position.

RNA probes were labeled with digoxigenin (DIG): The tube contained 500 ng purified DNA, 2 μl 10x NTP labeling mixture Dig-labeled dNTP, 2 μl 10x SP6 Transcription buffer, 1 μl RNase inhibitor, 2 μl SP6 polymerase were mixed gently and centrifuged briefly. The reaction was carried out for 2 hr at 37. 1 μl DNaseI and 2 μl DNase buffer were added to remove DNA template. The tubes were incubated for 15 min at 37°C.

Probe purification using Ethanol precipitation. The RNA-DIG-labeled samples were incubated with 8 μl NH4OAc and 200 μl EtOH absolute for 24 h at -20°C and then centrifuged for 30 min at 13000 rpm, 4°C. The pellets were washed with 500 μl 70% EtOH, centrifuged 15 min at 13000 rpm, 4°C and resuspended in 25 μl nuclease-free water.

The concentration were measured by nanodrops.

The probe purity was checked by electrophoresis: 1 μl RNA sample was mixed with 2x loading dye for 5 min at 65°C and loaded on a 1% agarose gel.

In vitro transcription of RNAi probe

The procedure was similar to the in vitro transcription of RNA probe for WISH without the DIG-labeling step. 1 mM of rATP, rUTP, rGTP, rCTP was used instead of DIG-labeled dNTP. The reaction was carried out for 3,5 hr 37°C. 1 μl Turbo DNse and 2 μl 10x buffer were added to remove DNA template. The tubes were incubated for 30 min at 37°C.

2.2.13   Agarose gel electrophoresis

1% Agarose gel was boiled in TBE buffer using microwave for approximately 2 min. The gel was cooled down for 5 min and Ethidium Bromide was added directly into the solution and mixed well before forming a solid gel. The gel was then fully covered with 1X TBE buffer in the electrophoresis chamber. GeneRuler DNA Ladder was used as a reference for DNA fragment lengths. DNA samples were mixed with 6x DNA loading dye and loaded into each well. The gel was run in 80 V for 10 min and increased up to 120 V at RT until blue dye has migrated half-way through the gel. DNA/dsRNA bands were visualized using Chemidoc Touch device (Biorad) under ultraviolet (UV) light.

2.2.14   RNAi injection

All animals were starved for one week before injection. Planarian were placed on the ice-filled-petri dish and injected with RNAi using Nanoject II (Drummond Scientific, USA), under the microscope (SMZ745T). Three pulses of 32.2 nl of dsRNA solution of 2 ng/nl *ABCC2, ABCB7, ATP2B1, TMEM128, TMEM215, GFP* (negative control) and beta-*catenin* (positive control) were injected ventrally
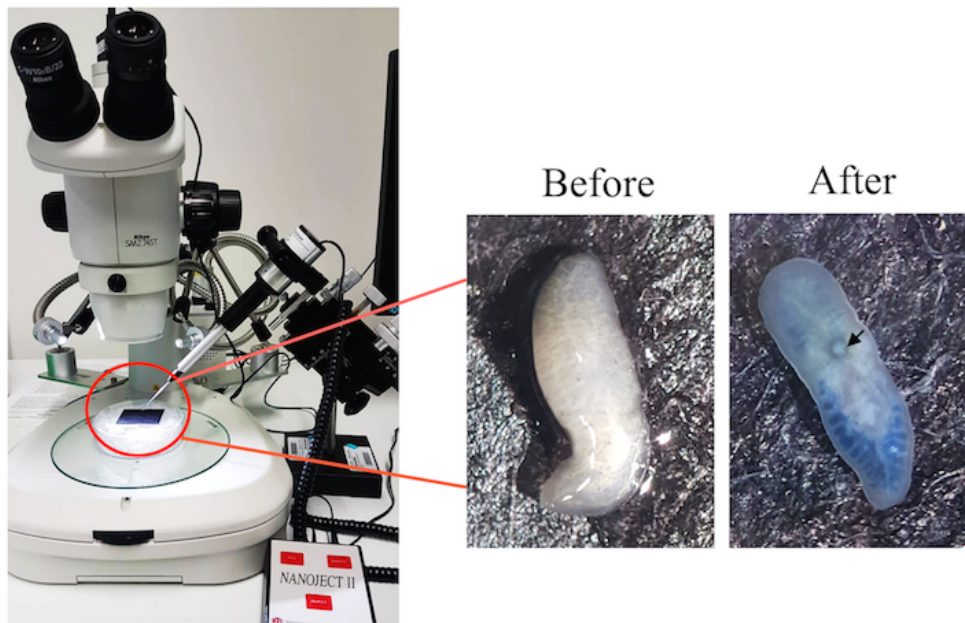
Figure 2.1: Planarian injection experiment. Live planarian was injected with trypan blue and the pictures were taken under the microscope. The arrow is the injection position, the blue color point out the gut branches filled with Trypan blue.

into planarian gut for three consecutive days and for two rounds. All animals were amputated prepharyngeally 1 day after the last injection. After 14 days of the regeneration, planarians were observed under the microscope for morphology and behavior testing or subjected to RNA extraction for qPCR. Images were taken with a stereo microscope (Nikon, ZM25, Japan). Primers for dsRNA are listed in the material part.

2.2.15 RNA sequencing (RNAseq)

For RNAseq analysis the 2 biological replicates of 6-9.2 X1- and 6-9.2 X1+ cells were sorted using FACS Aria III and subjected to RNA isolation kit NucleoSpin (Macherey&Nagel). 84-100 ng of high quality total RNA were used to generate mRNAseq libraries using the Agilent 2100 Bioanalyzer. Libraries were made according to the protocol Smart-seq2 (Simone Picelli et al., 2014) which is modified for higher input of purified total RNA.

Protocol: 2.5 μl total RNA in H2O (100 ng)

Reverse transcription

Priming Mix: 0.5 μl 20 μM oligo dT Primer, 0.5 μl 20 mM dNTPs

RT mix

Component	μl / sample
SuperScript II RT (200 U / μl)	0.5
RNase inhibitor (40 U / μl)	0.4
Superscript II first-strand buffer (5 x)	2
DTT (100 mM)	0.5
Betaine (5 M)	2
MgCl2 (0.1 M)	0.6
TSO (20 μM)	0.5

Add 1 μl Priming Mix to each sample. Vortex thoroughly, spin down. Denature at 72 °C for 3 min and immediately place on ice. Add 6.5 μl RT mix to each sample. Mix by gentle pipetting,

spin down and incubate in a heated-lid thermocycler.

42°C	90 min	
50°C	2 min	10 x
42°C	2 min	
70°C	15 min	
4°C	hold	

PCR preamplification

Component for PCR Master Mix	μl / sample
KAPA HiFi HotStart Ready Mix (2 x)	12.5
IS PCR primers (10 μM)	0.25
nuclease-free water	2.25

Add 15 μl PCR MM to each sample. Vortex, spin down and incubate in a heated-lid thermocycler.

98°C	3 min	
98°C	20 s	
67°C	15 s	5
67°C	6 min	
72°C	5 min	
4°C	hold	

PCR purification

Add 25 μl Ampure XP beads (1:1 ratio) to each sample. Incubate for 8 min at room temperature. Magnetic separation for 5 min. Discard supernatant. Wash twice with 200 μl freshly prepared 80 % EtOH. Let beads dry for 5 min at room temperature. Elute cDNA in 9 μl EB solution (or nuclease-free water). Transfer 7 μl of eluted cDNA into a fresh PCR-stripe.

Quality control

Measure sample concentration with Qubit HS. Expected yield 10 – 12 ng. Check size distribution of cDNA on a Agilent HS DNA Bioanalyzer Chip (1 μl).

Tagmentation: Standard Nextera Kit

Tagmentation in 20 μl reaction volume. 5 ng cDNA, 1 μl Tn5, 10 μl 2X TD Buffer, ddH2O. 10 min, 55 °C. MinElute Purification (100 μl PB, Elution in 10.5 μl EB)

PCR: 10 μl Template + 15 μl NEB-MM + 1 μl AD1 + 1 μl AD2 + 3 μl ddH2O

72°C – 5 min, 98°C – 30 sec, 98°C – 10 sec, 63°C – 30 sec, 72°C – 1 min, 72°C – 5 min. All steps for 7 cycles. Add 0.9 X Ampure XP Bead Purification (45 μl beads).

Libraries quality and quantity checking

Resulting short fragment libraries were checked for quality and quantity using the Bioanalyzer (Aligent) and Qubit Fluorometer (Life Technologies).

Equal molar libraries were pooled, requantified and sequenced on the Illumina HiSeq 2500 instrument using HiSeq Control Software 2.2.38. Following sequencing, Illumina Primary Analysis version RTA 1.18.61.0 and Secondary Analysis version CASAVA-1.8.2 were run to demultiplex reads for all libraries and generate FASTQ files. Sequencing reads from each library were mapped to the *S. mediterranea* cDNA sequences from Planmine database (http://planmine.mpi-cbg.de/planmine), dd_smed_v6 transcriptome assembly. Reads were aligned using Salmon (Patro et al. 2017) with default parameters.

Detection of differentially expressed genes

Read counts was imported into DESeq2 (Love, Huber, and Anders 2014) with the Bioconductor package tximportData. The differential expression of genes/contigs was performed by DESeq2 function in R. P-values were adjusted as previously described (Benjamini and Hochberg, 1995). A FPM (Fragment per million reads) matrix were exported and differentially expressed genes/contigs were detected. Here, contigs among the top 1% highest expressed contigs were excluded in order to avoid bias. The low expressing contigs (base mean less than 20) were filtered out of from the generated matrix. To verify the accuracy of our transcription profiling results, we selected 21 genes (*SoxP2, SoxP1, Gapdh, zfp_1, p53, fgfr1, gata456, pcna, inx13, egr-1, prox-1, prog-1, nkx2.2, smedwi-1, myhc-1, fgfr-4, agat-1, NB22.1e, SoxP3, smad6/7, cyclinB*) which were already validated in qPCR results. Obtaining the reproducibility of expression profiles between qPCR and RNAseq data, we then sorted the list of contigs that have two criteria simultaneously: a statistical test (adjusted P-value < 0.01) and a log2 fold change of ± 1. All gene expression fold changes were calculated relative to the expression of the respective gene in 6-9.2 X1+ compare to 6-9.2 X1- samples. Vocano plot was generated from Log2 Fold change of positive group versus negative group and adjusted pvalue using R package.

2.2.16 Whole mount in *situ* hybridization (WISH)

The WISH procedure followed the protocol from Dr. Kerstin Bartscherer's lab (Max Planck, Münster) modified by Henning Schmitz.

2% ice-cold HCl (hydrochloric acid) solution was used to kill animals and wash the mucus away. Animals were placed in a petri dish containing HCl for 2 min with vigorously sharking. The samples were then transferred into fresh ice-cold Carnoy solution for 2 hrs on a horizontal shaker at 4°C. Carnoy solution was removed and replaced with 100% methanol for 1hr at 4°C. Samples were then treated with fresh bleaching solution (6% H2O2 in methanol) for 16 hrs under a lamp in a cold room (4°C). Bleached specimens were washed three times with methanol at RT in 30 min and hydrated by washing in a series of 75%, 50%, and 25% methanol in PBTx, for 10 min each step. The specimens were then treated with 20 μg/ml Proteinase K for 8 min at 37°C without shaking. The samples were washed briefly with PBTx and fixed with 4% PFA for 30 min and

washed three times with PBTx in 30 min. The worms were incubated with 0.1 M TEA pH 7.6 buffer in ddH2O for 15 min, two times. 0.25% acetic anhydride was added into sample tubes in the second TEA incubation for 15 min. 0.25% acetic anhydride was added again and incubated for 15 min. The worms were rinsed with PBTx two times for 10 min and then transferred into 1.5 ml tubes and incubated with 500 μl of pre-heated prehybridization mixed with PBTx (1:1) in 10 min. Specimens were incubated with prehybridization buffer at 56°C for two hrs on a shaker inside a hybridization oven (Stuart SI30H). 0.5 ng/μl DIG-labeled RNA probes in hybridization buffer was denatured at 72°C for 10 min and cooled down on ice for 5 min. The prehybridization buffer was replaced by hybridization solution containing RNA probes and shaking for approximately 16 hrs at 56°C in the oven. The samples were washed stepwise with Wash Hyp1, Wash Hyp2, Wash Hyp3, Wash Hyp4 (15 min each step), 2x SSC solution (three times , 20 min each), 0.2x SSC solution (four times, 20 min each). The samples were then transferred to a 12 well plate, washed with MABTx buffer two times in 20 min, and blocked with MABTxB buffer for 1 hr. The samples were incubated with alkaline phosphatase (AP)-conjugated anti-DIG antibody (α-DIG-AP) with MABTx overnight at 4°C. After washing with MABTx buffer for at least 8 times (20 min each), samples were washed with AP buffer for 10 min, and then incubated with development NBT/BCIP buffer in dark until reaching the desired staining signals. The samples were washed with PBTx and fixed with 4% PFA in PBTx for 20 min and wash again twice in PBTx. The animals were incubated in 50% ethanol in PBTx until they sunk down and rinsed one last time with PBTx. The specimens were mounted on glass slides with mounting media (Aqua-Poly/Mount).

2.2.17   Fluorescent in *situ* hybridization (FISH)

FISH protocol followed the similar process of WISH except the antibody incubation and fluorescent development steps. A peroxidase (POD)-conjugated anti-DIG antibody (α-DIG-POD) was used in this study. TSATM Plus Cyanince 3/Fluorescine System was used to amplify the fluorescent signals, according to the standard manufacturer's instructions. Samples were incubated with FITC or tyramine (1:50) for 60 min and rinsed four times in 1 hr with MABTx. Samples were then fixed in 4% PFA in MABTx for 20 min and stained with 0.5 μg/ ml Hoechst 33342 for 2 hrs.

2.2.18 Protein extraction

Planarian samples were rinse 2 times with ddH2O and placed in 1.5 ml tube with 1 ml RIPA buffer containing protease inhibitor (0589279100, Roche) (see material section). Samples were then sonicated in sonication device (Bandelin Sonopuls HD 200) for 10 seconds and placed on ice for 45 mins. Centrifuge samples with13000 rpm for 30 mins at 4°C. Harvest the suspension and store samples at -80°C.

2.2.19 Western Blot

The protein concentrations were measured by nanodrops using ddH2O as a blank sample. 4-20% mini Protean TGX gels (BioRad) were placed into electrophoresis chamber in Running buffer. Add 4X SDS loading buffer into protein samples, heat at 90C for 10 mins and place on ice for 5 mins. Run the gel at 30 mA until the samples reach the black line of the chamber. Transfer the gels to the PVDF membrane and place the membrane sets into the Trans-blot TURBO transfer system (BioRad) and run for 3 mins. Block the membranes in 5% skim milk in TTBS buffer for 1 hr at RT. Incubate the membrane with 10% 6-9.2 antibody supernatant in skim milk, shaking overnight (Heidolph Polymax 1040) at 4°C. Wash the membrane with TTBS for 2 times, in 30 mins. Add secondary antibody mouse IgM into the membrane (1:1000 in TTBS). Shaking for 1 hr. Wash the membrane 4 times in 1 hr. The membrane were stained with Immun-Star WesternC chemiluminescence by adding the mixed solution onto the top of the membrane for 1 min. The signals were detected by Chemidoc Touch Imaging system (BiroRad).

2.2.20 Protein membrane protein isolation

Planarian samples were lysed in lysis buffer and isolated by magnetic beads, as described by the standard protocol of Qproteome™ Plasma Membrane kit (QIAGEN).

Briefly, the animals were snap frozen in liquid nitrogen and ground with a pestle to homogenize the tissues. The samples were then incubated in a hypotonic buffer with mild detergent (PM buffer containing protease inhibitor) and homogenized again by mechanical disruption using a needle and syringe, placed on ice for 30 min. Cell lysates were centrifuged at 12,000 x g, 4°C for 20 min.

The supernatants contains cytosolic proteins, endoplasmatic reticulum, Golgi vesicles, and plasma membranes were harvested. Added 40 μl of reconstituted Binding Ligand PBL (specific for molecules on the plasma membrane) into supernatants and incubated the reaction with gentle agitation for 1 hr on a shaker at 4°C.

During the incubation, StrepTactin Magnetic Beads were equilibrated and vortexed vigorously to obtain a homogenous suspension. 300 μl of the bead suspension were transferred into a new 1.5 ml tube. The tubes were magnetized for 1 min on a magnetic rack (BioRad) and removed supernatant with a pipette. 500 μl Lysis Buffer PM with protease inhibitors were mixed with the beads and separated the buffer again with a magnet for 1 min. The beads were added 100 μl Lysis Buffer PM with protease inhibitors, gently vortexed the suspension and placed on ice.

The equilibrated magnetic beads were then added into the reaction mix and incubated for 1 hr with gentle agitation on a shaker at 4°C. The tubes were then placed on a magnetic rack for 1 min to remove the supernatant. Washed the pellet 2 times with 500 μl of Lysis Buffer PM with protease inhibitors, resuspended beads by gently vortexing and placed on ice for 5 min. The suspension were magnetized using magnet for 1 min and completely remove and discard supernatant. After washing, plasma membrane vesicles were eluted with 500 μl of Elution buffer PME, vortexed gently, incubated on ice for 5 min, and separated the supernatant by magnet for 1 min. The process was repeated three times and four eluates were combined in a single tube.

The protein fractions were added with four volumes of ice-cold acetone and incubated for 15 min on ice. The samples were centrifuged for 10 min at 12,000 x g in a pre-cooled microcentrifuge at 4°C. The pellets were harvested, dried on air briefly and separated into two tubes. One tube was resuspended with 100 μl sample buffer and the other one was subjected to immunoprecipitation assay to enrich the 6-9.2 proteins.

2.2.21 Immunoprecipitation

The 6-9.2 enriched protein samples were performed by immunoprecipitation of plasma-membrane proteins using 6-9.2 antibody.

SureBeads protein A/G magnetic beads (BioRad) were vortexed vigorously to obtain a homogenous suspension. 20 μl of magnetic beads were added into a tube containing 100 μl of 6-9.2 antibody and incubated for 1 hr on a shaker at 4°C. The plasma-membrane proteins isolated from Qproteome^{TM} Plasma Membrane kit were incubated with the mixture of 6-9.2 antibody and magnetic beads for 1 hr on a shaker at RT. The samples were magnetized on a magnetic rack for 1 min at RT and were separated into two fractions:

- The supernatant contained unbound magnetic proteins were harvested in a new tube and washed with lysis buffer contains protease inhibitor. The tube sample was vortexed and placed on a magnetic rack for 1 min to remove all the left over beads. The supernatant contained only unbound proteins (6-9.2- sample).

- The pellet contained 6-9.2 proteins were harvested, washed twice to completely removed the unbound proteins with lysis buffer contains protease inhibitor. The pellets was eluted by elution buffer, vortexed and magnetized by placing the tubes on a magnetic rack for 1 min. The magnetic beads bound to the magnet area and the purified 6-9.2 protein were harvested in a supernatant.

2.2.22   Mass Spectrometry

<u>Protein extraction</u>

Protein samples including membrane enriched sample, 6-9.2 enriched proteins, and 6-9.2- proteins isolated from "Protein membrane protein isolation" step, and the whole cell lysate sample were used for Mass Spectrometry. In order to maximize and cross-check the protein identity, we used two distinct protein-processing methods, namely, NU-PAGE gel (Sigma Aldrich) for in-gel digestion and Western blot for membrane digestion.

In-gel digestion: 30 μg of protein was separated under reducing conditions on 4 – 12 % NuPAGE gradient gels (Invitrogen). The gel was fixed and stained by Novex Colloidal Blue (Thermo). Placed the gel on the gel-cutting board. The selected protein size around 20, 25, 37 and 50 KDa were cut with a new clean scalpel and transfered to 1.5 ml tube separately and processed as described in

Shevchenko's method (Shevchenko et al., 2006) for gel digestion. Briefly, the gel cube were washed two times with 500 μl 50 mM ABC/50% EtOH for 20 min each and dehydrated with 500 μl EtOH absolute for 20 min, removed EtOH by SpeedVac for 10 min. 100 μl of 50 mM ABC/10 mM DTT were added into the tube and incubated for 45 min at 56°C with 900 rpm rotation. The supernatants were removed and the gels were alkylated by adding 100 μl 50 mM ABC/55 mM IAA, incubated for 30 min in dark, removed supernatants. The washing and dehydration steps were repeat two times and the samples were dried in SpeedVac until gel pieces became solid. Gel pieces were incubated in 50 μl 12.5 ng/μl Trypsin in 50 mM ABC for 15 min, added 50 μl 50 mM ABC and incubated overnight at 37°C. Supernatants were collected into new tubes and extracted using a gradient of ACN buffer. The sample tubes were incubated with 100 μl 30% ACN/3% TFA for 20 min and transferred supernatants to tubes. Samples were incubated with 100 μl 70% ACN for 20 min, transferred supernatants to tubes, repeated and incubated with 100 μl 100% ACN for another 20 min. The protein samples were concentrated in SpeedVac to a final volume of about 80 μl and proceeded stage-tipping step.

Membrane digestion: 30 μg of protein for each sample were separated under 4 - 12% SDS-PAGE gradient gels (BioRad) and performed Western blot (See Western blot section). The membrane were then immunized with 6-9.2 antibody for overnight at 4°C in skim milk solution. The membrane was then incubated with secondary antibody mouse IgG for 1 hr at RT on a shaker. The membrane was then washed and the protein bands below 50 KDa were cut and placed in 1.5 ml tube separately and processed membrane digestion protocol. Membrane proteins were washed with water for 5 min with agitation using a thermomixer at RT and 1000 rpm. Samples were incubated at 37°C for 30 min with 1 ml 0.5 PVP-40/0.1 M acetic acid to block nonspecific proteins (trypsin) binding sites on the nitrocellulose with gentle agitation at 300 rpm. Membranes were washed 6 times with 1 ml water to completely remove PVP-40 and transferred to new tubes. Membranes were incubated overnight at 37°C with 50 μl 12.5 ng/μl Trypsin in 50 mM ABC and fully covered with additional volume of 50 mM ABC, gently agitated at 300 rpm. After the digestion step, membranes were dried under the vacuum and added with 100 μl of aceton, vortexed and incubated for 30 min at RT. The samples were centrifuged for 10 min at 14000 g and the remained aceton were carefully removed. Precipitated peptides were air-dried, re-suspended in 20 μl 2% ACN/0.1 % FA, and sonicated for 10 min.

Stage-tipping

Production of stage tips: 200 μl yellow tips were filled with C18-material by using blunt luer lock needle (Hamilton) to punch out a small piece of C18 matrix from matrix disc. A small piece of C18-material were pushed into a tip using HPLC capillary running with the luer lock needle. 4 layers of C18 were pressed onto the top of the tip. Added 20 μl MeOH into the yellow tip and centrifuged for 3 min at 300 rpm. Added 20 μl solution B (80% ACN, 0.1 % FA) into a tip and centrifuged for 3 min at 300 rpm. Added 20 μl solution A (0.1% FA) into a tip and centrifuged for 3 min at 300 rpm, repeated this step one more time. The concentrated protein samples were mixed with an equal volume of solution A and added into the prepared stage tips. The tips were centrifuged at 300 rpm until they were empty and washed with solution A, centrifuged for another 3 min at 300 rpm. The tips contained C18-bound peptides were eluted with 40 μl solution B into a 96-well plate. The volume were reduced to 2-3 μl in SpeedVac for 20-30 min. Added 8 μl solution A into each well and subjected the samples to Mass Spec.

Mass Spectrometry Analysis and Bioinformatics

This process was performed by Dr. Hannes Drexler from Max Planck, Münster. LC-MS/MS analysis was performed on a LTQ Orbitrap Velos mass spectrometer (Thermo Scientific) online coupled to an Easy nano-LC system (Proxeon) via a nano electrospray source (Proxeon).

Protocol in brief: Peptides were separated by reversed-phase chromatography on fused silica capillary chromatography columns (15cm length, ID 75μm; New Objectives) Peptides extracted from in-gel and membrane digested fractions were separated using linear gradients from 2-7% buffer B (80% acetonitril, 0.5% acetic acid; 5 min), 7-35% B (90 min), 35-60% B (20 min), 60-80% B (4 min) and 80-98% B (2 min). Each of these gradients lasted 190 min and was followed by a gradient over 10 min to 90% B and further elution at 90% B for 5 min before the column was equilibrated again with starting buffer A (0.5% acetic acid). The mass spectrometer was operated in data-dependent mode (positive ion mode, source voltage 2.1kV) automatically switching between a survey scan (mass range m/z = 350-1650, target value = 1 x 106; resolution R = 60K; lock

mass set to background ion 445.120025) and MS/MS acquisition of the 15 most intense peaks by collisional induced dissociation in the ion trap (isolation width m/z =2.0; normalized collision energy 35%; dynamic exclusion enabled with repeat count 1, repeat duration 30.0, exclusion list size 500 and exclusion duration set to 90 s; double charge and higher charges were allowed).

MaxQuant software (v1.3.0.5) was used to process the raw data. The search was performed against a *Schmidtea mediterranea* database from Dr. Jochen Rink's lab. 1 unique peptide was filtered and all contaminants were removed, as well as reverse hits from the database search and proteins that were identified by a modified peptide only. Protein groups contained protein identifications based on at least two different peptides with a false discovery rate (FDR) set to 1% for all peptide and proteins.

Sequence alignment and 6-9.2 antigen discovery

From western blot results, we already confirmed that the proteins bind to 6-9.2 antibody were located at 20, 25, 37 and 50 KDa protein bands on the membrane. The dataset was first selected from the common peptides represented in both in-gel digested and membrane digested samples. The contigs that highly expressed in both 6-9.2 enriched sample and plasma-membrane enriched sample but had low expression in 6-9.2- protein sample were selected. The transcriptome data set of this candidates were then blasted to human and other species using blastn tool in NCBI data base. The short list of genes that match with predicted genes express in the cellular membrane were sorted.

To confirm the sequence identification, we converted the transcriptome data set into peptide sequences using ExPASy tool (University of Geneva, Switzerland) and blasted peptide sequences into human and other species using blastp tool from NCBI. The short list of peptides that match with predicted protein express in the cellular membrane were sorted.

We then combined the results from blastn and blastp and selected the contigs that predicted to be located on the cellular membrane and have sizes ranging from 20 to 50 KDa. These putative genes were then confirmed by RNAi experiments.

2.2.23   Bioinformatics

R was used for bioinformatics analysis and the script used are shown below:

PCA
pca_model = prcomp(file name ,scale. = F)
biplot
biplot(file name,family="serif",xlim=XLIM,ylim=XLIM)

Vocano plot
Select Log2 Folchange and padj value.
data_1=data.frame(file name)
data=data_1[,c(,)]
data=as.matrix(data_1)
library(plotrix)

plot(data, main="p-value versus fold-change", xlab="log2 fold change", ylab="-log10 p-value")
points(data[,1], data[,2], col=color.scale(data[,2], c(0.75, 0, 0), 0.8, 1, color.spec="hsv"))

MA plot
library(affy)
x <- normalize.quantiles(data)
ma.plot(rowMeans(x), $log2(x positive) - log2(x negative)$, cex=1)

q-q plot
library(ggplot2)
qqnorm(data$attribute)

Violin plot
library(ggplot2)
ggplot(data, aes(factor(p-value), log2FoldChange)) + geom_violin(aes(fill = factor(p-value)))

2.2.24   Statistical analysis

R and Excel was used for statistical analysis. The statistical significance was calculated with Student t-test.

p-value: t.test()

padj (adjusted p-value in RNA sequencing data) was calculated in DESeq2 package using Wald-test.

Chapter 3

RESULTS

3.1 Stem cell classification using novel surface antibody 6-9.2.

Planarian adult stem cells (neoblasts) have been identified as a heterogeneous population. The key techniques commonly used in planarian currently are whole-mount in situ hybridization (WISH) to visualize gene transcripts within cells and tissues, and the RNA interference (RNAi) to study gene function. Recently, high-dimensional single cell transcriptome emerged as a powerful tool to resolve the heterogeneity of the neoblasts, multiple sub-classes have been found; and among them, σ-Neoblasts are pluripotent cells that mostly encompass the c-Neoblast population and lay upstream of other neoblast sub-classes (table 1). However, these techniques could only provide the understanding on molecular criteria while the information in cellular level is lacking or poorly understood. Another obstacle, there are few antibodies available to visualize protein expressions which also detain the cell signaling research. Therefore, to understand the planarian stem cell biology, the new tools that allow tracking the fate of individual transplanted cells are required. In 2012, our group raised a library of monoclonal antibodies specific for planarian plasma membrane proteins. Among them, 6-9.2 antibody recognized sub-populations of stem cells in FACS gate (Moritz et al., 2012), offers a promising antibody-based labeling to specifically stain subsets of stem cells to trace their behaviors *in vivo*. Therefore, we further investigate the possibility to use this antibody as a novel stem cell marker for neoblasts, the characteristic of this 6-9.2 surface protein and its role in planarian stem cells. This study is a

major step to build up a live cell tracking system (Figure 3.1) to answer the long-standing question of how individual neoblasts behave and how the regeneration mode is regulated.
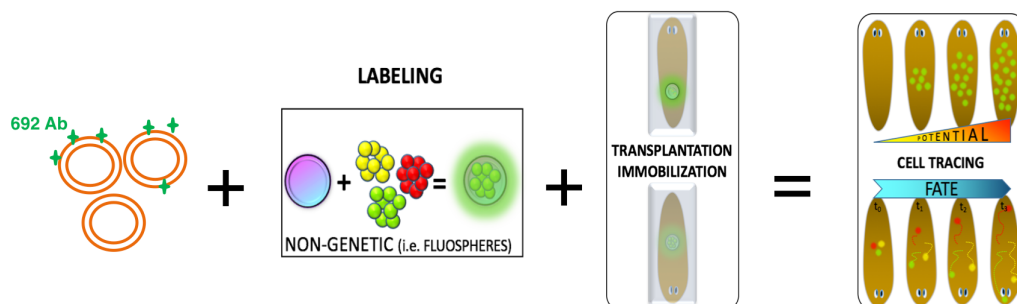
Figure 3.1: The overview of live cell tracking method using surface antibody and fluorescent bead-based labeling approach. From left to right: the stem cell subclasses are isolated by 6-9.2 antibody; cell non-genetic labeling using fluorescent beads that allow to stain cells in different colors; labeled cells are transplanted into immobilized planarians; the live tracking of different fluorescent cells in planarians.

3.2 Surface antibody 6-9.2 recognized committed stem cells in neoblasts X1 FSC/SSC population.

In order to develop a live cell tracking system, we first confirmed and examined the characteristics of cell sub-populations isolated from 6-9.2 antibody. As shown in figure 3.2, the planarian cells were dissociated and subjected for fluorescence-activated cell sorting (FACS) experiments to isolate different cell subgroups. The stem cell population were stained live immuno fluorescence with surface antibody 6-9.2 and the two sub-groups that are negative and positive binding with this antibody were then subjected to molecular techniques: qPCR and RNAseq.

Neoblasts are the only dividing cells in planarian and also the most sensitive cells to irradiation (Bardeen and Baetjer, 1904). Therefore, they can be isolated by FACS when compare the cell distribution of wild type and irradiated samples on FACS plots (Moritz et al., 2012; Reddien et al., 2005; Hayashi et al., 2006). As shown in Figure 3.3A, planarian cells populated in three populations: the two X ray-sensitive populations 1 and 2 (X1 and X2), and one X ray-insensitive cells (Xin). Neoblasts are in both the X1 (dividing cells in S-G2/M phase of the cell cycle) and the X2 (cells in G1) gates. In irradiated sample, the whole X1 and a part of X2 populations disappeared (as X2 contains a mixture of
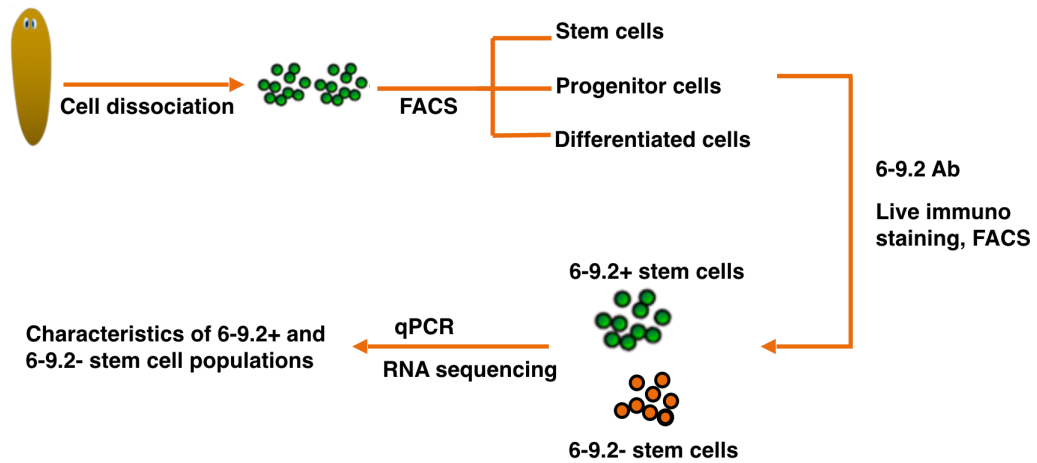
Figure 3.2: Proposed experimental plan of 6-9.2 antibody in isolating neoblast sub-populations.

neoblasts and post-mitotic neoblast progeny). Planarian stem cells X1 gate were then isolated further using 6-9.2 antibody live immuno staining. The result showed two populations separated in histogram in FITC channel (green fluorescence), where 35% of the stem cells negatively bind to 6-9.2 antibody (6-9.2- X1) and approximately 40% stem cells positively bind to 6-9.2 antibody (6-9.2+ X1) were populated on the right peak (Figure 3.3B).

These cell sub-types X1, X2, Xin, 6-9.2+ X1 and 6-9.2- X1 were then sorted in CMFH buffer and subjected to qPCR to examine the differences in gene expression levels. σ-Neoblasts has been published as pluripotent stem cells that lay upper the badland landscape and have an ability to commit into every cell types (Tran and Gentile, 2018). Therefore we used the marker gene set of σ class and its defined committed ζ and γ-classes to see the relationship of 6-9.2+ X1 and 6-9.2- X1 with σ, ζ and γ-Neoblasts. We first confirmed whether the stem cells in X1 gate were well isolated by FACS analysis by performed qPCR with stem cell marker gene sets: pan-Neoblast (*PCNA, smedwi-1*), σ class (*Inx13, smad6/7, SoxP-1, SoxP-2*), ζ class (*Egr-1, Fgfr-1, SoxP-3, zfp-1*), γ-class (*gata456, hnf-4, nkx2.2, prox-1*), post-mitotic markers (*Agat-1, Prog-1*), and one differentiated marker *myhc-1*. qPCR results showed a significant high gene expression levels of pan-neoblast markers but significant low level of differentiated marker in X1 stem cells compare to Xin cells, indicating the well isolation of stem cells from differentiated cells by FACS gating. The X1 and X2 cells (stem cells in S-G2/M and G1 phases of the cell cycle) expressed a high level of σ gene markers, whereas X2 cells expressed higher level in post-mitotic

markers, which indicated the well separation of stem cells from post-mitotic or progenitor cells. Interestingly, X2 cells had higher gene expression levels of ζ and γ-classes (Neoblasts derived from σ class) (Figure 3.5A). Since the isolation of X1 stem cell population was confirmed by qPCR, we then examined the gene expression level of the stem cell marker genes in 6-9.2+ X1 and 6-9.2- X1 sub-classes. Figure 3.5B showed the dramatically high gene expression level of 6-9.2+ X1 in ζ class (*Egr-1, Fgfr-1, SoxP-3*), γ-class (*gata456, hnf-4, nkx2.2, prox-1*), and post-mitotic markers (*Agat-1, Prog-1*), while 6-9.2- X1 had higher gene expression level in σ class (*SoxP-1, smad6/7, Inx13*) (p value *leq* 0.05). 6-9.2+ X1 and 6-9.2- X1 cells expressed relatively similar level of pan-Neoblast markers (*PCNA, H2B, smedwi-1*) and differentiated marker *myhc-1*. A few other markers from σ, ζ, and γ-classes were not differed. Altogether, we concluded that 6-9.2- X1 cells are potential pluripotent stem cells that co-express the same gene set with σ-Neoblast and 6-9.2+ X1 cells are stem cells derived from σ-Neoblast that highly express ζ and γ-Neoblast markers, as well as some post-mitotic markers (Figure 3.5C). These data suggested the 6-9.2 antibody offers the advantage of specifically isolate the pluripotent stem cells from committed cells and 6-9.2 antigene (protein membrane) is a novel marker for stem cell isolation. To further investigate the molecular characteristic of these two stem cell sub-groups 6-9.2+ X1 and 6-9.2- X1, we isolated these stem cells and sorted by FACS in CMFH buffer. In 30.000 events we collected 6.4% of stem cell population X1, in which 6-9.2- X1 and 6-9.2+ X1 cells were approximately 35% (Figure 3.4).
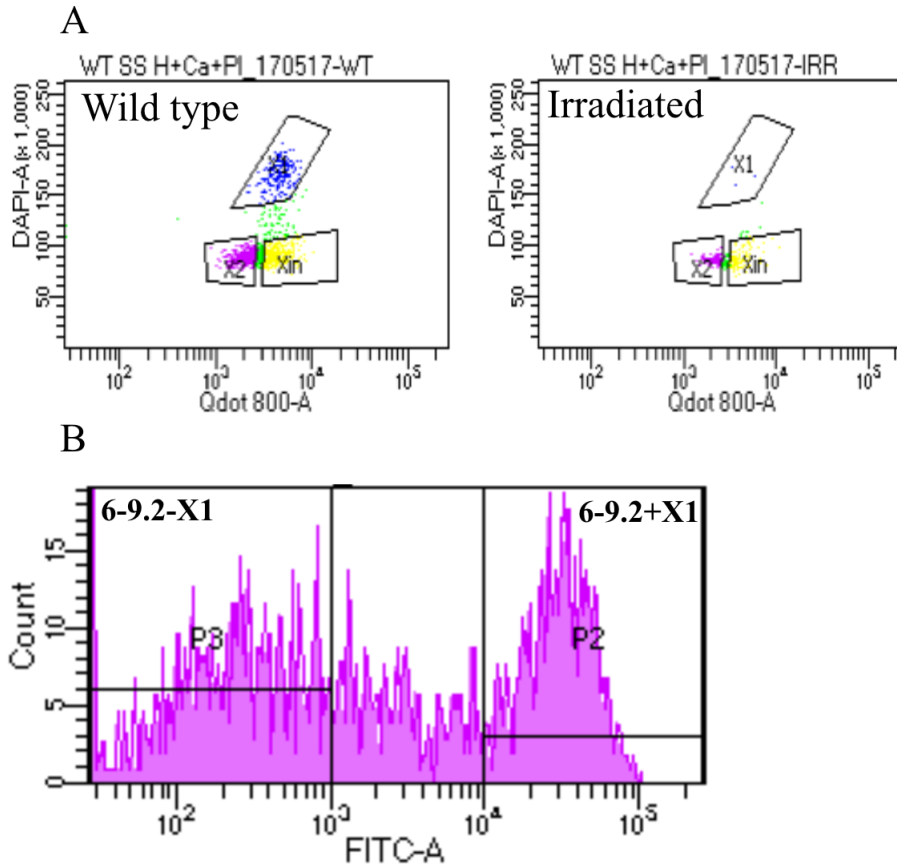
Figure 3.3: Neoblast subclasses isolated by FACS. A, Irradiated and wild type planarians were dissociated and stained with Hoechst and PI dyes, and subjected to FACS analysis. B, Stem cells X1 gate were stained with 6-9.2 antibody (1:8) and secondary antibody Alexa Fluor 488 goat anti-mouse IgM (1:1000) and two sub-populations were separated in the histogram based on the fluorescent signals of FITC channel.
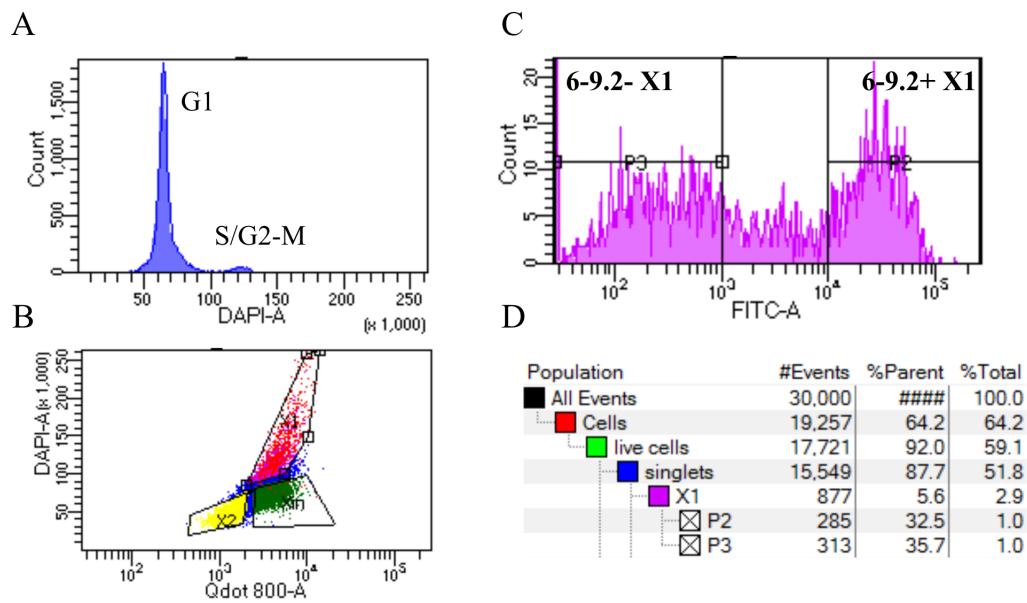
Figure 3.4: The isolation of 6-9.2- X1 and 6-9.2+ X1 cells in planarian. A, Cell cycle histogram. B, Different cell populations (stem cells, progenitor cells, differentiated cells) isolated by FACS gating using Hoechst blue (DAPI-A channel) and Hoechst red (Qdot 800-A). C, Two sub-population of X1 cells isolated by 6-9.2 antibody live-immuno staining with Alexafluor 488 secondary antibody (FITC-A channel). D, Number of cells in different groups in 30.000 events. The data represent one biological experiment.
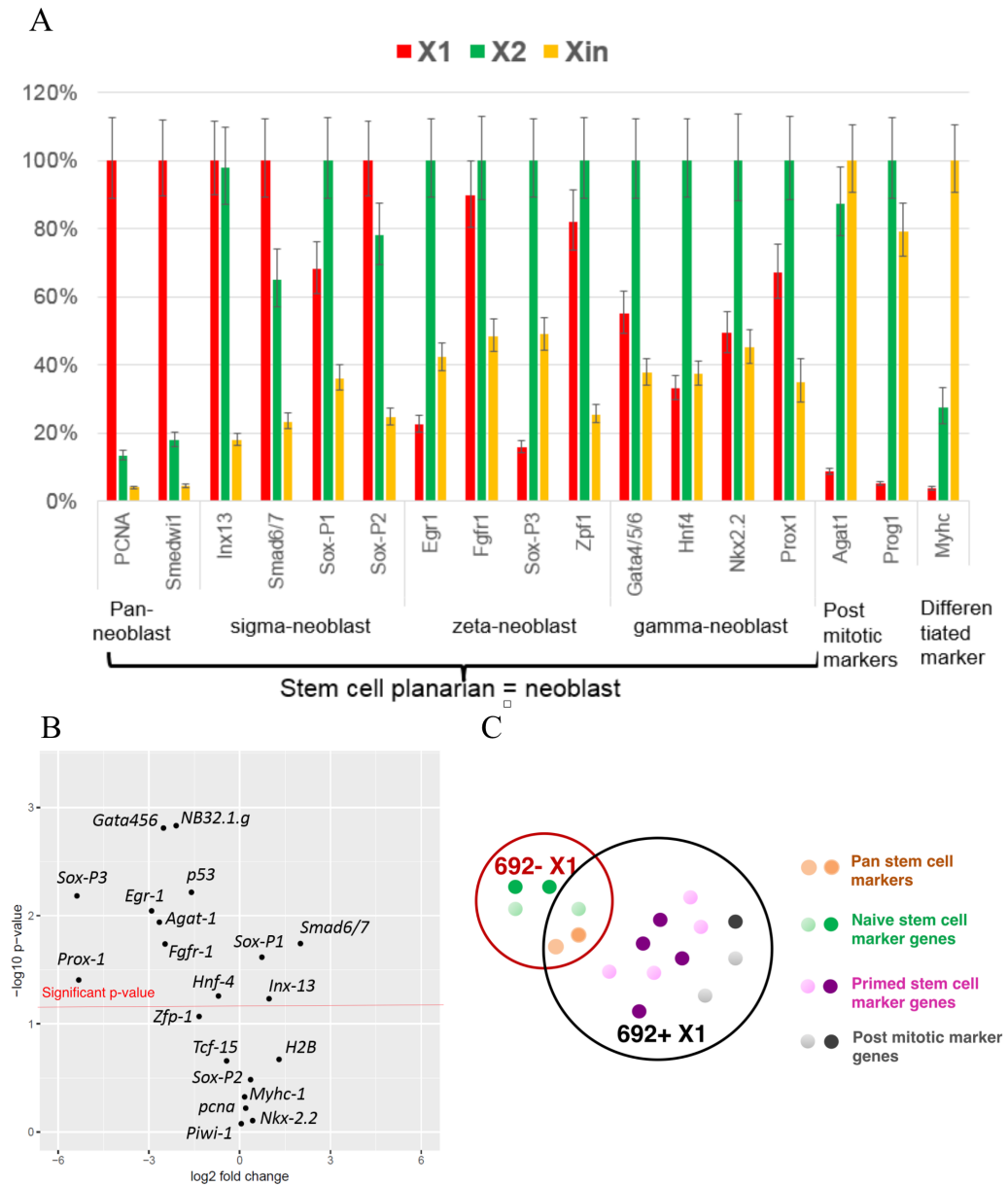
Figure 3.5: Gene expression level of different gene markers from qPCR. A, Relative gene expression level (%) of cells isolated from X1, X2, and Xin gates. B, Relative gene expression (Log2 fold change) of 6-9.2- X1 cells compared to 6-9.2+ cells. The gene markers lay upper the red line are significant different (p-value $\leq$ 0.05 or -log10 p-value $\geq$ 1.3). Data were analyzed from three independent experiments. C, The relationship of 6-9.2+ X1 and 6-9.2- X1 cells in gene expression level of different stem cell marker sets. Light and dark colors of the dots in each cell population indicate that it might comprise different sub-classes.

RNA was extracted from at least 100.000 cells per samples with two biological replicates to build up libraries for RNA sequencing. Sequencing reads from each library were mapped to the *S. mediterranea* dd_smed_v6 transcriptome from PlanMine database (http://planmine.mpi-cbg.de/planmine). Reads were aligned using Salmon (Patro et al. 2017) with default parameters (Materials and Methods, section 2.2.9). Data showed the fragment length distribution around 200-300 bp (base pair) with the mapping rate of 36.2 to 48.8%. The differential expression of genes/contigs was performed by DESeq2 function in R. A FPM (Fragment per million reads) matrix were exported and analyzed. The raw data showed that 99% read count less than 418.18, more than 50% read count less than 10, and the maximum value was very significant (80,000 to 100,000), in total around 10,000 contigs. To avoid bias, we removed the top 1% highest and also the low expressed contigs (FPM less than 10) from the matrix. The contribution of the read counts in raw and normalized data of each biological samples were performed in q-q (quantile-quantile) plots. The normalized data in q-q plot showed the right-skew distribution with major of contigs distributed at the lower part of the plot (Figure 3.6).
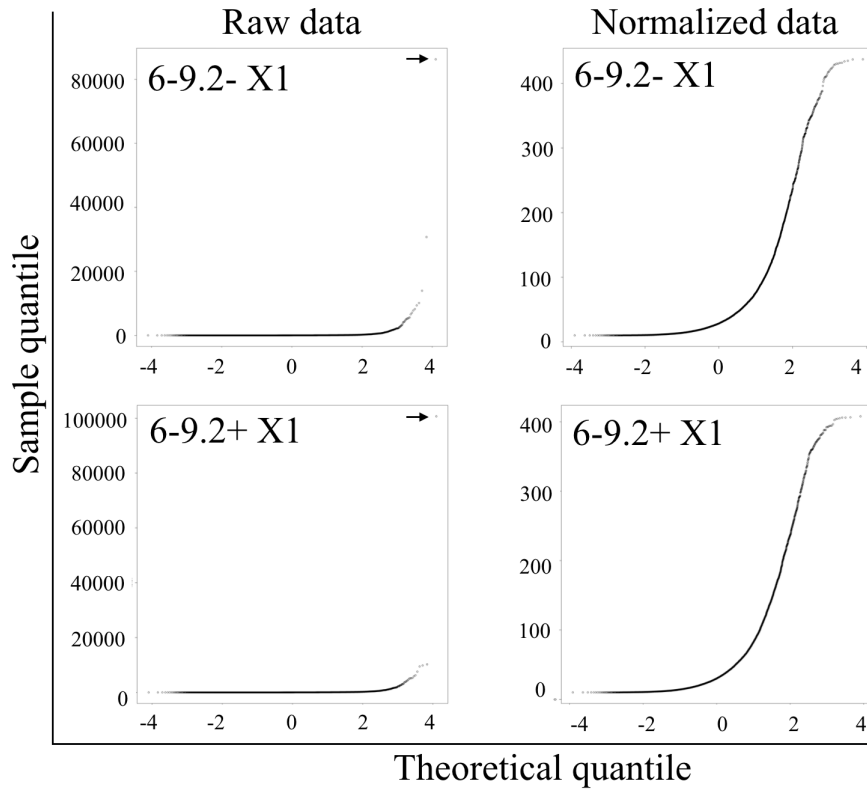
Figure 3.6: The distribution of read counts in 6-9.2- X1 and 6-9.2+ X1 samples. The y-axis represents the sample quantile and x-axis represent the theoretical quantile of two biological replicates. The arrow shows the maximum read count of each sample before the normalization.

The differential expression of genes/contigs analyzed by DESeq2 function was performed in Log2 Fold change (Log2 FC) of 6-9.2+ X1 samples compared to 6-9.2- X1 samples. We showed the distribution of Log2 FC ratio between 6-9.2+ X1 to 6-9.2- X1 samples and the mean average of FPM values (read count) of two samples in MA plot. The red line is LOESS (locally estimated scatterplot smoothing) that estimate the whole distribution of 6-9.2+ X1 to 6-9.2- X1 samples. When the mean average of read counts of all samples (x-axis) are less than 100, the Log2 FC ratios are positive and when the mean average values are increased, the Log2 FC ratios are negative, which means the long contig gene sequences were up-regulated in 6-9.2- X1 samples (Figure 3.7A). As showed in violin plot, in total 19321 contigs, 1165 contigs have adjusted p value (padj) $\leq$ 0.01 and among that 113 contigs have Log2 FC greater than 0, which indicated that this 113 gene contigs were upregulated in 6-9.2+ X1 samples (Figure 3.7B, C).
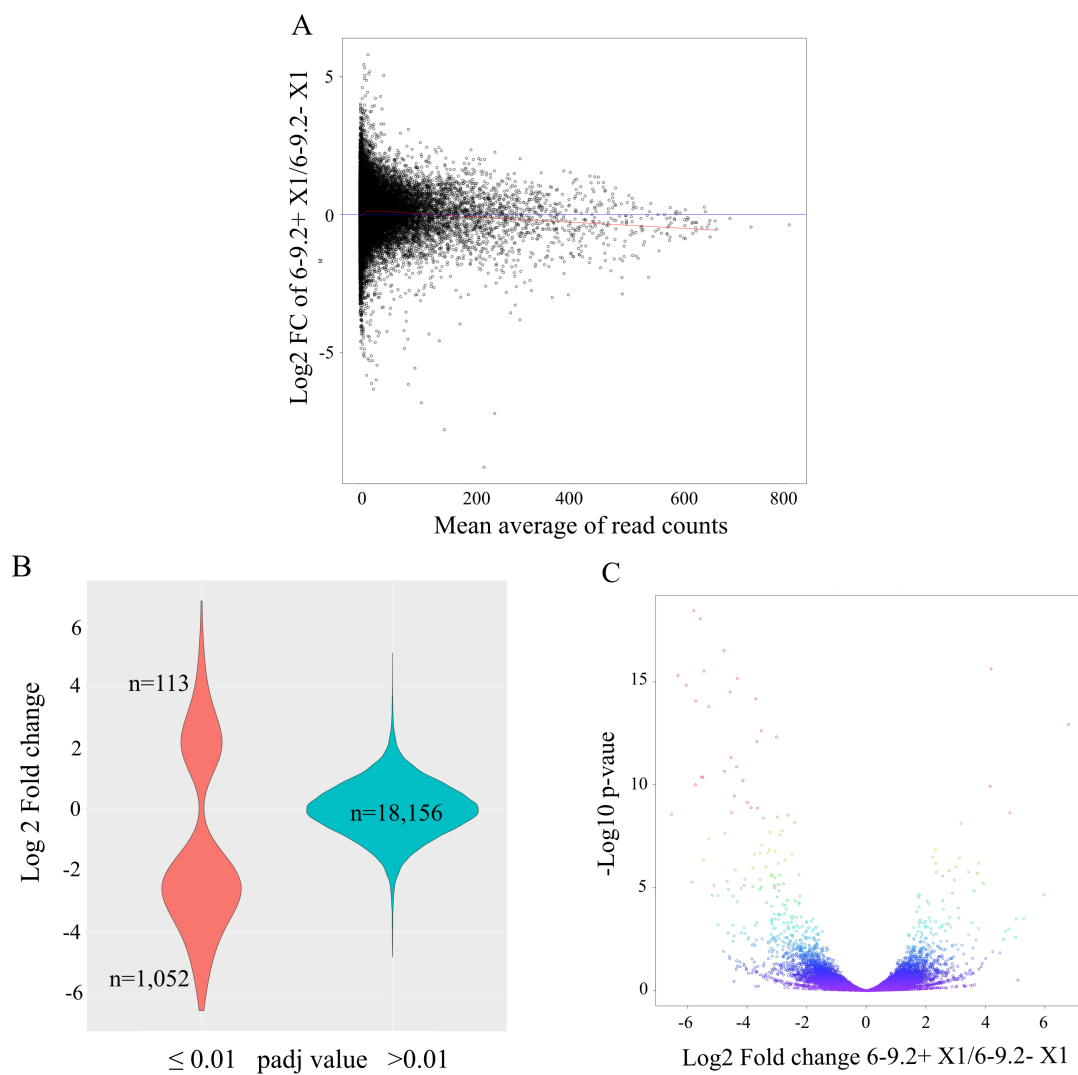
Figure 3.7: The distribution of Log2 FC ratio of 6-9.2+ X1 versus 6-9.2- X1 samples. A, MA plot visualized the mean average read count-related Log2 FC ratio of 6-9.2+ X1 versus 6-9.2- X1 samples. B, Violin plot, visualized the distribution of contigs based on the Log2 FC and adjusted p value (padj). C, Vocano plot, displayed the distribution of contigs based on the Log2 FC and -Log10 p-value. Data represent two biological replicates.

## 3.2 Surface antibody 6-9.2 recognized committed stem cells in neoblasts X1 FSC/SSC population.

We filtered out all the contigs in DESeq2 data analysis that have base mean (the mean of all samples) less than 20, Log2 FC of 6-9.2+ X1 compared to 6-9.2- X1 $\leq$ -2 or $\geq$ 2, and adjusted p value (padj) > 0.01. By that way, we selected 152 contigs that have Log2 FC $\leq$ -2, meaning that these gene sequences were enriched in 6-9.2- X1 cells; and 53 contigs that have log2 FC $\geq$ 2 (these gene sequences were enriched in 6-9.2+ X1 cells). All the selected contigs were blasted onto the genome database of *Schmidtea mediterranea, homo sapien*, and other species. Only the contigs that have E-value close to 0 were selected for further investigation. In 152 contigs that were enriched in 6-9.2- X1, 77 contigs have significant found when blasting on the genome database and 56% of these contigs blasted to *S.mediterranea* clone with unknown function. The rest contigs showed that 6-9.2- X1 cells highly express the *nanos*-like gene, which is an essential gene for germ cell development and regeneration (Wang et al., 2007), and *lectin* gene that previously reported as a marker for differentiated secretory cells in planarians (Zayas et al., 2010). The positional control genes activin and follistatin were also upregulated in 6-9.2- X1 cells. Interestingly, the follistatin antagonized activin and promotes regeneration of anterior identity and influences the specification of cell types in the anterior tissue (Roberts-Galbraith and Newmark, 2013). The co-expression of activin and its inhibitor follistatin implied the multiple direction of 6-9.2- X1 cells to commit into different lineages from anterior to posterior identities. 6-9.2- X1 cells also expressed the Ast-1, -6, -7 protein encoding genes but their functions in planarian is still unknown. Further investigations in all the unknown clones that are highly expressed in 6-9.2- X1 cells are needed to draw a firm conclusion. All the contigs highly expressed in 6-9.2+ X1 cells were then blasted onto genome database and inspected their functions (Table 2). Notably, 6-9.2+ X1 cells showed the high expression of heat shock proteins (hsp) which are consistent with previous report that hsps are highly enriched in planarian stem cells (Isolani et al., 2012). It has been shown that hsp proteins play key roles in maintaining protein homeostasis, stem cell activity, regeneration and tissue repair in planarian (Isolani et al., 2012, Conte et al., 2009, 2010, Fernandez - Taboada et al., 2011). Knockdown of some hsp proteins showed the defect in planarian homeostasis and they were unable to uptake food and died in a few weeks (Isolani et al., 2012). Fork head box transcription factors FoxA1 and FoxJ1 were also up-regulated in 6-9.2+ X1 cells. Previous results suggested that *FoxA* (a new name for a gene group containing HNF3 alpha, beta, and gamma) is specifically expressed in the cells participating in pharynx and digestive tract

formation (Koinuma et al., 2000). Interestingly, *FoxJ1* plays an essential role in the differentiation of motile cilia and knockdown of *FoxJ1* gene disrupted the locomotion of planarian (Vij et al., 2012). Another highly expressed transcription factor in 6-9.2+ X1 cells was AP2, the important gene regulates the transcription of neuronal involved genes during mouse embryogenesis (Mitchell et al., 1991). Wenemoser and colleagues have found that RNAi of AP2 gene impaired the regeneration of a subtype of neurons in planarian (Wenemoser et al., 2012). 6-9.2+ X1 cells also expressed high level of putative *Strawberry notch* homolog 1 gene. It is unclear the role of this gene in planarian but in *Drosophila* this transcription factor regulates gene products that required in many developmental stages including the fate determination of eyes, wings, and legs (Coyle-Thompson and Banerjee, 1993). Beside that, 6-9.2+ X1 cells expressed *Calpain*, a gene plays an essential role in embryogenesis by mediating the survival of human placental trophoblast (Takano et al., 2011), or in mice (Dutt et al., 2006) and *Drosophila* (Vieira et al., 2017) embryos. Further investigations are needed to characterize the function of other enriched genes in 6-9.2+ X1 cells. However, the RNAseq data shown that 6-9.2+ X1 cells expressed the gene set that are essential for the differentiation of different tissues such as pharynx, digestive tract, neuron, cilia. It is consistent with our hypothesis that 6-9.2+ X1 cells are committed cells and might derived directly from sigma-Neoblast due to the co-expression of stem cell marker set and at the same time emerge other gene sets that determine the later fates.

3.3　The characterization of 6-9.2 antigen.

The membrane protein that is recognized by 6-9.2 antibody emerges as a promising marker for pluripotent stem cell isolation (Figure 3.5). The antibody was generated by immunized the whole planarian membrane proteins into mouse and did ELISA screening process but the characteristic of this membrane protein is unclear. Hence, we investigated the identity of this 6-9.2 antigen, its name, sequence, and function in planarian homeostasis and regeneration. As shown in figure 3.8, the planarian protein extractions were load onto two SDS-PAGEs to separate proteins based on their molecular weights. One SDS-PAGE gel were then performed western blot using 6-9.2 antibody and subjected to membrane digestion. The other gel was used as a control and subjected to gel digestion. All protein fragments were performed Mass Spec and the contigs generated from this process were analyzed by MaxQuant. List of

RefSeq candidate sequences			
CONTIG ID	**BLAST HOMOLOGY**	**E-VALUE**	**SPECIES**
dd_Smed_v6_12112_0_1	G-protein alpha subunit	0.0	Schmidtea mediterranea
dd_Smed_v6_320_0_1	Heat shock protein 70	0.0	Schmidtea mediterranea
dd_Smed_v6_6854_0_15	clone H.85.4a	4E-67	Schmidtea mediterranea
dd_Smed_v6_14357_0_1	clone Dj_aH_227_J11.full, expressed in adult head	9E-32	Dugesia japonica
dd_Smed_v6_6878_0_2	maf domain containing protein, Raf	0.0	Schmidtea mediterranea, Dugesia japonica
dd_Smed_v6_3995_0_3	metastasis-associated protein MTA3	1E-18	Bemisia tabaci
dd_Smed_v6_10718_0_2	forkhead box A-1	0.0	Schmidtea mediterranea
dd_Smed_v6_15104_0_1	Transcription factor AP2	0.0	Schmidtea mediterranea
dd_Smed_v6_758_1_1	Heat shock protein 903	0.0	Schmidtea mediterranea
dd_Smed_v6_11874_0_1	clone H.14.11c, phosphatase with EF-hand domain 2	0.0, 1E-12	Schmidtea mediterranea, Homo sapien
dd_Smed_v6_14635_0_1	forkhead box J1-like protein	0.0	Schmidtea mediterranea
dd_Smed_v6_8198_0_1	ERCC excision repair 2	5E-31	Homo sapien
dd_Smed_v6_11493_0_1	sodium/hydrogen exchanger-like, slc9a-9	0.0, 1E-102	Schmidtea mediterranea
dd_Smed_v6_10374_0_1	strawberry notch homolog 1 (SBNO1)	1E-46	Homo sapien
dd_Smed_v6_25466_0_1	GCR062	0.0	Schmidtea mediterranea
dd_Smed_v6_22802_0_1	GCR008	0.0	Schmidtea mediterranea
dd_Smed_v6_8673_0_1	Calpain-A	8E-42	Lingula anatina
dd_Smed_v6_10483_0_4	DNA methyl-transferase mRNA	0.0	Schmidtea mediterranea

Table 2: BLAST homologies to gene sequences enriched in 6-9.2+ X1 cells. Gene sequences coming from DESeq2 with Log2 FC $\geq$ 2 and adjusted p-value $\leq$ 0.01 were mapped onto the genome database of *Schmidtea mediterranea* and other species. Gene sequences that have the low E-value are shown.

contigs were generated by blasting on TSGene data base and the gene candidates were pulled out by blasting on the transcriptome and proteome data base of different species (human, mouse, sheep, planarian, elegans, drosophila).
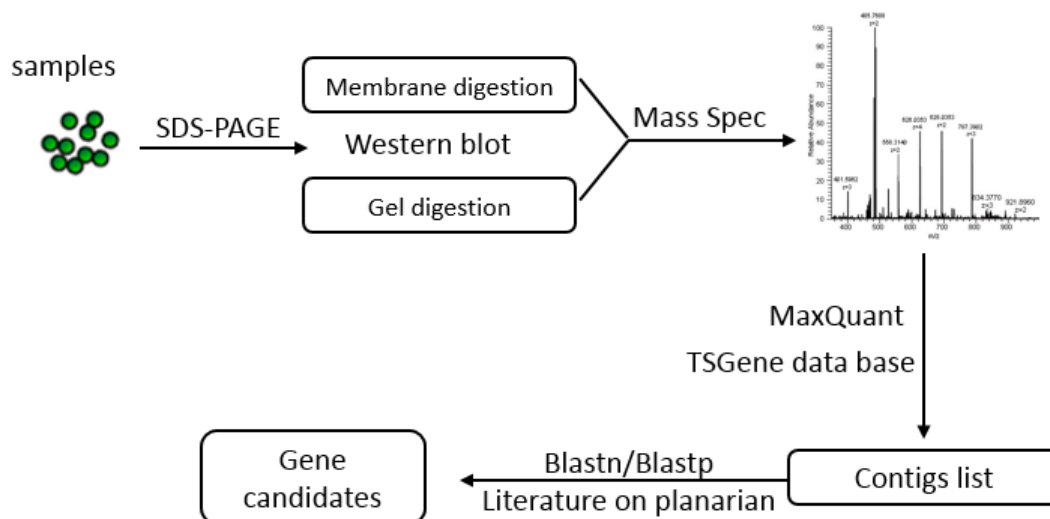
Figure 3.8: The experimental plan of 6-9.2 antigen characterization. Blastn: the query is a nucleotide sequence and the data base is a nucleotide data base. Blastp: the query is a amino acid sequence and the data base is an amino acid data base.

To examine the correct protein size and sequence of 6-9.2 antigen we harvested different protein fractions to compare: whole cell lysate fraction (WL) that contained all the proteins from planarian tissues, membrane fraction (M) that contained all the membrane proteins, IP fraction (IP) contained the enriched 6-9.2 membrane proteins that were immunoprecipitated using 6-9.2 antibody and magnetic beads, supernatant fraction (Sup) was the supernatant removed from immuno-precipitation process that contained no/low 6-9.2 proteins. All the fractions were subjected to SDS-PAGE gels to separate proteins by their size and stained the gel with coomassie blue. As shown in figure 3.9A, all the proteins with the same size were separated with a line. WL contained all kinds of protein ranging from 10 - 170 KDa, membrane fraction had 4 clear bands at 15, 17, 20, and 34 KDa. It was consistent with IP fraction that showed the same protein bands from 15 - 34 KDa. The strong and thick band around 50 - 72 KDa in IP and Sup fractions are the heavy chain of the 6-9.2 antibody that left over after the immuno-precipatation process. IP fraction showed more bands around 72, 130, 170 KDa compared to the membrane sample. This could be due to the higher amount of protein input in the IP than a membrane fraction from the enrichment process or due to the

70

accumulation of magnetic beads in some proteins which also showed up in supernatant sample. As expected, some proteins that appeared in membrane and IP fractions were disappeared in sup fraction (17, 20, 34 KDa) (Figure 3.9A). We further performed western blot to determine the protein bands detected by 6-9.2 antibody. Figure 3.9B showed the three clear bands at 17, 20, 34 KDa in both membrane and IP samples. No band was detected in Sup and WL, this could be due to the amount of protein input since the membrane and IP samples were the enrichment samples of the proteins. Altogether, we confirmed that proteins at 17, 20, and 34 KDa are 6-9.2 protein or its dimerization form/cleavage form/isoform.

Figure 3.9: Detection of protein 6-9.2 by electrophoresis. A, protein bands were detected by SDS-PAGE gel and coomasive blue staining. B, proteins were detected by western blot using 6-9.2 antibody. Membrane fraction was enriched by Qproteome kit and Immuno-precipitation (IP) was performed using magnetic beads.

To perform Mass Spectrometry, proteins with different sizes were cut from the gel and western blot membrane for digestions and subjected to Mass Spec. The raw data from Mass Spec were analyzed using MaxQuant by Dr. Hannes Drexler (Max Planck institute for Molecular Biomedicine, Münster). We collected 6,614 contigs that have 2 peptides 1 unique and among them 876 contigs are appeared only in IP sample. We then shortened the list with 19 contigs in IP fraction that appeared in both western blot and gel. All 19 contigs were then blasted in NCBI with different organisms (human, mouse, planarian, C. elegans) and the putative protein information were checked in GeneCard Human data base (https://www.genecards.org/). 6-9.2 antigene is a plasma membrane protein so we only sorted the proteins that localize on the

membrane. Among 19 contigs, we finally selected 5 contigs that have membrane locations (Table 3). dd_Smed_v6_6609_0_1 and dd_Smed_v6_6005_0_1 sequences blasted with the putative ATP binding cassette subfamily ABCC2 and ABCB7 genes in human genome (respectively), whereas dd_Smed_v6_3_0_1 blasted with ATPase plasma membrane ATP2B1. dd_Smed_v6_318_0_1 sequence blasted with both transmembrane proteins TMEM215 and TMEM128 so we named this contig TMEM215. dd_Smed_v6_360_0_1 blasted with TMEM128 and CMTM6 so we named it shortly TMEM128. Interestingly, the putative proteins of TMEM215, TMEM128, and ABCC2 have molecular weight in human data base also match with the protein bands on the western blot of planarian tissue (Table 3).

We further investigated whether one of these 5 gene candidates is 6-9.2 antigen by RNAi experiments. Short and double strand RNA for single gene were designed by E-RNAi web tool (http://www.e-rnai.org/) following the RNAi protocol for invertebrate model (Horn and Boutros, 2011). Planarian does not express GFP gene so we designed GFP RNAi as a negative control. Beta-catenin is a positional control gene that control the regeneration of posterior tissue (tail); in the lacking of beta-catenin, planarians fail to regenerate the tail so they regenerate a head instead. RNAi of beta-catenin gives a clear morphological readout so we pick it as a positive control for successful RNAi injection. As shown in figure 3.10, planarians were injected with dsRNAi of each single gene (section 2.2.12. RNAi injection) and amputated 1 day post-injection. The intact and regenerated animals were examined for the RNAi efficiency, animal's phenotype, stem cell gene expression, and the 6-9.2 expression.
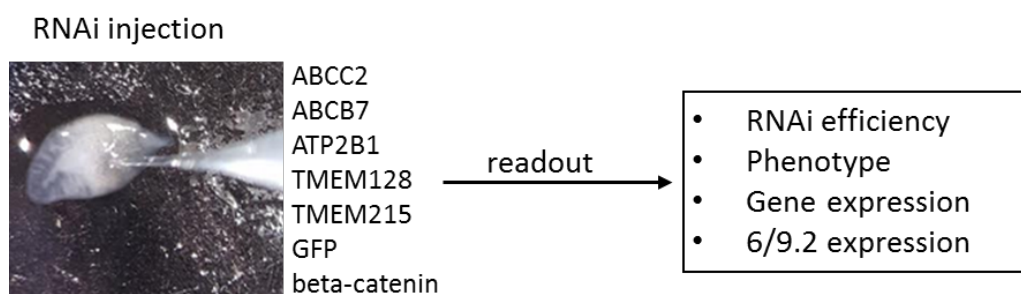
Figure 3.10: Experimental plan of RNAi injection in planarian for 6-9.2 antigen characterization. Beta-catenin: positive control, GFP: negative control.

To check for RNAi efficiency, we collected RNA extraction of RNAi injected planarians with *GFP, ABCC2, BCB7, ATP2B1, TMEM215*, and *TMEM 128*

	Organism	Alternate name	Localization	Notes	Mol mass (Kda)	Identity
dd_Smed_v6_3_0_1	human	ATP2B1	Plasma membrane	ATPase plasma membrane Ca2+ transporting 1 (ATP2B1).	150	72-78%
dd_Smed_v6_318_0_1	human	TMEM215	membrane	Transmembrane protein (no information)	26	84%
	human	TMEM128	membrane	Transmembrane protein (no information)	16-18	84%
dd_Smed_v6_360_0_1	human	TMEM128; CMTM6	membrane	Transmembrane protein TMEM128. CKLF like MARVEL transmembrane domain containing 6 (CMTM6). This gene is widely expressed in many tissues, but the exact function of the encoded protein is unknown.	20; 20	86;80%
dd_Smed_v6_6005_0_1	human	ABCB7, ATP binding cassette subfamily B, member 7	membrane, mitochondria	This protein may play a role in metal homeostasis.	77	68%
dd_Smed_v6_6609_0_1	human	ATP binding cassette subfamily C member 2 ABCC2	membrane	ABC proteins transport various molecules across extra- and intra-cellular membranes. This protein is a member of the MRP subfamily which is involved in multi-drug resistance. T	174 or 34	75%

Table 3: Gene candidates for 6-9.2 antigen from Mass Spec data.

73

after 7 days post-amputation and performed qPCR with *ABCC2, ABCB7, ATP2B1, TMEM215, TMEM 128* primers, and 1 house keeping gene Gapdh. The results showed that interfering of *ABCC2, ABCB7, ATP2B1, TMEM215, TMEM128* genes affected on the expression of not only the target genes but also other genes. For example, ABCB7 RNAi resulted in the significant decrease of *ABCC2*, or TMEM215 RNAi also down-regulated the *ABCC2, ABCB7*, and *TMEM128* gene expression. In *ABCC2* RNAi animals, the expression of *ABCC2* was slightly decreased, while expression of *TMEM128* was increased 4 folds compare to control sample. It is hard to interpret all the up- and down-regulations of RNAi on one sample due to the direct and indirect effects of each silencing gene inside the animals. Therefore, we only focused on the silencing of genes we targeted. The significant decrease of target genes *ABCB7, ATP2B1, TMEM215* and *TMEM128* compare to GFP control sample (orange column) in respective RNAi animals indicated the high efficiency of RNAi design, probe synthesis, and RNAi injection experiments (Figure 3.11).
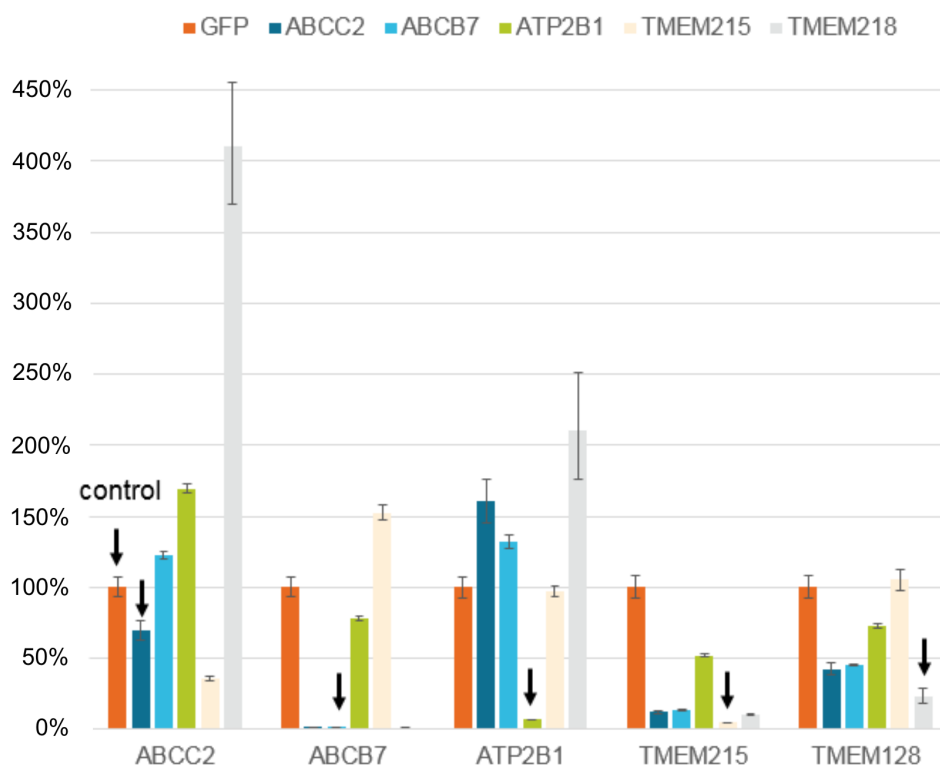
Figure 3.11: Relative gene expression level of 5 candidate genes in RNAi animals. qPCR result calculated from Delta-delta CT (Cycle Threshold) method. GFP, control sample, set as 100% of gene expression. y-axis, gene expression level of RNAi samples (%), x-axis, target gene names. The arrow shows the target gene of each RNAi sample.

Previous data showed the correlation of 6-9.2- X1 cells with the σ-Neoblast while the 6-9.2+ X1 population is more likely to be committed cells that highly express ζ and γ-Neoblast markers (Figure 3.5). This reveals that 6-9.2 surface antigen might play an important role in stem cell commitment process and lacking of this 6-9.2 antigen might cause the animal fail to maintain their homeostasis and regeneration. For this hypothesis, we next examined the phenotype of planarians after the injection with 6-9.2 candidate genes. Planarian were injected with *GFP, beta-catenin, ABCC2, BCB7, ATP2B1, TMEM215, and TMEM 128* for three consecutive days in two weeks and amputated into head and tail fragments 1 day post-injection. After 7 days of amputation, planarian regenerative abilities were observed under the light microscope. As expected, the negative control *GFP* RNAi animals showed normal regenerative phenotype in both tail and head fragments. The positive control *beta-catenin* RNAi showed the normal regeneration from the tail fragment but failed to regenerate the tail from the head fragment and regenerated two heads instead due to the lacking of posterior control gene *beta-catenin*. These phenotypes confirmed the efficiency of RNAi experiments where the negative control did not show any effect and the positive control gave a strong evidence of knocking down the correct target gene (Figure 3.12A). In 5 candidate genes for 6-9.2 antigen, animals knocked down of *TMEM215* and *TMEM128* failed to regenerate both head and tail from amputated tissues with the regeneration rates are only 10-30% (Figure 3.12B). *ABCC2, ABCB7*, and *ATP2B1* RNAi did not show any effect in the regenerative ability of planarians (Figure 3.12A, B). We also observed the effect of RNAi on the survival rate of both intact and regenerated planarians. *ATP2B1* RNAi showed a slight decrease in planarian survival ability while *ABCC2* and *ABCB7* had no effect. Knock down of *TMEM215* and *TMEM128* significantly decreased the survival rate of both intact (homeostasis) and regenerated animals (Figure 3.12C).

The planarian homeostasis and regeneration were strongly affected by *TMEM215* and *TMEM128* knockdown, which means the stem cell population was also dramatically affected. Therefore, we performed qPCR to check the gene expressions level of different stem cell markers in RNAi animals and examined which neoblast subclass was highly regulated by the gene knockdown. As expected, knockdown two transmembrane encoding genes *TMEM128* and *TMEM215* had strong effects in stem cell gene expressions whereas *ABCC2, ABCB7*, and *ATP2B1* RNAi animals did not affect in almost all stem cell

subgroups. *TMEM128* RNAi especially down-regulated pan-neoblast, zeta, gamma, and post mitotic makers (*H2B, Smedwi-1, PCNA, fgfr-1, zfp-1, p53, SoxP-3, hnf-4, nkx2.2, Agat-1, Prog-1*), while *TMEM215* RNAi down-regulated post-mitotic markers (*Agat-1, Prog-1*) but up-regulated gamma markers (*gata456, nkx2.2, prox-1*) (Figure 3.13). The significant effect in committed neoblast markers (zeta, gamma classes) and progenitor markers indicated that *TMEM128* and *TMEM215* plays an important role in the stem cell compartment, which is consistent with the hypothesis of 6-9.2 antigen since 6-9.2 protein is a surface protein expresses in committed cells.
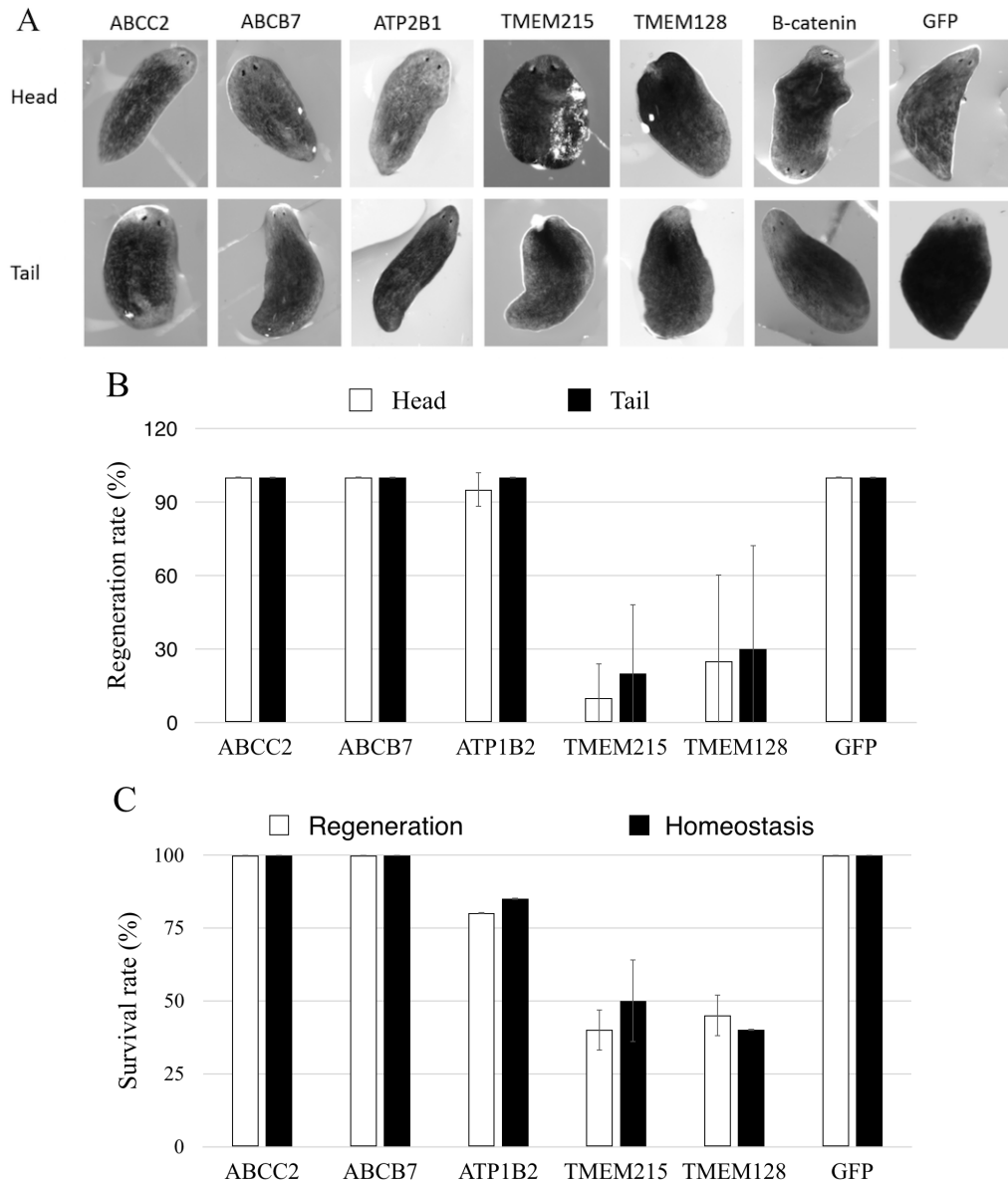
Figure 3.12: Planarian homeostasis and regeneration in RNAi condition. A, planarian regeneration phenotype 7 days post-amputated under the light microscope. B, Regenerative ability of amputated planarian after 7 days. C, Survival rate of planarian in intact and regenerative conditions. Data represent mean ± SD of three biological replicate (n=9 for each replicate)
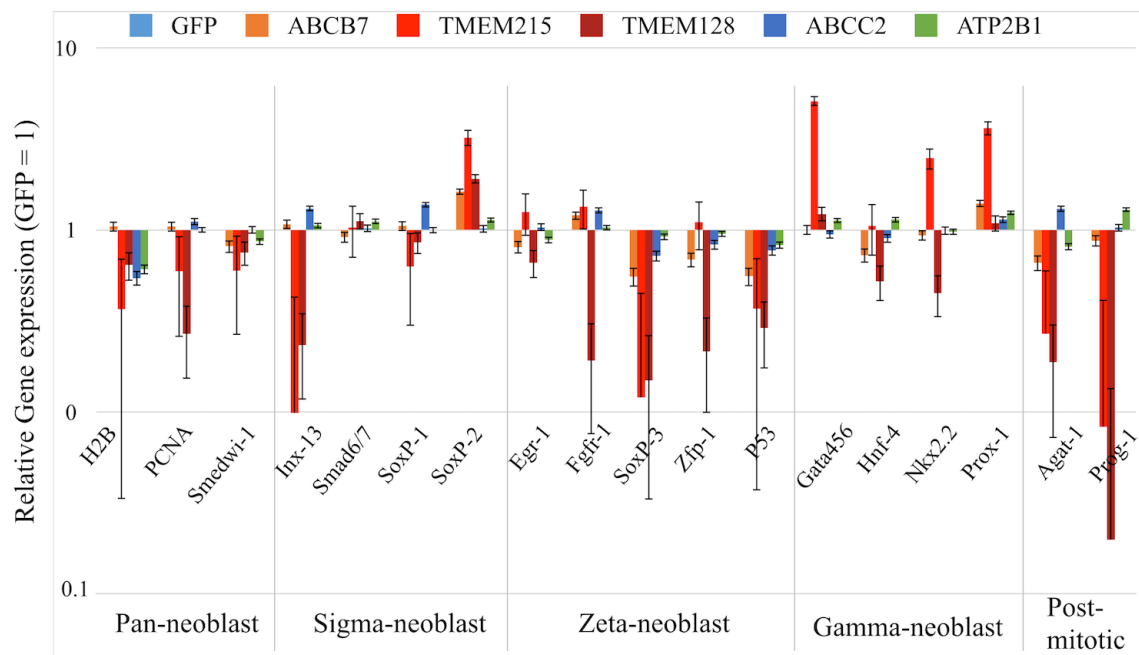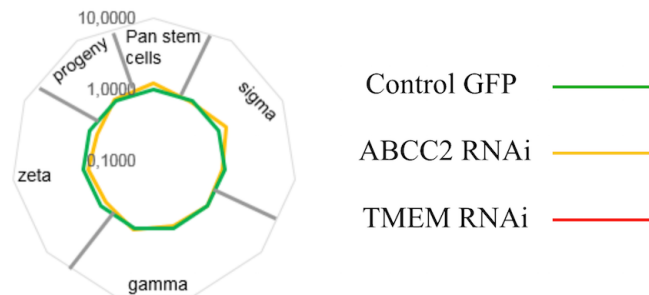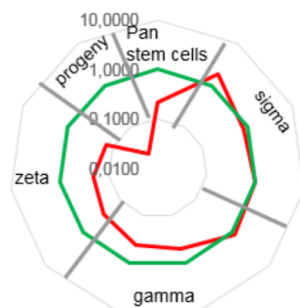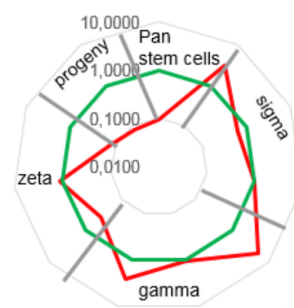
Figure 3.13: The gene expression level of stem cell markers in RNAi animals. The graph showed the relative gene expression of RNAi animals compared to control *GFP* sample. Radar chat indicated the significant effect in stem cell gene expression of *TMEM128* and *TMEM215* RNAi samples, compared to *ABCC2* RNAi animal. Data represent the mean ± SEM of two biological replicates.
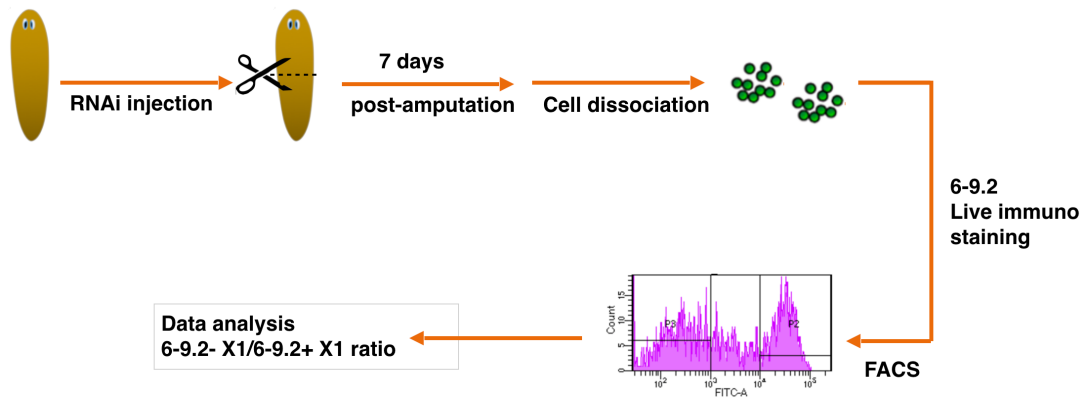
Figure 3.14: Experimental design for 6-9.2 antigen identification.

Putative genes *TMEM215* and *TMEM128* showed as the most promising candidate for 6-9.2 antigen due to their significant effects in stem cell compartment as the animals failed to regenerate new tissues from amputated fragments (Figure 3.12) and knock down of these two genes had strong impact in stem cell marker genes, especially committed neoblast markers (Figure 3.13). To confirm whether the transmembrane protein *TMEM* is 6-9.2 surface protein, we injected animals with *TMEM215* and *TMEM128* dsRNAi and animals were amputated 1 day post-injection. After 7 days of regeneration, cells were dissociated and then subjected to live-immuno staining with 6-9.2 antibody and analyzed the 6-9.2- X1 and 6-9.2+ X1 populations based on FACS gating (Figure 3.14).

We chose GFP RNAi injection as a control sample to compare the changing in 6-9.2- X1 and 6-9.2+ X1 population. If one of these putative transmembrane genes *TMEM215* or *TMEM128* is 6-9.2 antigen, the knocking down of these genes can impair the expression of 6-9.2 proteins, which results in the loss of cells detected by 6-9.2 antibody immuno staining. Our hypothesis assumed that the ratio between 6-9.2- X1 and 6-9.2+ X1 cells would be dramatically increased compared to the control sample due to the efficiency of RNAi technique that proved in figure 3.11. As shown in figure 3.15, the ratio of 6-9.2- X1/6-9.2+ X1 cells were slightly increased from $32.7 \pm 0.5\%$ (*GFP* RNAi samples) to $41.6 \pm 1.3\%$ (*TMEM215* RNAi) and $50.7 \pm 11.8\%$ (*TMEM128* RNAi). One possible reason for the modest change in 6-9.2- X1/6-9.2+ X1 ratio could be due the large portion of 6-9.2+ X1 cells already lost during the regeneration process since the RNAi of TMEM had strong effect in stem cells compartment, which made a minor change in the ratio.
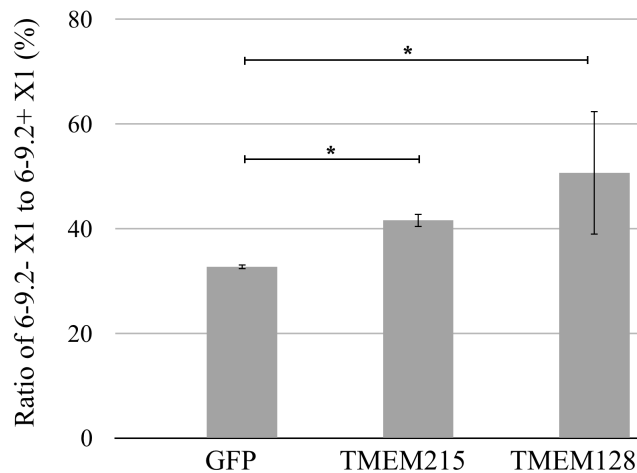
Figure 3.15: The ratio of 6-9.2- X1 compared to 6-9.2+ X1 in RNAi samples. The graph showed the ratio of *GFP, TMEM215, TMEM128* RNAi cells after live immuno staining of 6-9.2 antibody. Alexa Fluor 488 IgM goat anti-mouse was used as secondary antibody. Cells were stained with Hoechst for nuclei and PI for dead cells. The fluorescent signals were detected by FACS. Data represent two biological replicates with mean ± SD, p value ≤ 0.05 (*).

The data suggested that both putative TMEM genes are potentially 6-9.2 antigen. *TMEM215* and *TMEM128* could be fragments of one protein or two different proteins but have one target binding site for 6-9.2 antibody. The gene expression level in RNAi efficiency data (Figure 3.11) indicated that knocking down of *TMEM215* also significantly down-regulated the expression of *TMEM128*, whereas the RNAi of *TMEM128* affected only the expression of TMEM128 but not *TMEM215*. This could partially explain the similar effect of RNAi of *TMEM215* and *TMEM128* in planarian regeneration and homeostasis. More investigations in the binding site of these putative proteins and the 6-9.2 antibody are needed to bring the final answer for the name of the 6-9.2 antigen. Altogether, our data showed the important role in the stem cell compartment of putative TMEM proteins. These protein sequences are highly expressed in the committed neoblasts 6-9.2+ X1, which is a useful marker for identifying the stem cell commitment. Furthermore, we also brought an opportunity to isolate different stem cell subgroups using the surface antibody 6-9.2 and these cells are alive for downstream studies unlike any other current methods.

3.4   Live cell tracking method using 6-9.2 surface antibody.

Current methods using in planarian studies are: i) RNA interference (RNAi), to study gene function; ii) BrdU labeling and whole-mount in situ hybridization (WISH), to visualize gene expression within cells and tissues; iii) Fluorescence-activated cell sorting (FACS), to identify and isolate planarian stem cells for ex vivo manipulation; iv) next generation sequencing and qPCR, to quantify gene expression quantification. Although these methods bring a breakthrough in our comprehension of planarian stem cell biology, the molecular characterization takes place after stem cell lysis, preventing any functional approach *in vivo*. Moreover, the full potential of planarian as a model system cannot be tapped until transgenesis is routinely achieved. Although proof of principle for planarian transgenesis has been produced in *Giradia tigrina* (Gonzalez-Estevez et al., 2003), some preliminary attempts to achieve transgenesis in *S. mediterranea* by injecting the animal with the Smed-Gapdh::EGFP::SV40pA construct and electroporating have not succeeded so far. As this might be attributed to problems at several levels – efficiency of DNA delivery into planarian stem cells, promoter strength, cell survival and codon usage – in the present application we propose a non-genetical method that using our novel surface antibody 6-9.2 for live cell labeling and tracking. In general, the tracking method comprises three important steps: i) finding a proper way to image the animal; ii) finding a cell labeling material; iii) isolating a sub-population of actively proliferating stem cells. Our data have shown the surface antibody 6-9.2 can isolate the stem cell population X1 into two sub-fractions, in which 6-9.2- X1 cells are pluripotent-like stem cells and 6-9.2+ X1 cells are committed stem cells. This provides the ability to isolate stem cell fractions, label them and transplant into planarians for live cell tracking.

The cell labeling were performed by using fluospheres with 40 nm in size. Planarian cells were dissociated and incubated with fluobeads for 30 min at RT and observed under the microscope. Figure 3.16A showed the cytoplasmic location of fluobeads inside the cells. It is unclear whether the beads were uptaken into cells by endocytosis pathway or by direct penetration. However, we observed that fluobeads-labeled cells are distributed equally between the daughter cells after a cell division, allowing tracking of the cell over presumably

several generations, coupled with *in situ* hybridization against markers for lineage-specific differentiation (Figure 3.16B).
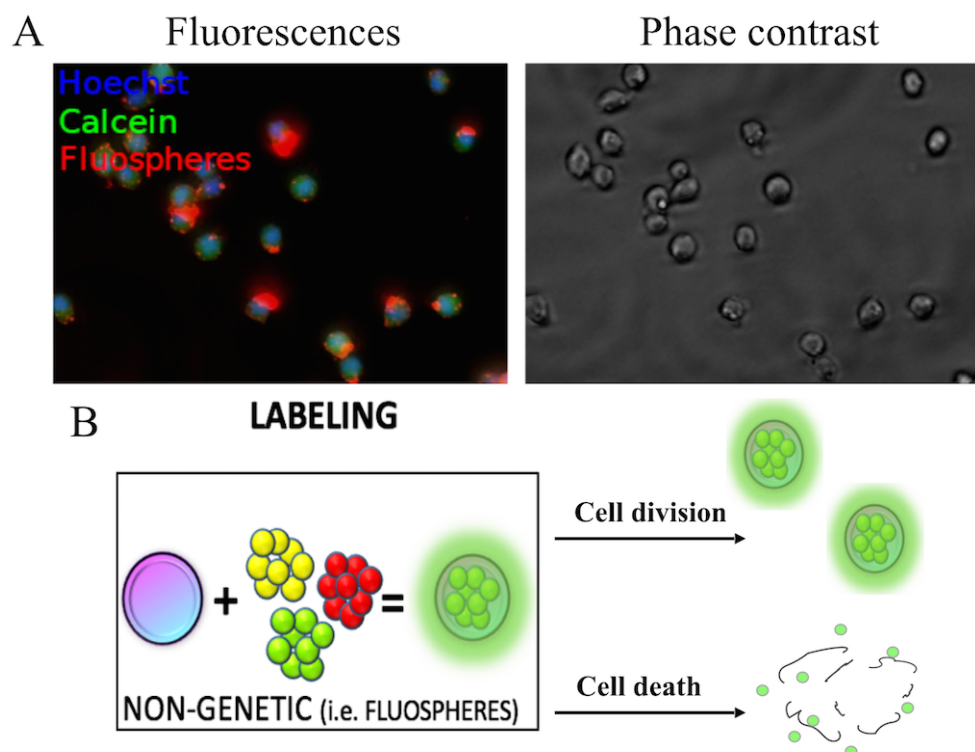
Figure 3.16: Fluophere labeling in planarian stem cells. A. The cytoplasmic location of fluobeads in X1 cells. Hoechst: nuclear staining, Calcein: cytoplasmic staining, Fluospheres: red nanoparticles. B. The fluobeads take up in normal cell, cell division and cell death.

Planarians are negatively phototactic in the visible spectrum, making the immobilization of the animal for in vivo imaging an essential step. Current methods for planarian immobilization include anesthetics (1,1,1-trichloro-2-methyl-2-propanol; ethanol (Talbot et al., 2011; Stevenson et al., 2010) or embedding in low melting point agarose. The Planarian Immobilization Chip (PIC) allows high resolution imaging (Dexter et al., 2014). However, this device is only effective for 5 hours, while regeneration spans several days (Tran and Gentile., 2018). Thanks to the expertise developed at Fraunhofer IBMT Dr. Michael Gepp and André Schulz in manipulating alginate hydrogels (Schulz et al., 2018), we propose to immobilize planarians embedding them in ultra-high viscosity (UHV) alginate, which allows long time-lapse imaging *in vivo* without causing injuries or drug-induced biochemical alteration. The use of Alginate hydrogel in numerous applications in biomedical sciences and engineering emerged as a powerful tool to enable immobilization, due to its

biocompatibility and ease of gelation. Alginate has structural similarities to extracellular matrices of living tissues (Lee et al., 2012). Covering a wound with alginate maintains a physiologic microenvironment, minimizes bacterial infections and facilitates wound healing (Lee et al., 2012). Furthermore, this biomaterial has been applied for cell transplantation and utilized to immobilize mammalian cells in biomedical studies (Gepp et al., 2009; Ehrhart et al., 2013; Schulz et al., 2018a; Schulz et al., 2018b). Hence, alginate could provide sufficient stability of immobilization for high-resolution, high-throughput days-long imaging. Figure 3.17A showed the brown algae Lessonia nigrescens (LN) and Lessonia trabeculata (LT) (Alginatec, Riedenheim, Germany) that used to extract high molecular alginates. In this project we used alginate solution with LN/LT 1:1 and 0.65% (w/v %). Figure 3.17B visualized the immobilization technique using alginate hydrogels. The bottom of the well plate was coated with poly-L-lysine to provide mechanical stability for alginate bindings. Planarians were placed in the middle of two alginate layers and the gels were cross linked with CaCl2 and replaced with planarian artificial media (PAM) (See Chapter 2. Materials and Methods). We examined the survival rate and the regenerative capacity of planarians after 7 days of immobilization in alginate hydrogels. Surprisingly, alginate embedding condition had no effect to planarian homeostasis and regeneration (Figure 3.17C, D). Only 1 intact planarian in total 20 tested animals and 1 tail fragment in total 21 fragments showed the lysis. However, it was due to the contact of the animal with the layer of poly-L-Lysine remaining at the bottom, which is toxic to the planarian. Therefore, the animals should be always placed in the middle of two alginate layers. Since the animals were effectively immobilized in the alginate hydrogels under the white light microscope. We then transplanted the 6-9.2+ X1 and 6-9.2- X1 fluorescent cells into planarian to check whether we can observe the fluorescent signals under the Biozero – Microscope (Keyence). Figure 3.17E showed the possibilities to observe the strong signal of single fluorescent dot when transplanted different kind of fluorescent cells. However, animal's head was moving under the exposure to fluorescent light, which is much stronger than the normal white light. The fluorescent signals were still detected but the partial immobilization made it hard to track the behavior of single cells inside planarians. We then tested whether the fluorescent signals can be detected in *in situ* hybridization so that we can trace the cells after a certain time point. Unfortunately, the fluorescence was too weak to be detected after bleaching steps (data not shown). With the limitation of time, we could not solve all the

obstacles but this preliminary data showed the promising technique to observe a single fluorescent cell in living-immobilized planarian. For further studies, we suggest to increase the alginate concentration to 1% and try different microscopes that have the possibility to adjust the temperature since the low temperature can impair the movement of planarians.
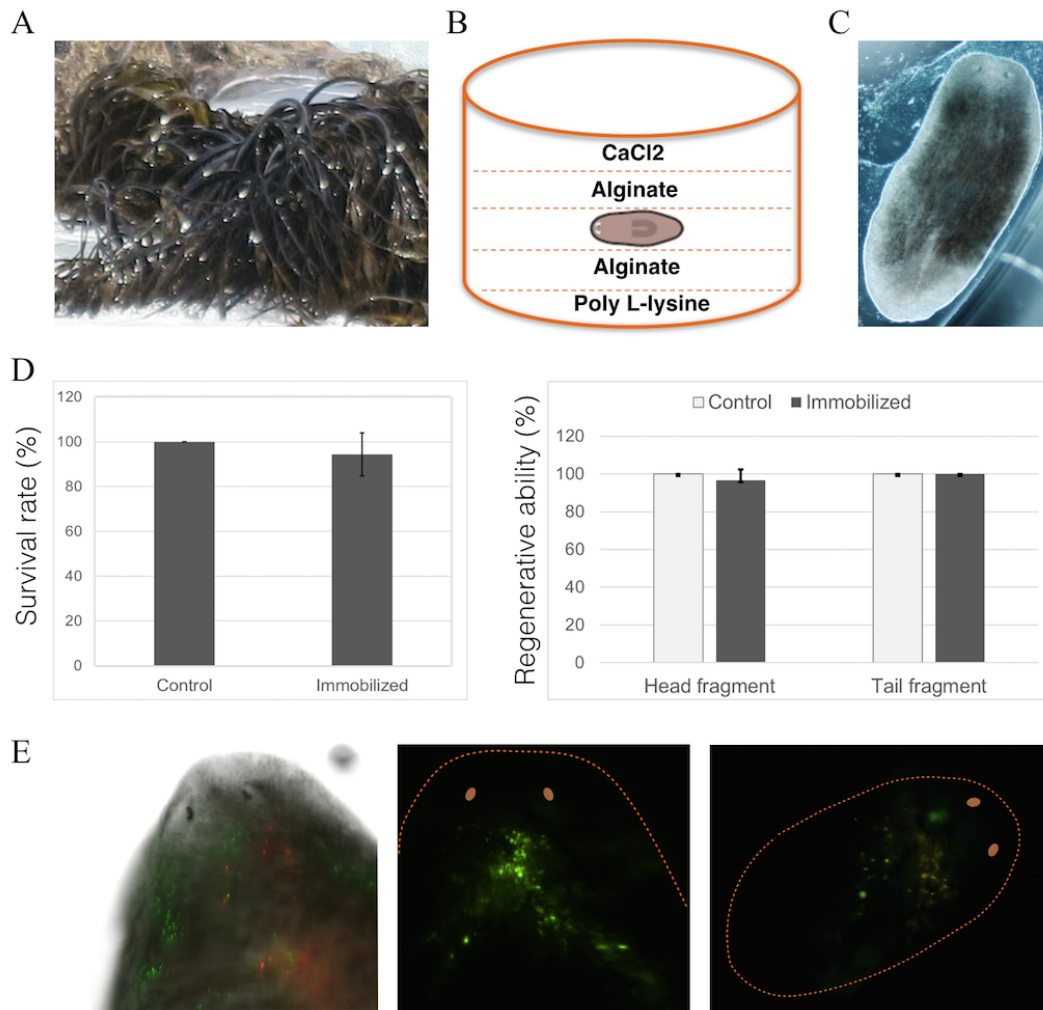
Figure 3.17: Live cell tracking method in planarians. A, brown algae Lessonia nigrescens (LN) that used to extract alginates. B, Immobilizing method for planarian. C, Immobilized planarian in alginate hydrogels under the phase contrast. D, The survival rate and regeneration of planarians in alginate condition. E, Left, merge channels in animal transplanted with red and green fluobead cells observed under the stereo microscope. Right, single channel in animal transplanted with green fluobead cells.

3.5 Planarian - From basic science to applied researches

3.5.1 Planarian - A beautiful model for environment toxicological study

Thao Tran, *Michelle Hesler, Oscar H. Moriones, Alba Jimeno-Romero, Benjamin Fischer, Neus G. Bastús, Victor Puntes, Sylvia Wagner, Yvonne L. Kohl, and Luca Gentile.* (2019). Assessment of iron oxide nanoparticle ecotoxicity on regeneration and homeostasis in the replacement model system Schmidtea mediterranea. ALTEX.

Planarians are invertebrates that living in both fresh water and marine. They are very sensitive to environmental exposure and thus allowing to determine the effect of different environmental toxicants (Savetti et al., 2015; Hagtrom et al., 2016; Kustov et al., 2014, van Roten et al., 2018). Planarians have a complex body structure (Introduction part 1.2) and especially an adult stem cell population that can differentiate to all kinds of cell types and regenerate the missing tissue in a short time scale. These stem cells are very sensitive to environmental changes so planarians can be used to evaluate toxic, genotoxic, and carcinogenic agents with an approach in line with the 3R (Reduce, Refine, Replace) principle (Russell and Burch, 1959). Fe3O4 Iron oxide particles (IOPs) are used in numerous applications such as medical contrast agents, cosmetics, food additives, biosensors, paints, coatings, pigmented thermoplastics, and drug delivery systems for targeted cancer therapy (Minard and Wind, 2002, Peng et al., 2008, Kornberg et al., 2017, Lee et al., 2008, Semelka et al. 2001, Gupta and Gupta, 2005, Shen et al., 2012, Thomas et al., 2010, Weinstein et al., 2009, Veiseh et al., 2010). However, as reviewed by Kornberg and colleagues, the toxicity of IOPs is unclear (Kornberg et al., 2017). Some in vitro studies showed the toxicity of IOPs in macrophages (Codali et al., 2013), mitochondria (Dwivedi et al., 2014), and DNA damage (Sighinolfi et al., 2016), whereas some other reports showed the non cytotoxic effect of IOPs exposure (Coricovac et al., 2017; Freyria et al., 2012). Not only workers, also consumers and the environment are exposed to IOPs since the nanoparticles are released along the complete lifecycle (Alejandro Caballero-Guzman et al., 2016). The characteristics of particles depend on their size, dose, surface charge and their

solvents (Bundschuh and Filser et al., 2018). The environmental impact of released engineered IOPs is unknown and there are no literature has reported so far whether the engineered IOPs have a greater or lesser toxicity than the starting materials in *in vivo*. In this study, we investigated the effect of IOPs (Figure 3.18) on regeneration and homeostasis of planarians. IOPs were synthesized (Figure 3.19), characterized and directly injected to the planarian gastrovascular system at environmental relevant concentrations (0.1 mg/ml and 1 mg/ml) for food safety test or incubated planarians in the media containing IOPs for environmental exposure test.

We examined the morphological changes, survival rate, and regenerative ability of planarians. The observation of IOPs exposed-planarians showed the normal homeostatic ability of planarian with 100% of survival rate compared to control group in both injection and incubation methods (data not shown). IOPs did not affect the planarian movement nor the negatively phototatic behavior (data not shown). Due to the agglomeration of particles at the bottom of the well in incubation method, the concentration of IOPs that affect the animals were not homogeneous. Hence, we decided to test further cellular and molecular experiments in only injection method due we can adjust the IOP concentration precisely. We then detected changes in the reactive oxygen species (ROS) level of planarian cells after IOPs exposure since the oxidative stress is a crucial contributor to the toxicity formation of environmental toxicants (Leung et al. 2008; Shvedova et al., 2012; Dayem et al., 2017). The effect of IOPs in the stem cell population were also examined after 14 days IOPs injection. Planarians were dissociated into single cells and stained with nuclear staining Hoechst, cytoplasmic staining Calcein and dead cell staining PI and subjected to FACS. As shown in figure 3.19, IOPs did not affect the cell viability of planarian cells (A) and neither the stem cell population X1 (B). IOPs treated animals had the comparable ROS production to control groups, while positive control Hydro peroxide H2O2 showed the significant increase in ROS level (Figure 3.20C). (Figure 3.20C).
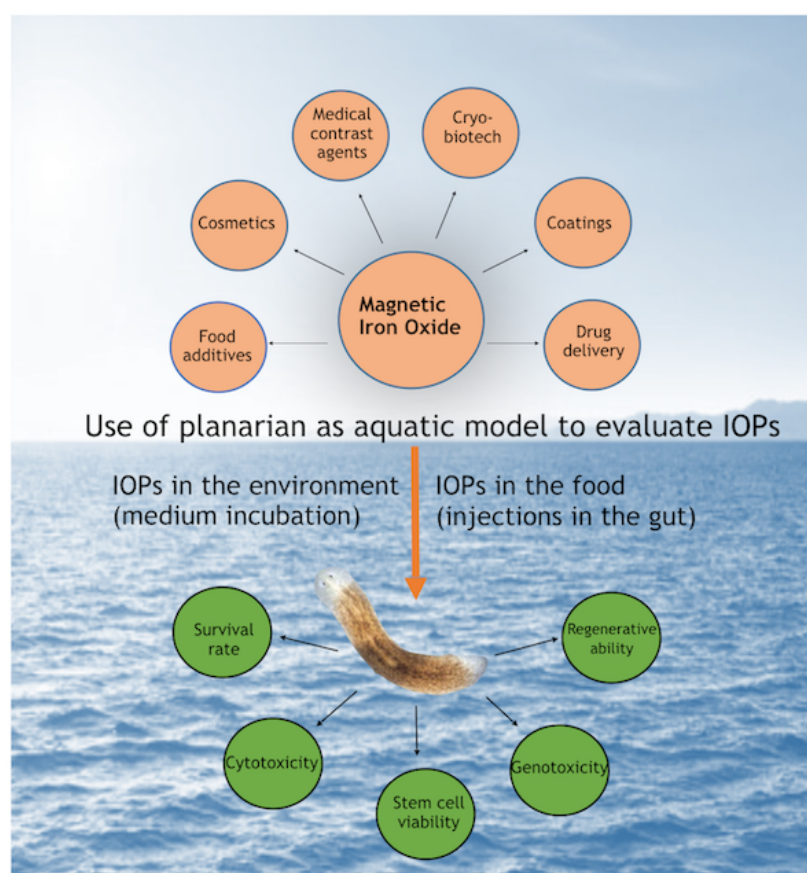
Figure 3.18: Use of planarians as model to evaluate the toxicity of Iron oxide particles (IOPs). The IOPs are used in many applications end up in water environment, or taken up with the food. In this study, we investigate the toxicity of IOPs in planarian with comprehensive studies on the planarian survival and regeneration, cell viability, and gene expression changes. Tran et al., 2019.
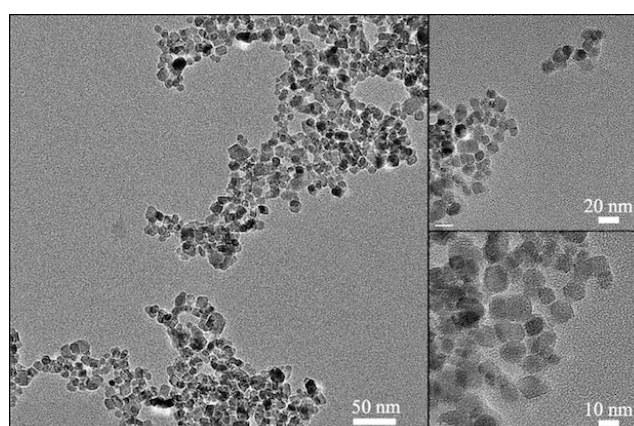
Figure 3.19: Synthesized IOPs. Mean size determined via TEM is 11 ± 1.8 nm. Pictures were taken from the Catalan Institute of Nanoscience and Nanotechnology (ICN2) (Tran et al., 2019).
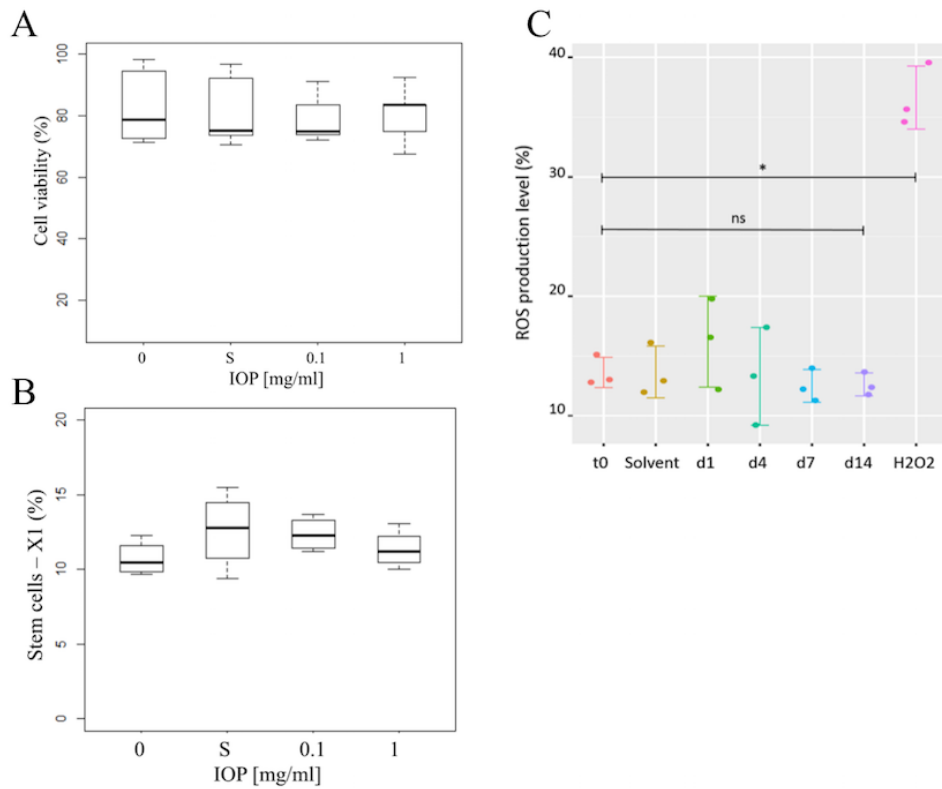
Figure 3.20: Effect of IOPs on cell viability, stem cell population and ROS production in planarian. Boxplot, displaying the cell viability (A) and stem cell population (B) (in %) and measured by FACS using propidium iodide (PI) and Calcein after 14 days post-injection of 0.1 and 1 mg/mL IOPs. B, Dot plot, displaying the ROS production of cells after different time points post injection with 1 mg/mL IOPs, measured by the fluorescence signals of Carboxy-H2DCFDA. H2O2 was used as positive control. Data represent mean ± SD of n = 3 biological replicates. * Significant difference with p<0.05; ns, no significant difference. Tran et al., 2019.

Some nanoparticles showed high impact in gene expression level but did not have any effect on the survival of tested animals (Bahadar et al., 2016). The planarian adult stem cells are very sensitive to stress (e.g. irradiation) and respond quickly with the situation to activate or impairing the recovery system (George et al., 2008, Hayashi et al., 2006). Hence, examination of stem and progenitor marker genes can indicate the effect of downstream cascade in cellular mechanism. We, therefore, tested whether IOPs altered the gene expressions in our two stem cell sub-populations: the pluripotent group 6-9.2-X1 and the committed cell group 6-9.2+ X1. We performed real time PCR analysis with different gene markers to examine the effect of IOPs: *Smedwi-1*, a pan stem cell marker (Scimone et al., 2014); *Smed-pcna* and *Smed-p53*, proliferating and self-renewal markers (Pearson and Sánchez Alvarado, 2010), *Smed-Agat-1, Smed-NB32.1.g, Smed-HB19.11.g*, post-mitotic makers (Wagner et al., 2012), *Smed-myhc-1*, muscle cell marker (Witchley et al., 2013), *Smed-Gapdh*, a house keeping gene (Barber et al., 2005). Figure 3.21A showed no significant difference in gene expression level except the pan-stem cell marker, *Smedwi-1*. Approximately 50% of *Smedwi-1* expression was reduced in IOPs treated animals (p-value <0.05 by Tukey post-hoc test). Some minor changes at the gene level could be due to a mild inflammatory process triggered by IOPs at the early day. The relative distribution of control and treated groups were performed by PCA (Principle Component Analysis) (Figure 3.21B). Both IOPs treated animals with 0.1 and 1 mg/ml were grouped together indicated the same effect on the gene expression levels regardless of the concentration. We have noticed that the gene expression level of *Smedwi-1* was decreased 50% but the number of stem cells in X1 gate was not altered (Figure 3.20B). Hence, we examined whether IOPs affected the other cell populations X2 and Xin. As shown in figure 3.22, the X2 population comprising stem cells at G1 phase and progenitor cells was decreased in IOPs 1 mg/ml, whereas the post mitotic cells (differentiated cells) Xin was increased. This data suggested that some stem cells were activated to differentiate into different kind of cell types to help animal recover from IOPs exposure (Tran et al., 2019).

We further examined whether IOPs affect the regenerative capacity after wounding, one of the most significant outcome to test the agent toxicity in planarian. Planarians were injected with IOPs (0.1 mg/ml and 1 mg/ml), and one day after the last injection, planarians were amputated into two fragments head and tail. Observing the regeneration after 14 days, all fragments (n = 16/group) from the 4 groups (untreated control, solvent alone control, 0.1
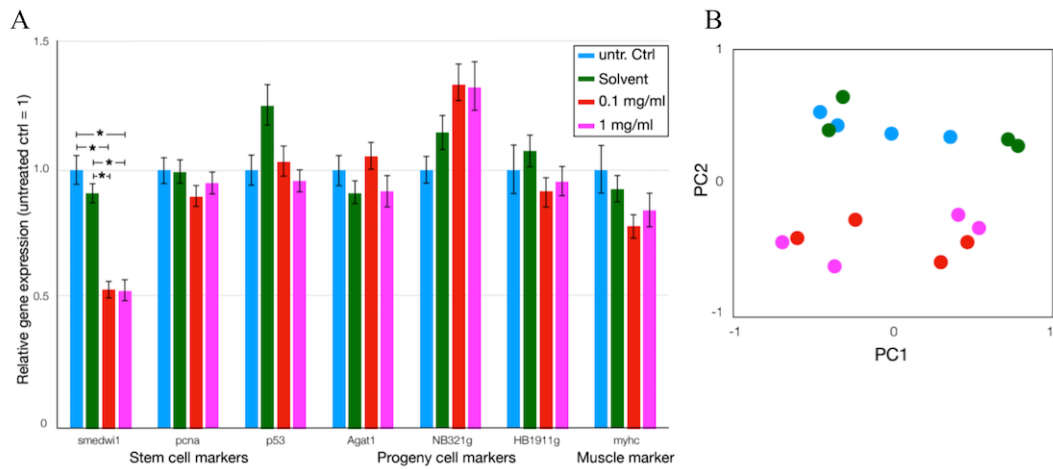
Figure 3.21: Effects of the gastrovascular exposure to IOPs on gene expression. A, Relative gene expression measured by qPCR of the untreated control (calibrator = 1) and IOPs treated samples. B, Principal component analysis showing how the analyzed samples group in clusters after IONs injection in the gastrovascular system. (*) $p \leq 0.05$. The analysis was carried out in animals at 14 dpi, n = 3 biological replicates and n = 2 technical replicates. Tran et al., 2019.
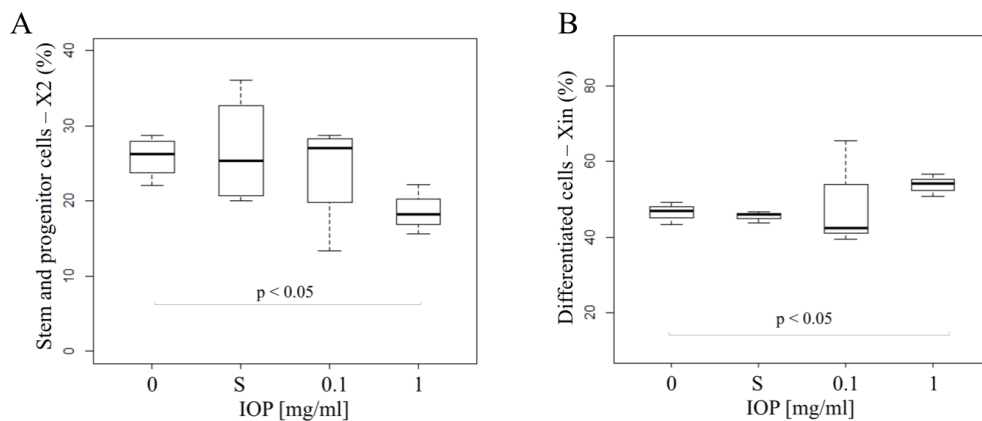
Figure 3.22: Effects of the gastrovascular exposure to IOPs on cell populations. Boxplot, displaying the X2 cell population (A) and post-mitotic cell population (B) (in %) and measured by FACS using propidium iodide (PI) and Calcein. (*) $p \leq 0.05$. The analysis was carried out in animals at 14 dpi, n = 3 biological replicates. Tran et al., 2019.
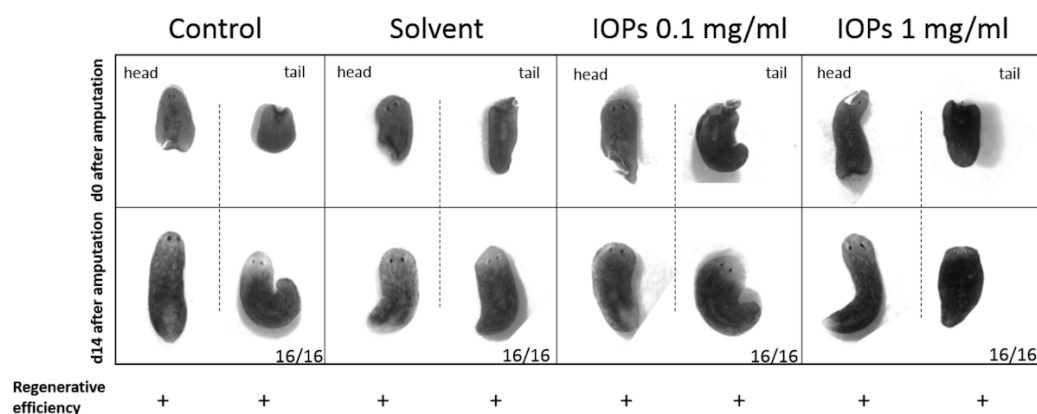
Figure 3.23: Effects of the IOPs on the regenerative capacities of planarians. Top panel, showing the morphology of freshly amputated head and tail fragments and lower panel shows the planarian regeneration at 14 dpi. The specimen shown are representative of all the fragments used (n = 16 fragments for each condition). Tran et al., 2019.

mg/ml IOPs and 1 mg/ml IOPs) were able to fully regenerate (Figure 3.23).

There is still an ongoing debate on IOPs toxicity, as described previously that IOPs caused fibrosis and inflammatory in mice model (Szalay et al., 2012, Srinivas et al., 2012, Park et al., 2010). However, in this report, we highlight the attention of testing the fate of IOPs in the environment since the characteristics of engineered and natural IOPs are far different (Kornberg et al., 2017). Our data showed that IOPs did not have any effect in planarian survival rate, cell viability, and regenerative capacity. IOPs might have a mild effect that cause the animal activated the differentiation of stem cells to balance the whole cell populations and maintained the homeostatic condition (the decrease in stem cells X2 gate and increase in differentiated cells Xin gate). Altogether, we confirmed the non-toxic effect of IOPs in planarian model with the high concentration after mid-term treatment 14 days (Tran et al., 2019).

3.5.2 Planarian - A suitable model for tumorigenesis

This data contributed in one publication in Disease Models & Mechanisms journal.

Andromeda Van Roten, Amal Zohir Abo-Zeid Barakat, Annelies Wouters, **Thao Anh Tran***, Stijn Mouton, Jean-Paul Noben, Luca Gentile, and Karen Smeets. (2018). A carcinogenic trigger to study the function of tumor suppressor genes in Schmidtea mediterranea. dmm032573.*

91

Recently, planarian has been successfully established as a paradigm for hyper-proliferation and tumorigenesis due to their remarkable regenerative capacity. In normal condition, thanks to the population of adult stem cells, planarian can regenerate to replace any missing tissues without tumor formation. However, these highly activating stem cells are also very sensitive to environmental toxicants so they can be used as a model for tumor suppressor genes (TSGs). The over-proliferation of cells is controlled by numerous TSGs such as p53, Rb, PTEN, Wt-1, APC through apoptotic stimulation or cell cycle suppression (Beausejour and Campisi, 2006). Mutation of these genes cause cancer by damaging genomic stability (Deng and Scott, 2000; Kwong and Dove, 2009; Levitt and Hickson, 2002; Scholz and Kirschner, 2011) and triggering metastasis by promoting Epithelial-Mesenchymal Transition process (Bullions et al., 1997; Hanahan and Weinberg, 2011). It has been well known that the tumor formations are often induced by the synergistic effect of genetic factors and environmental factors. Cadmium (Cd) is one of the top agents that plays as a human carcinogen factor for many human cancer types (Akesson et al., 2008; IARC, 1993, McElroy et al., 2006; Waalkes, 2003). In Planarian, Cd induced the tumor formation in *Dugesia dorotocephala* species but there is no reports for the effect of Cd in planarian *Schmidtea mediterranea* (Plusquin et al., 2012). It has been reported that the planarian regeneration process is regulated by MMPs. Knocking down of *MmpB*, the planarian ortholog of vertebrate MMP19, resulted in tissue dysplasia, lesion formation, and regeneration defect (Isolani et al., 2013). Interestingly, using *in silico* screening and a proteomic screening after exposure to the human carcinogen Cd, we found the down-regulation of *MmpB* gene in planarian *S.mediterranea*. To have a deeper understanding of *MmpB* function, we knocked-down *MmpB* by dsRNAi and concomitantly exposed planarians with Cd. The regulation of genetic and environmental factor Cd in this project could bring an important information for regenerative therapies and tumor prevention.

Planarian asexual *S.mediterranea* were injected with *MmpB* dsRNAi and treated with or without 10 μM CdCl2 for 30 min post-amputation. Surprisingly, as shown in figure 3.24A, *MmpB* knocked down planarian could complete the regeneration process but epidermal blisters with large outgrowths appeared in one quarter of the *MmpB* RNAi animals (n = 6/24). Some animals were found death without blisters and incomplete regeneration. The affected animals developed 1 to 4 blisters with teratoma-like structures. Remarkably, the *MmpB* knock down effect did not vary in Cd-exposed and unexposed animals (data not

shown). To investigate which cell type resembled in the blisters, we perform *in situ* hybridization (ISH) with the stem cell marker *smedwi-1* and immuno histochemistry (IHC) with serine 10-phosphorylated histone 3 (H3P) antibody, a G2/M phase marker. Figure 3.24B showed the accumulation of *Smedwi-1*$^+$ cells in the blister of *MmpB* RNAi specimens. As expected, these cells were proliferating stem cells that co-expressed the H3P protein, a marker for dividing cells (Figure 3.24C). This observation raised a question whether *MmpB* RNAi globally induced the number of proliferating cells, as well as the effect of this knock down on other stem cell gene expression levels. We then selected four regions of planarian ISH/IHC specimens and counted the number of *Smedwi-1*$^+$ and *H3P+* cells. Interestingly, the number of stem cells *Smedwi-1*$^+$ and proliferating cells H3P+ were not altered in all the treatment conditions compared to control specimens (Figure 3.25). We further investigated the effect of *MmpB* RNAi in different sub-populations of planarian stem cell that has been described 6-9.2- X1 comprises sigma-Neoblast (*Smad6/7, SoxP-1, SoxP-2, Inx-13*), 6-9.2+ X1 comprises zeta- and gamma-Neoblasts (*Egr-1, Fgfr-1, SoxP-3, Zpf-1*), *Gata4/5/6, Hnf-4, Nkx2.2, Prox-1*). We performed qPCR to quantify the expression level of these gene markers. We found that *MmpB* RNAi animals significantly upregulated 6/12 markers (four sigma-neoblast markers, one zeta- and one gamma-neobalst markers). Cd treatment and Cd + *MmpB* RNAi co-treatment showed mild effects in the gene expression levels (Figure 3.26). This data suggested that Cd treatment affected in both pluripotent stem cell 6-9.2- X1 and committed stem cell 6-9.2+ X1 sub-groups. Especially, all four markers of sigma neoblast cells were highly upregulated. This could explained the hyper-proliferation to form blisters of treated animals, since the 6-9.2- X1 subclass (including sigma class) has the ability to do self-renew.

Altogether, we conclude that *MmpB* knock down significantly induced the blister formation and outgrowth of planarian, which is different from previous report (Isolani et al., 2013). Cd alone did not induce tumorigenesis and treatment with or without Cd did not vary the effect of *MmpB* RNAi. Planarians could fully regenerate in *MmpB* RNAi condition and epidermal blisters were only observed after the regeneration process had completed. This tumor-like formation comprised the proliferating cells under the epidermal layer. Once these tumor-like tissues invaded throughout the entire body, the animals were found death, which is similar to the malignant characteristics. The appearance of blisters after the regeneration process suggests a dual role of
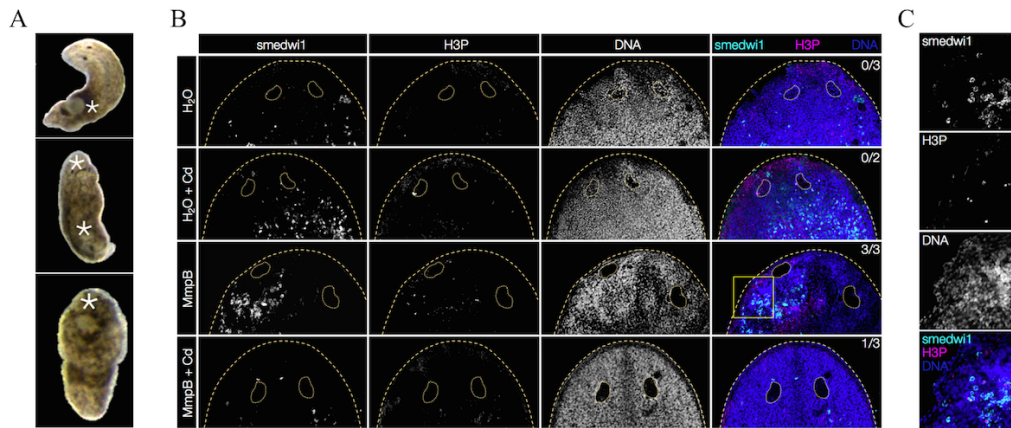
Figure 3.24: Tissue invasion and tumor formation in MmpB(RNAi) animals. A, The large outgrowth (white arrowheads) in MmpB(RNAi) animals with and without Cd treatment. B, Confocal acquisition of the sample with smedwi1/Ser10-phospho-histone H3 (H3P) double WISH/IHC. *Smedwi-1*^{+} MmpB(RNAi) animals, either in presence (n=1/3) or absence (n=3/3) of Cd. C, 63x magnification of the skin blister showed the co-expression of *Smedwi-1*^{+} and H3P markers in the blister. Van Roten et al., 2018.
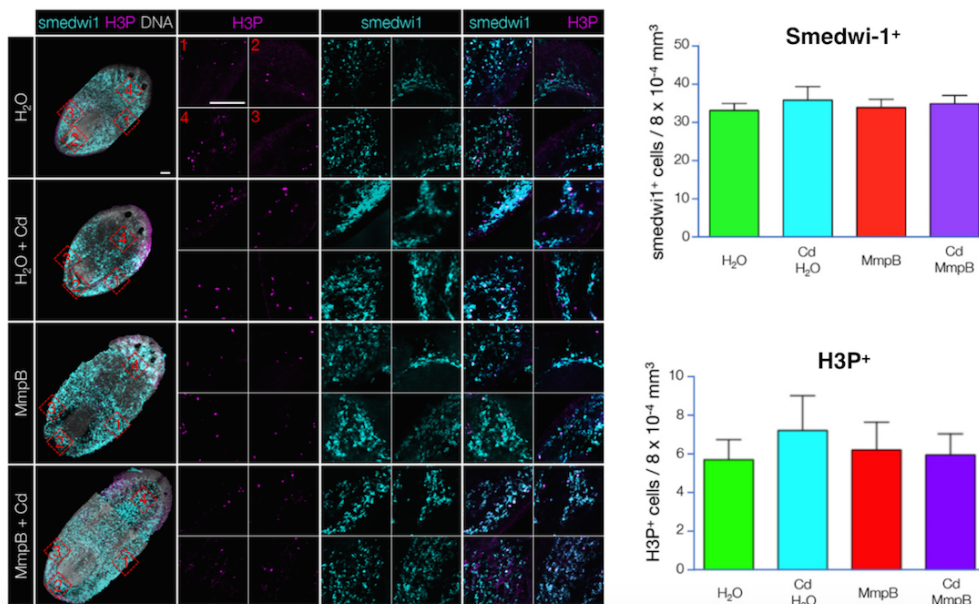
Figure 3.25: Body-wide distribution of *smedwi1*[+] and H3P^{+} cells. Left column, stitched maximum confocal projection of the whole animal (20^x magnification). Middle and right columns, the location of *Smedwi-1*^{+} and H3P^{+} cells at the lateral pre-pharyngeal (1), posterior back-stripe (2), lateral post-pharyngeal (3) and head/neck (4) areas, corresponding to the red frames shown in the left column, are presented in a clockwise arrangement. Scale bars: 100 μm. The graphs represent the total number of *Smedwi-1*^{+} and H3P^{+} cells were scored from 4 selected regions. Van Roten et al., 2018.
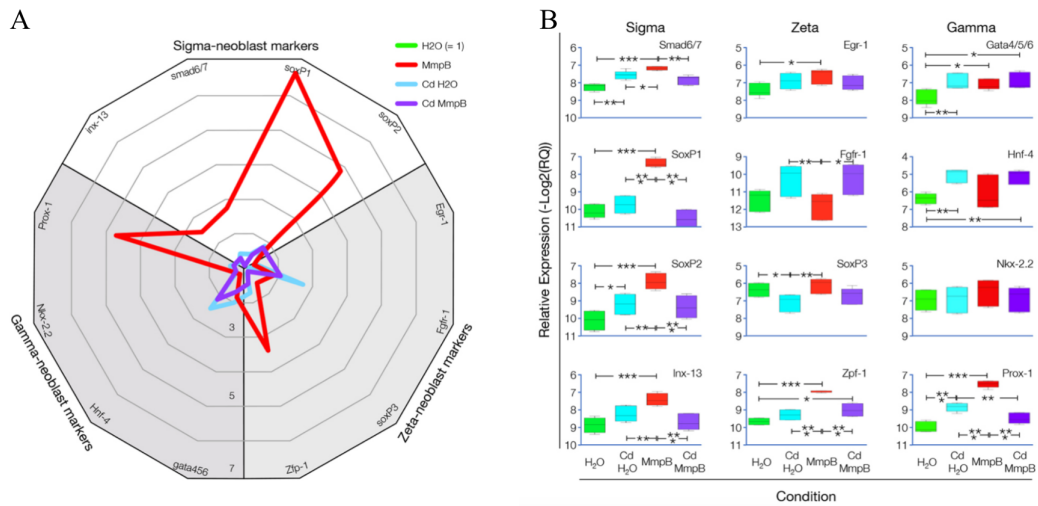
Figure 3.26: The effect of *MmpB* RNAi in stem cell gene expression levels. A, Radar chart showing the relative enrichment in the expression of subsets of sigma-, zeta- and gamma-neoblast markers in the four experimental conditions tested (n=3; H2O control=1 and collapsed to the center). B, Boxplots showing the significant differences in the relative expression of the 12 markers tested. (*) P≤0.05; (**) P≤0.01; (***) P≤0.0001. Van Roten et al., 2018.

Smed-MMPB enzyme. We hypothesized that Smed-MMPB plays a role in the tissue remodeling and stem cell restoration for the regeneration process (George and Dwivedi, 2004). This could explain why in some fragments knock down of *MmpB* gene impaired planarian regeneration. However, in another role, once the animal is fully regenerated due to the unnoticed tumor development, Smed-MMPB preserves as the cell proliferating controller, suppress the over-proliferation of stem cells. Therefore, lacking of *MmpB* gene can trigger dysplastic lesions (epidermal blisters, epidermal lesions and large outgrowths), the phenotype of malignant cells (DeGregori, 2017). Additionally, by gene expression performance, we have found that both stem cell sub-populations 6-9.2- X1 and 6-9.2+ X1 were dramatically affected in the lacking of Smed-MMPB, suggesting the essential role of Smed-MMPB in maintaining the balance between pluripotent stem cells and committed/progenitor cells. All together, we suggested the tumor suppressor function of Smed-MMPB that control the extracellular matrix and the epithelial mesenchymal transition process to prevent the hyper proliferation and invasion of planarian stem cells. Its role in stem cell compartment and regeneration depends on the microenvironment.

Chapter 4

DISCUSSION AND FUTURE DIRECTION

Planarian is a unique model to study pluripotent stem cells, as its whole body displays an *in vivo* cell culture dish that allow elucidating not only the stem cell behavior but also their descendants during homeostasis and regeneration. Planarian stem cells, called neoblasts, maintain in the adulthood and play a key role in regeneration, tissue turn over and gonad formation (Reddien et al., 2004). These neoblasts were long known as a homogeneous population (Baguña 1989), until the study from Wagner and colleagues showed a small population, named clonogenic neoblasts (cNeoblasts), had the ability to rescue stem cell depleted animals (Wagner et al., 2011). Recently, the single cell RNA sequencing (SCS) is one of the most advanced technique that attracted the planarian research community. SCS approach has contributed a great knowledge in the lineage transition states and patterning information of planarian system. Multiple prominent classes of planarian stem and progenitor cells have been found using single cell analysis (Scimone et al., 2011, Moritz et al., 2012, Lapan et al., 2011, Wenemoser et al., 2012, Cowles et al., 2013, Currie et al., 2013, van Wolfswinkel et al., 2014, Scimone et al., 2014, He et al., 2017). In 2018, Reddien and colleagues provided a near complete discovery of cell type transcriptome atlas for the planarian *Schmidtea mediterranea* using SCS of thousands of cells (Fincher et al., 2018). This piece of work allows us to determinate all differentiated cell types and lineage precursors, uncover rare cell types and novel patterning genes. They have found a novel cell class: *cathepsin*$^+$ cells together with eight known clusters protonephridia,

parenchymal, epidermal, intestine, muscle, pharynx, neoblast, and neural. These studies revealed the highly heterogeneous in transcript sets and potencies of planarian stem cells as a whole population. It is unknown how the cell fate determination is regulated in planarian so that cells are patterned in a correct way to replace missing tissues during the regeneration process. In comparison to different animal models, planarian shares many common signaling pathways that promote stem cell maintenance and compartment such as Wnt-, EGFR-, AKT-, JNK- signalings. Especially, the similarity of planarian and the first bilateral animal - acoels in positional control genes (Raz et al., 2017) support the hypothesis that the boundary between regenerative and non-regenerative animals may not due to the pluripotent capacity but more likely rely on the overall control of stem cells in the body scale. However, many questions remain to be answered. For example, do new cells come from specialized neoblasts or are there dedifferentiation and transdifferentiation process in planarian? Are cNeoblasts similar to mammalian embryonic stem cells? Are there a restrict tree-like hierarchy of pluripotent cells and their progenitors? The direct evidence of individual pluripotent cell transition including cell fate and patterning re-establishment are the effort for novel approach investment. We proposed a future direction for planarian stem cell study using live cell tracking method, a crucial need to enable the identification of the downstream of pluripotent stem cells. In order to do so, we developed a novel surface antibody 6-9.2 that binds to an unknown membrane protein highly expressed in a sub-population of neoblasts. Using this surface antibody 6-9.2, we could isolated two neoblast subgroups: 6-9.2- X1 cells that co-expressed with the sigma neoblast markers; and 6-9.2+ X1 cells that co-expressed with the zeta, gamma neoblast markers and also emerged some other genes required for the differentiation of many tissues such as pharynx, intestine, neuron, and cilia (Figure 3.5, table 2). Our previous studies showed the single cell transplantation of 6-9.2- X1 cell in irradiated planarian had the ability to form multiple colonies and could increase the engraftment rate while 6-9.2+ X1 cells failed to do so (Figure 4.1, Zhang, 2012). We proposed a Continuum of LOw-primed UnDifferentiated planarian stem/progenitor cells (CLOUD-PSPCs) (Chapter 1, Introduction) instead of a discrete tree-like hierarchy where the potency of stem cell strictly follows stepwise reduction. The co-expression of activin and its antagonized follistatin in our RNA sequencing data provided an indirect evidence for the fluidity of our CLOUD model. The regeneration of posterior identity is regulated by activin, whereas follistatin

promotes the specification of anterior identity (Roberts-Galbraith and Newmark, 2013). This implied the upper position of 6-9.2- X1 cells in the badlands where the cell has more chance to change the cell type manifestation from anterior to posterior identities than the subsequent lineages. Altogether, we conclude that 6-9.2- X1 cells are pluripotent-like stem cells that co-expressed the sigma-neoblast markers and have c-Neoblast characteristic (Wagner et al., 2011); and 6-9.2+ X1 cells are committed neoblasts that might derived directly from 6-9.2- X1 neoblast and express 6-9.2 antigen (a putative transmembrane protein TMEM). Knocking down of this antigen TMEM215/128 significantly affected neoblast subclasses and subsequently impaired the planarian regeneration. Together with previous reports, these findings about 6-9.2 story helped us defining the stem cell transition with a fluidic identity, where pluripotent stem and progenitor cells gradually restrict their potential and have multiple directions to commit to later states (Figure 4.1). In the badlands, 6-9.2- X1 subclass might locate at the upper part with c-Neoblast and sigma-Neoblast due to its ability to form multiple colonies in irradiated animals and the co-expression of *smedwi-1* and sigma-neoblast markers. As discussed in our review (Tran and Gentile, 2018), the difference among these lineages may be very small in terms of gene expression, they might share the similar molecular profile but locate in different portions on the landscape. 6-9.2+ X1 subclass comprises the zeta and gamma-Neoblasts and locate in the middle of the badlands. When differences in the molecular signature and potential of these lineages increase, the border between them gradually becomes impassable. Not surprisingly, the CLOUD model was also shown in numerous neoblast subclasses proposed in the study of Fincher and colleagues (Fincher et al., 2018). Gamma-Neoblast expressed four marker genes *prox-1*, *hnf-4*, *nkx2.2*, and *gata4/5/6* (van Wolfswinkel et al., 2014). Among them, *hnf-4* co-expressed with *nkx2.2* and *gata4/5/6* in intestinal clusters, but also co-expressed with *cathepsin*+ cells. *hnf-4* also expressed with *ETS1* and *FOXF1*, which have been shown to function in pigment cell lineage (He et al., 2017). This suggested that *hnf-4* is expressed in more than two distinct lineages. Due the multiple distinct cell types cluster in one major group, they systematically subclustered each major cluster group. They have found a gradual decrease of *smewi-1* expression level across subclusters. For example, *smedwi-1* highly expressed within cells at the center of the parenchymal cells and gradually decline its expression in all directions into seven major subclusters. Each subcluster enriched at least one transcription factor. This data is consistent with our hypothesis of a CLOUD
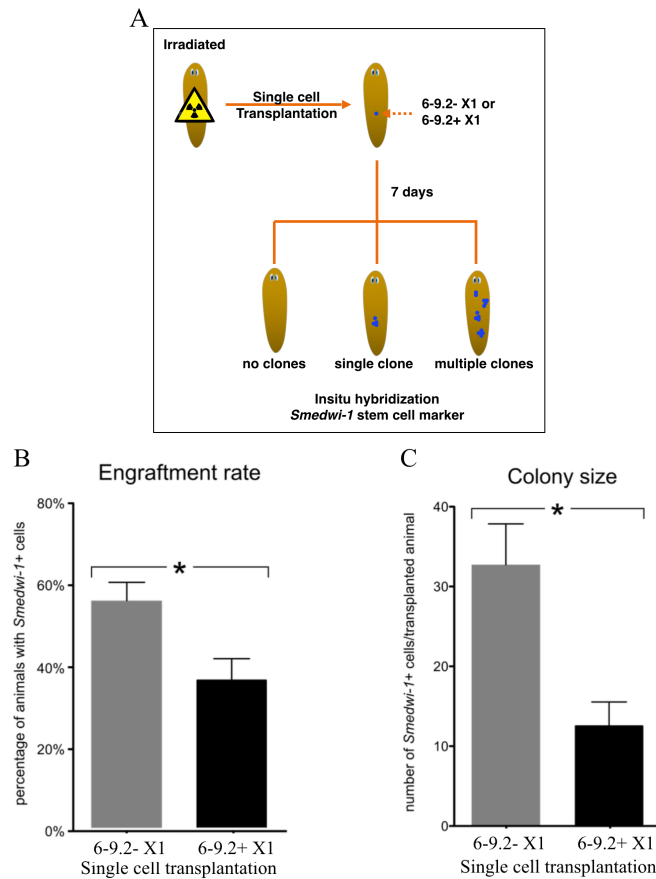
Figure 4.1: Adapted figure from Yudong Yang master thesis. A, experimental design for clonogenic ability test of transplanted planarian. B, The percentage of animals with $Smedwi-1^+$ cells after single cell transplantation with 6-9.2- X1 and 6-9.2+ X1 cells. C, The number of $Smedwi-1^+$ cells in transplanted animals. Data represent three biological replicates, p value ≤ 0.05 (*).

model that the cells present at the upper part of the badlands are more flexible than their subsequent lineages. However, there are no exact boundaries to distinguish a stem cell and its early committed cells.

Our study in 6-9.2 surface antibody shed light on using it as a novel marker to isolate pluripotent neoblasts for live cell tracking. One of the challenges of live tracking method is a lacking of an *in vivo* tool which enable the planarian immobilization without inducing injury or biochemical alteration during time-lapse imaging *in vivo*. Alginate hydrogels behaved as a perfect material for planarian immobilization due to their biocompatible characteristics (Schulz et al., 2018a; 2018b). We have shown the possibilities to immobilize the planarian in alginate hydrogels for 7 days without any harm to animal's homeostasis and regeneration. Under this condition, planarians were immobilized and fluorescent signals from transplanted cells could be detected under the fluorescent

microscope. The only obstacle of this method is the strong exposure to fluorescent light stimulated the movement of planarian and also increased the heat surrounding samples. Even though the live cell tracking experiments of transplanted 6-9.2- X1 and 6-9.2+ X1 animals were negative, we suggested the future studies with low temperature-adjustable microscope to minimize the heat effect and also impair the movement of planarians. We also recommend to continue using alginate hydrogels and increase the hydrogel concentration to 1% (we tested with 0.65%) to enhance the thickness and stability of the gels. With this preliminary data, we believe that this method would be a powerful tool to understand how pluripotent transitions are regulated in planarian and also confirm our proposed model of a lineage CLOUD for planarian stem cell commitment.
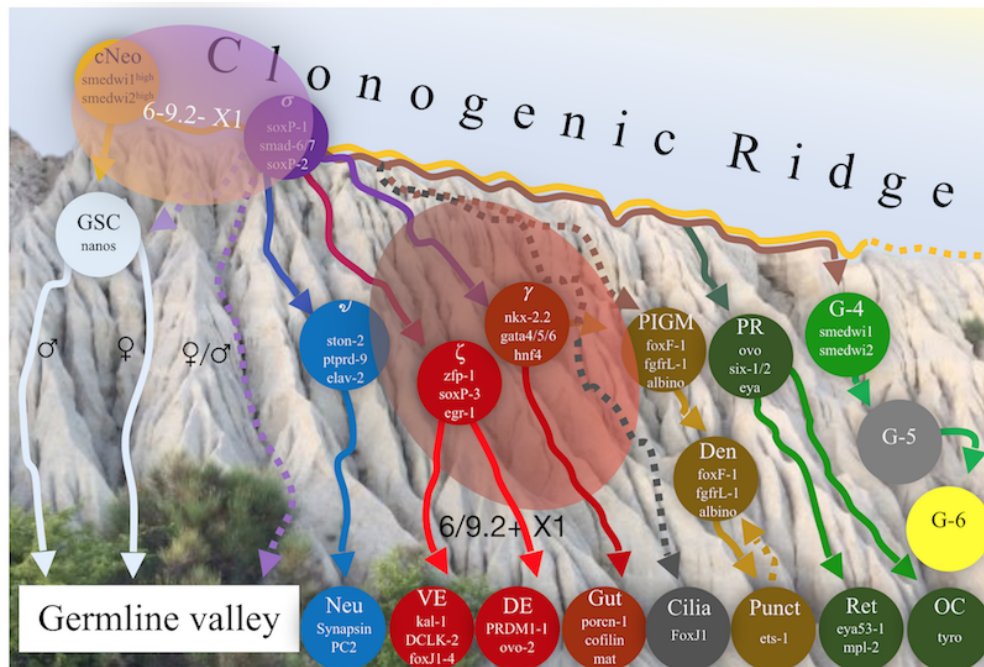
Figure 4.2: Bad land landscape showing the relationship of 6-9.2-X1 and 6-9.2+ X1 groups in planarian neoblast sub-classes. cNeo: clonogenic neoblast, cgsc: germ stem cell, gut: gut lineage, neu: neural lineage, DE: dorsal epidermis, VE: ventral epidermis, oc: optic cup cells, pr: photoreceptors, ret: retinol cells, DEN: Dendritic cells, PIGM: pigment cells, G4/5/6: Group 4/5/6, ♀/♂: female/male gametes. The possible connections between two subclasses are shown as dash lines.

Planarians, an exceptional model system to study pluripotency-based regeneration among bilaterians, also emerges as a suitable model for many research fields such as: drug action and abuse issues due to their mammalian-like behaviors when exposed to additive substances (Rawls et al., 2011; Kusayama and Watanabe, 2000), neurodegenerative drugs (Gentile et al.,

2011; Raffa et al., 2013), evolution (Witchley et al., 2013), tumorigenesis (van Roten et al., 2018) and environmental toxicological studies (Savetti et al., 2015; Hagtrom et al., 2016; Kustov et al., 2014). Recent decades, the massive usage of nanoparticles in industry and daily life products raises a high concern about the effects of nanoparticle exposure on the environment and living organisms including human health. Invertebrate species like planarian can be used as alternatives to vertebrates in toxicological studies. This model reduces the cost of maintenance and the difficulty of experimental manipulation but also yields useful toxicological information from individual to population or community level. Thanks to a large population of adult stem cells that readily regenerate any missing tissues, planarian displays as a wonderful model to study the effects of nano-pollutants on stem cells and regenerative ability. In this study, we investigated the effects of iron oxide particles (IOPs), one of the most common used particles in many researches and industrial fields, on both regeneration and homeostasis of planarians. We incubated planarians with IOPs under waterborne condition or directly injected IOPs into the gut system to examine the effects of IOPs in aquatic environment and food safety. The results indicated that IOPs did not affect to the cell viability and stem cell population, resulting in normal homeostasis and regenerative ability of planarian. We also examined the gene expression levels of stem and progenitor cell markers to test whether IOPs instabilized any cell groups. Surprisingly, the stem cell marker *Smedwi-1* was decreased 50% but the number of stem cells in X1 gate was not altered (Figure 3.20B and 3.21). We found that the number of cells in X2 gate was decreased together with the increase of cells in Xin gate (Figure 3.22. As shown in our previous data, 6-9.2- X1 and 6-9.2+ X1 cells are both *Smedwi-1*$^{+}$ cells and can appear in both X1 and X2 gates depend on their cell cycle phase (G1 or G2/M). The transition of these stem cells to their progenitors could explain the decrease in *Smedwi-1* marker and in the X2 gated cells to compensate the loss of certain cell types caused by the mild effect of IOPs exposure. The findings obtained in this study provided an important information for the examination of magnetic iron oxide particles at environmental releasing fates. The biocompatibility of IOPs could enhance the development and translation of this particles into medical studies.

The remarkable ability in regeneration of planarian without tumor formation also provides a beautiful model for tumorigenesis studies. We have found several putative tumor suppressor genes which are down-regulated in the exposure of human carcinogenic agent Cadmium by *in silico* and proteomic screening. One

of them is *MmpB*, the family member of Matrix Metalloproteinase. We decided to investigate the tumor prevention role of *MmpB* in planarian, since there have been no reports so far for its function. The RNAi of *MmpB* genes showed the significant effect in planarian morphology with epidermal blisters and large outgrowths. The *in situ* hybridization (ISH) and immunohistochemistry (IHC) of *Smedwi-1* and H3P markers showed the localization of proliferating stem cells inside blisters, suggesting the tumor-like formation in the lacking of *MmpB*. Interestingly, the effect of *MmpB* RNAi did not depend on the Cd exposure. To investigate which stem cell subclass regulated this tumor progression, we performed qPCR with different stem cell markers of pluripotent cells 6-9.2- X1 and committed stem and progenitor cells 6-9.2+ X1. The data showed the increase in sigma-, zeta- and gamma- neoblast markers, which implied that both 6-9.2- X1 and 6-9.2+ X1 are effected in *MmpB* RNAi (Figure 3.26). Especially, all four markers of pluripotent stem cell sub-class were significantly upregulated, which is consistent with the localization of active proliferating cells inside the blister in ISH and IHC data (Figure 3.24). However, the total number of proliferating cells across the whole animal were not significant different compared to control groups (Figure 3.25). We hypothesized that knock down of *MmpB* induced the hyper-proliferation of only a small portion of stem cells. The local imbalance between stem cells and progeny might cause the migration of this dividing cells and ultimately formed a tumor. The loss of *MmpB* gene caused the death of the animal when the tumor start its invasion state and spread throughout the whole body. Therefore, unlike other MMP family members that are regarded as tumor promoters, MMPB plays a role in tumor suppression. By testing the gene expression level of 6-9.2 stem cell sub-classes, we elucidated that the change in a small sub-population of pluripotent stem cells could gravely damage the planarian homeostasis. We hypothesized the dual function of Smed-MMPB protein in promoting regeneration process and controlling the over-proliferation of stem cells. This finding is informative for studying the tumor suppression mechanism and the role of MMPB in stem cell niche could be investigated more for cancer therapy.

Conclusion

Although planarians are a promising paradigm for numerous approaches, especially for stem cell and regeneration studies, the lack of transgenesis technique and stem cell maintenance by cell culture leave us without a molecular insight of stem cell compartment and the regulatory mechanism in *in vivo*. To circumvent this impediment, the non-transgenesis live cell tracking can serve as a powerful method for studying stem cell compartment. Even though

the further development of live cell tracking tool is needed, our data on the 6-9.2 surface antigen brought a comprehensive information to isolate the pluripotent stem cell sub-class for *in vivo* tracking. Together with the qPCR, RNA sequencing and single cell transplantation, we concluded that 6-9.2- X1 cells are naive-like stem cells that locate at the upper part of the badland landscape and might derive to committed cells - the 6-9.2+ X1 subclass. Our data contributed in defining the fluidic identity of the stem cell transition in a CLOUD model. The two major subgroups found by using 6-9.2 surface antibody have also been applied in examining the effect of environmental toxicological and tumorigenesis studies. The change in the gene expression level of marker sets suggested the change in the balance between stem cells and progenitor cells. Therefore, we could define the effect of our toxicants or gene knock down on different cell types and predict the outcome. Moreover, our Mass Spec data and RNAi experiments indicated the putative name for 6-9.2 antigen: a transmembrane protein TMEM215/128. Knock down of *TMEM215/128* gene dramatically impaired the planarian regeneration and homeostasis. Further studies of these genes could explore a novel key player in stem cell compartment and differentiation across bilaterial animals. Altogether, the knowledge we gain on the planarian system could be applied broadly to diverse organisms. Further studies will aid in the understanding of human stem cell mechanisms and how to actively promote human stem cell reprogramming in the hope that we can eventually apply in the field of regenerative medicine.

REFERENCES

Agata, K., Nakajima, E., Funayama, N., Shibata, N., Saito, Y., Umesono, Y. (2006). Two different evolutionary origins of stem cell systems and their molecular basis. Seminars in Cell & *Developmental Biology.* 17: 503–509.

Akesson, A., Julin, B. and Wolk, A. (2008). Long-term dietary cadmium intake and postmenopausal endometrial cancer incidence: a population-based prospective cohort study. *Cancer Res 68*, 6435-41.

Azuma, K., Iwasaki, N., and Ohtsu, K. Absorption Spectra of Planarian Visual Pigments and Two States of the Metarhodopsin Intermediates. (1999). *Photochem Photobiol.* 69: 99–104, doi:10.1111/j.1751-1097.1999.tb05312.

Baguna, J, Salo E., and Auladell, C. (1989). Regeneration and pattern formation in planarian. III. Evidence that neoblast are totipotent stem cells and the source of blastema cells. *Development.* 107: 77–86.

Baguna, J. The planarian neoblast: the rambling history of its origin and some current black boxes. 2012. *Int J Dev Biol* 56:19-37.

Baguna, J., and Romero, R. (1981). Quantitative analysis of cell types during growth, degrowth and regeneration in the planarians Dugesia mediterranea and dugesia tigrina. *Hydrobiologia.* 84: 181–194.

Bahadar, H., Maqbool, F., Niaz, K., Abdollahi, M. (2016). Toxicity of Nanoparticles and an Overview of Current Experimental Models. *Iran Biomed J.* 20(1): 1–11. doi: 10.7508/ibj.2016.01.001.

Balestrini, L., Isolani, M.E., Pietra, D., Borghini, A., Bianucci, A.M., Deri, P. (2014). Berberine exposure triggers developmental effects on planarian regeneration. *Scientific Reports.* 4, 4914.

Barber, R.D., Harmer, D.W., Coleman, R.A., Clark, B.J. (2005). GAPDH as a housekeeping gene: analysis of GAPDH mRNA expression in a panel of 72 human tissues. *Physiol Genomics.* 21(3):389-395.

Barberán, S., Fraguas, S., Cebrià, F. (2016). The EGFR signaling pathway controls gut progenitor differentiation during planarian regeneration and homeostasis. *Development.* 143(12): 2089–102.

Bardeen, C.R, and Baetjer, F.H. (1904). The inhibitive action of the Roentgen rays on regeneration in planarians. *J. Exp. Zool.* 1: 191–195.

Baumann, J., Köser, J., Arndt, D., Filser, J. (2014). The coating makes the difference: acute effects of iron oxide nanoparticles on Daphnia magna. *Sci Total Environ.* 484: 176-184.

Baxendale, S., Davison, C., Muxworthy, C., Wolff, C., Ingham, P.W., and Roy, S. (2004). The B-cell maturation factor Blimp-1 specifies vertebrate slow-twitch muscle fiber identity in response to Hedgehog signaling. *Nat. Genet.* 36: 88–93.

Beausejour, C. M. and Campisi, J. (2006). Ageing: balancing regeneration and cancer. *Nature* 443, 404-5.

Bourgkard, E., Wild, P., Courcot, B., Diss, M., Ettlinger, J., Goutet, P., Hemon, D., Marquis, N., Mur, J.M., Rigal, C., et al. (2009). Lung cancer mortality and iron oxide exposure in a French steel-producing factory. *Occup. Environ. Med.* 66, 175–181.

Brockes, J.P; Kumar A., and Velloso, C.P. (2001). Regeneration as an evolutionary variable. *J. Anat.* 199: 3–11.

Bullions, L. C., Notterman, D. A., Chung, L. S. and Levine, A. J. (1997). Expression of wild-type alpha-catenin protein in cells with a mutant alpha-catenin gene restores both growth regulation and tumor suppressor activities. *Mol Cell Biol* 17, 4501-8.

Bundschuh, M., Filser, J., Lüderwald, S., McKee, M.S., Metreveli, G., Schaumann, G.E., Schulz, R., Wagner, S. (2018). Nanoparticles in the environment: where do we come from, where do we go to? *Environ Sci Eur.* 30(1): 6.

Cebrià, F., and Newmark, P. (2005). Planarian homologs of netrin and netrin receptor are required for proper regeneration of the central nervous system and the maintenance of nervous system architecture. *Development.* 132, 16, 3691–3703.

Chan, K. C., Ko, J. M., Lung, H. L., Sedlacek, R., Zhang, Z. F., Luo, D. Z., Feng, Z. B., Chen, S., Chen, H., Chan, K. W. et al. (2011). Catalytic activity of Matrix metalloproteinase-19 is essential for tumor suppressor and anti-angiogenic activities in nasopharyngeal carcinoma. *Int J Cancer* 129, 1826-37.

Chera, S., Ghila, L., Dobretz, K., Wenger, Y., Bauer, C., et al. (2009).

Apoptotic cells provide an unexpected source of Wnt3 signaling to drive hydra head regeneration. *Dev. Cell.* 17: 279–289.

Christen, B., Robles, V., Raya, M., Paramonov, I., and Belmonte, J.C. (2010). Regeneration and reprogramming compared. *BMC Biol.* 8: 5. doi: 10.1186/1741-7007-8-5.

Coricovac, D.E., Moaca, E.A., Pinzaru, I., Cîtu, C., Soica, C., Mihali, C.V., Pacurariu, C., Tutelyan, V.A., Tsatsakis, A., Dehelean, C.A. (2017). Biocompatible Colloidal Suspensions Based on Magnetic Iron Oxide. Nanoparticles: Synthesis, Characterization and Toxicological Profile. *Front. Pharmacol.* 8, 154.

Coward, S.J. (1974). Chromatoid bodies in somatic cells of the planarian: observation on their behavior during mitosis. *Anat Rec.* 180: 533–545.

Cowles, M.W., Brown D.D., Nisperos S.V., Stanley B.N., Pearson B.J., Zayas R.M. (2013). Genome-wide analysis of the bHLH gene family in planarians identifies factors required for adult neurogenesis and neuronal regeneration. *Development.* 140: 4691–4702.

Currie, K.W., Pearson, B.J. (2013). Transcription factors lhx1/5-1 and pitx are required for the maintenance and regeneration of serotonergic neurons in planarians. *Development.* 140: 3577–3588.

Curtis, W.C, and Hickman, J. (1926). Effects of X-rays and radium upon regeneration in planarian. *Anat. Rec.* 34: 145–146.

Dayem, A.A., Hossain, M.K., Lee, S.B., Kim, K., Kumar, S.S., Yang, G.M., Choi, H.Y., Cho, S.G. (2017). The Role of Reactive Oxygen Species (ROS) in the Biological Activities of Metallic Nanoparticles. *Int J Mol Sci.*18(1): 120.

DeGregori, J. (2017). Connecting cancer to its causes requires incorporation of effects on tissue microenvironments. *Cancer Res.*

Deng, C. X. and Scott, F. (2000). Role of the tumor suppressor gene Brca1 in genetic stability and mammary gland tumor formation. *Oncogene* 19, 1059-64.

Denker, E., Manuel, M., Leclere, L., Le Guyader, H., Rabet, N. (2008). Ordered progression of nematogenesis from stem cells though differentiation stages in the tentacle bulb of Clytia hemisphaerica (Hydrozoa, Cnidaria). *Dev Biol.* 315: 99–113.

Dexter, J.B., Tamme, M.B., Lind, C.H., Collins, E.M.S. (2014). On-chip immobilization of planarians for in vivo imaging. *Sci. Rep.* 4: 6388. doi:

10.1038/srep06388.

Ehrhart, F., Mettler, E., Böse, T., Weber, M.M., Vasquez, J.A., and Zimmermann, H. (2013). Biocompatible coating of encapsulated cells using ionotropic gelation. *PLOS ONE*. 8, e73498.

Eisenhoffer, G.T., Kang, H., Sánchez Alvarado, A. (2008). Molecular analysis of stem cells and their descendants during cell turnover and regeneration in the planarian Schmidtea mediterranea. *Cell Stem Cell*. 3: 327–339.

Fincher, C.T., Wurtzel, O., de Hoog, T., Kravarik, K.M., Reddien, P.W. (2018). Cell type transcriptome atlas for the planarian Schmidtea mediterranea. *Science*. 25; 360(6391).

Fraguas, S., Barberán, S., Cebrià, F. (2011). EGFR signaling regulates cell proliferation, differentiation and morphogenesis during planarian regeneration and homeostasis. *Dev Biol*. 354(1):87–101.

Galloni, M. (2012). Global irradiation effects, stem cell genes and rare transcripts in the planarian transcriptome. *Int J Dev Biol*. 56: 103–116.

Gasperini, L., Mano, F.J., and Reis, R.L. (2014). Natural polymers for the microencapsulation of cells. *J R Soc Interface*. 11(100): 20140817.

Gautier, E.L., Shay, T., Miller, J., Greter, M., Jakubzick, C., Ivanov, S., Helft, J., Chow, A., Elpek, K.G., Gordonov, S. et al. (2012). Gene-expression profiles and transcriptional regulatory pathways that underlie the identity and diversity of mouse tissue macrophages. *Nat. Immunol*. 13: 1118–1128.

Gehrke, A.R., Srivastava, M. (2016). Neoblasts and the evolution of whole-body regeneration. *Current Opinion in Genetics & Development*. 40: 131–137.

George, S. J. and Dwivedi, A. (2004). MMPs, cadherins, and cell proliferation. *Trends Cardiovasc Med* 14, 100-5.

Gepp, M., Ehrhart, F., Shirley, S.G., Howitz, S., and Zimmermann, H. (2009). Dispensing of very low volumes of ultra high viscosity alginate gels: a new tool for encapsulation of adherent cells and rapid prototyping of scaffolds and implants. *Biotechniques*. 46: 31–43.

Gepp, M., Fisher, B., Schulz, A., Dobringer, J., Gentile, L., Vásquez, J.A., Neubauer, J.C., Zimmerman, H. (2017). Bioactive surfaces from seaweed-derived alginates for the cultivation of human stem cells. *Journal of Applied Phycology*. 29, 5: 2451-2461.

Goldstein, B., King, N. (2016). The future of cell biology: Emerging model

organisms. 26: 818–824.

González-Estévez, C. (2009). Autophagy meets planarians. *Autophagy.* 5(3): 290-297.

Gonzalez-Estevez, C., Felix, D.A., Aboobaker, A.A., and Salo, E. (2007). Gtdap-1 and the role of autophagy during planarian regeneration and starvation. *Autophagy.* 3: 640–642.

Gonzalez-Estevez, C., Momose, T., Gehring, W.J., and Salo, E. (2003). Transgenic planarian lines obtained by electroporation using transposon-derived vectors and an eye-specific GFP marker. *Proc Natl Acad Sci USA.* 100: 14046–14051.

Hagstrom, D., Cochet-Escartin, O., Zhang, S., Khuu, C., Collins, E.-M.S. (2015). Freshwater planarians as an alternative animal model for neurotoxicology. *Toxicological sciences: an official journal of the Society of Toxicology.* 147: 270–285.

Hall, F., Morita, M. and Best, J. B. (1986). Neoplastic transformation in the planarian: I. Cocarcinogenesis and histopathology. *J Exp Zool* 240, 211-27.

Hanahan, D. and Weinberg, R. A. (2011). Hallmarks of cancer: the next generation. *Cell* 144, 646-74.

Hay, E.D., and Coward, S.J. (1975). Fine structure studies on the planarian, Dugesia: I. Nature of the "neoblast" and other cell types in non-injured worms. *J Ultrastruct Res.* 50: 1–21

Hayashi, T., Asami, M., Higuchi, S., Shibata, N., Agata, K. (2006). Isolation of planarian X-ray-sensitive stem cells by fluorescence-activated cell sorting. *Dev Growth Differ.* 48(6):371-80.

Hayashi, T., Shibata, N., Okumura, R., Kudome, T., Nishimura, O., Tarui, H., Agata, K. (2010). Single-cell gene profiling of planarian stem cells using fluorescent activated cell sorting and its "index sorting" function for stem cell research. *Dev Growth Differ.* 52: 131–144.

Hikasa, H., and Sokol, S.Y. (2013). Wnt Signaling in Vertebrate Axis Specification. *Cold Spring Harb Perspect Biol.* 5(1): a007955.

Hori, I. (1982). An ultrastructural study of the chromatoid body in planarian regenerative cells. *J Electron Microsc.* 31: 63–72.

Hynes, R. O. (2009). The extracellular matrix: not just pretty fibrils. *Science*

326, 1216-9.

IARC. (1993). Bertllium, Cadmium, Mercury and the Exposures in the Glass Manifacturing INdustry. *In Bertllium, Cadmium, Mercury and the Exposures in the Glass Manifacturing INdustry*, vol. 58. Lyon, France: IARC.

Ishino, K., Kato, T., Kato, M., Shibata, T., Watanabe, M., Wakabayashi, K., Nakagama, H., Totsuka, Y. (2015). Comprehensive DNA adduct analysis reveals pulmonary inflammatory response contributes to genotoxic action of magnetite nanoparticles. *Int. J. Mol. Sci.* 16, 3474–3492.

Isolani, M. E., Abril, J. F., Salo, E., Deri, P., Bianucci, A. M. and Batistoni, R. (2013). Planarians as a model to assess in vivo the role of matrix metalloproteinase genes during homeostasis and regeneration. *PLoS One* 8, e55649.

Jochen, C. (2013). Stem cell systems and regeneration in planaria. *Dev Genes Evol.* 223(1-2): 67–84.

Kim, S. H., Turnbull, J. and Guimond, S. (2011). Extracellular matrix and cell signalling: the dynamic cooperation of integrin, proteoglycan and growth factor receptor. *J Endocrinol* 209, 139-51.

Kobayashi, K., Arioka, S., Hase, S., Hoshi, M. (2002). Signification of the sexualizing substance produced by the sexualized planarians. *Zool Sci.* 19:667–672.

Kobayashi, K., Hoshi, M. (2002). Switching from asexual to sexual reproduction in the planarian Dugesia ryukyuensis: change of the fissiparous capacity along with the sexualizing process. *Zool Sci.* 19:661–666.

Kodali, V., Littke, M.H., Tilton, S.C., Teeguarden, J.G., Shi, L., Frevert, C.W., Wang, W., Pounds, J.G., Thrall, B.D. (2013). Dysregulation of macrophage activation profiles by engineered nanoparticles. *ACS Nano.* 7, 6997–7010.

Kornberg, T.G., Stueckle, T.A., Antonini, J.A., Rojanasakul, Y., Castranova, V., Yang, Y., Wang, L. (2017). Potential Toxicity and Underlying Mechanisms Associated with Pulmonary Exposure to Iron Oxide Nanoparticles: Conflicting Literature and Unclear Risk. *Nanomaterials.* 7(10), 307.

Kusayama, T., and Watanabe, S. (2000). Reinforcing effects of methamphetamine in planarians. *Neuroreport.* 3; 11(11):2511-2513.

Kustov, L., Tiras, K., Al-Abed, S., Golovina, N., Ananyan, M. (2014). Estimation of the toxicity of silver nanoparticles by using planarian flatworms.

Alternatives to laboratory animals. ATLA. 42, 51–58.

Kwong, L. N. and Dove, W. F. (2009). APC and its modifiers in colon cancer. *Adv Exp Med Biol* 656, 85-106.

Labbe, R.M., Irimia, M., Currie, K.W., Lin, A., Zhu, S.J., Brown, D.D.R., Ross, E.J., Voisin, V., Bader, G.D., Blencowe, B.J., et al. (2012). A comparative transcriptomic analysis reveals conserved features of stem cell pluripotency in planarians and mammals. *Stem Cells.* 30: 1734–1745.

Lange, C.S. (1968). Studies on the cellular basis of radiation lethality. I. The pattern of mortality in the whole body irradiated planarian (Tricladida, Paludicola). *Int. J. Radiat. Bill. Relax. Stud. Phys. Chem. Med.* 13: 511–530.

Lapan, S.W., Reddien, P.W. (2011). dlx and sp6-9 Control Optic Cup Regeneration in a Prototypic Eye. *PLoS genetics.* 7:e1002226.

Lavin, Y., Winter, D., Blecher-Gonen, R., David, E., Keren-Shaul, H., Merad, M., Jung, S., and Amit, I. (2014). Tissue-resident macrophage enhancer landscapes are shaped by the local microenvironment. *Cell.* 159: 1312–1326.

Lee, K.Y., and Mooney, D,J. (2012). Alginate: properties and biomedical applications. *Prog Polym Sci.* 37(1): 106–126.

Lei, C., Zhang, L., Yang, K., Zhu, L., Lin, D. (2016). Toxicity of iron-based nanoparticles to green algae: Effects of particle size, crystal phase, oxidation state and environmental aging. *Environ Poll.* 218: 505-512.

Lei, K., Vu, H.T.K., Mohan, R.D., Gotting, K., Workman, J.L., Sanchez Alvarado, A. (2016). Egf signaling directs neoblasts repopulation by regulating asymmetric cell division in planarians. *Developmental Cell.* 38: 1–17.

Lender, T. (1962). Factors in morphogenesis of regenerating fresh-water planaria. *In Advances in Morphogenesis, M. Abercrombie and J. Brachet. New York: Academic Press.* 305–331.

Lensch, M.W., Daley, G.Q. (2004). Origins of mammalian hematopoiesis: in vivo paradigms and in vitro models. *Curr Top Dev Biol.* 60: 127–196.

Levitt, N. C. and Hickson, I. D. (2002). Caretaker tumour suppressor genes that defend genome integrity. *Trends Mol Med* 8, 179-86.

LoCascio, S.A., Lapan, S.W., Reddien, P.W. (2017). Eye absence does not regulate planarian stem cells during eye regeneration. *Developmental Cell.* 40: 381–391.

Lowe ,J.R., Mahool, T.D., Staehle, M.M. (2015). Ethanol exposure induces a delay in the reacquisition of function during head regeneration in Schmidtea mediterranea. *Neurotoxicology and teratology.* 48, 28–32.

Martin, F.A., Perez-Garijo, A., Morata, G. (2009). Apoptosis in Drosophila: compensatory proliferation and undead cells. *Int. J. Dev. Biol.* 53: 1341–1347

McElroy, J. A., Shafer, M. M., Trentham-Dietz, A., Hampton, J. M. and Newcomb, P. A. (2006). Cadmium exposure and breast cancer risk. *J Natl Cancer Inst* 98, 869-73.

Merdad, A., Karim, S., Schulten, H. J., Dallol, A., Buhmeida, A., Al-Thubaity, F., Gari, M. A., Chaudhary, A. G., Abuzenadah, A. M. and Al-Qahtani, M. H. (2014). Expression of matrix metalloproteinases (MMPs) in primary human breast cancer: MMP-9 as a potential biomarker for cancer invasion and metastasis. *Anticancer Res* 34, 1355-66.

Minard, K.R., Holtom, G.R., Kathmann, L.E., Major, P.B., Thrall, B.D., Wind, R.A. (2014). Magnetic Resonance in Medicine. 52, 495-505.

Molinaro AM, Pearson BJ. (2016). In silico lineage tracing through single cell transcriptomics indentifies a neural stem cell population in planarian. *Genime Biol.* 17: 87.

Mollereau, B., Perez-Garijo, A., Bergmann, A., Miura, M., Gerlitz, O., Ryoo, H.D., Steller, H., Morata, G. (2013). Compensatory proliferation and apoptosis-induced proliferation: a need for clarification. *Cell Death Differ.* 20: 181.

Moritz, S., Stockle, F., Ortmeier, C., Schmitz, H., Rodriguez-Esteban, G., Key, G., Gentile, L. (2012). Heterogeneity of planarian stem cells in the S/G2/M phase. *Int J Dev Biol.* 56: 117–125.

Moulin, J.J., Clavel,T., Roy, D., Dananche, B., Marquis, N., Fevotte, J., Fontana, J.M. (2000). Risk of lung cancer in workers producing stainless steel and metallic alloys. *Int. Arch. Occup. Environ. Heal.* 73, 171–180.

Mouton, S., Willems, M., Houthoofd, W., Bert, W., Braeckman, B.P. (2011). Lack of metabolic ageing in the long-lived flatworm Schmidtea polychroa. *Exp Gerontol.* 46:755-761.

Newmark, P.A., Sánchez Alvarado, A. (2000). Bromodeoxyuridine specifically labels the regenerative stem cells of planarians. *Developmental Biology.* 220: 142–153.

Ogawa, Y., Kobayashi, T., Nishioka, A., Kariya, S., Ohnishi, T., Hamasato, S., Seguchi, H., Yoshida, S. (2004). Reactive oxygen species-producing site in hydrogen peroxide-induced apoptosis of human peripheral T cells: involvement of lysosomal membrane destabilization. *Int J Mol Med.*13(3):383-388.

Onal, P., Grün, D., Adamidi, C., Rybak, A., Solana, J., Mastrobuoni, G., Wang, Y., Rahn, H-P., Chen, W., Kempa, S., et al. (2012). Gene expression of pluripotency determinants is conserved between mammalian and planarian stem cells. *EMBO.* 31:2755–2769.

Ozhan, G., Weidinger, G. (2015). Wnt/β-catenin signaling in heart regeneration. *Cell Regeneration.* 4(1): 3.

Pearson, B.J., and Sánchez Alvarado, A. (2010). A planarian p53 homolog regulates proliferation and self-renewal in adult stem cell lineages. *Development.* 137(2): 213–221.

Pearson, B.J., Eisenhoffer, G.T., Gurley, K.A., Rink, J.C., Miller, D.E., Sánchez Alvarado, A. (2009). A Formaldehyde-based Whole-Mount In Situ Hybridization Method for Planarians. *Dev Dyn.* 238(2): 443–450.

Pearson, B.J., Sánchez Alvarado, A. (2008). Regeneration, stem cells, and the evolution of tumor suppression. *Cold Spring Harb Symp Quant Biol.* 73:565–572.

Pederson, K.J. (1959). Cytological studies on the planarian neoblast. *Zeischrift fuer Zellforschung.* 50: 799–817.

Pelletieri, J., Fitzgerald, P., Watanabe, S., Mancuso, J., Green, D.R., Sanchez Alvarado, A. (2010). Cell death and Tissue remodeling in planarian regeneration. *Dev Biol.* 1, 338(1): 76–85.

Pellettieri, J., Sanchez Alvarado, A. (2007). Cell turnover and adult tissue homeostasis: from human to planarians. *Annu. Rev. Genet.* 41: 83–105.

Peng, X.H., Qian, X., Mao, H., Wang, A.Y., Chen, Z.G., Nie, S., Shin, D.M. (2008). Targeted magnetic iron oxide nanoparticles for tumor imaging and therapy. *Int. J. Nanomed.* 3, 311–321.

Plusquin, M., Stevens, A. S., Van Belleghem, F., Degheselle, O., Van Roten, A., Vroonen, J., Blust, R., Cuypers, A., Artois, T. and Smeets, K. (2012). Physiological and molecular characterisation of cadmium stress in Schmidtea mediterranea. *Int J Dev Biol* 56, 183-91.

Pra, D., Lau, A.H., Knakievicz, T., Carneiro, F.R., Erdtmann, B. (2005).

Environmental genotoxicity assessment of an urban stream using freshwater planarians, *Mutation Research* 585, 79–85.

Raffa, R.B., Danah, J., Tallarida1, C.S., Zimmerman, C., Gill, G., Baron, S.J., Rawls, S.M. (2013). Potential of a planarian model to study certain aspects of anti-Parkinsonism drugs. *Advances in Parkinson's Disease*. 2, 70-74.

Rawls, S.M., Patil, T., Tallarida, C.S., Baron, S., Kim, M., Song, K., Ward, S., and Raffa, R.B. (2011). Nicotine behavioral pharmacology: clues from planarians. *Drug Alcohol Depend*. 118(2-3): 274–279.

Raz, A.A., Srivastava, M., Salvamoser, R., Reddien, P.W. (2017). Acoel regeneration mechanisms indicate an ancient role for muscle in regenerative patterning. *Nature communication*.

Rebscher, N., Volk, C., Teo, R., Plickert, G. (2008). The germ plasm component Vasa allows tracing of the interstitial stem cells in the cnidarian Hydraactinia echinata. *Dev Dyn*. 237: 1736–1745.

Reddien, P.W., Bermange, A.L., Kicza, A.M., and Sanchez Alvarado, A. (2007). BMP signaling regulate the dorsal planarian midline and is needed for asymmetric regeneration. *Development*. 134: 4043–4051.

Reddien, P.W., Oviedo, N.J., Jennings, J.R., Jenkin, J.C., Sánchez Alvarado, A. (2005b). SMEDWI-2 is a PIWI-like protein that regulates planarian stem cells. *Science*. 310: 1327–1330.

Reddien, P.W., Sánchez Alvarado, A. (2004). Fundamentals of planarian regeneration. *Annu Rev Cell Dev Biol*. 20:725-57.

Resch, A.M., Palakodeti, D., Lu, Y-C., Horowitz, M., Graveley, B.R. (2012). Transcriptome analysis reveals strain-specific and conserved stemness genes in Schmidtea mediterranea. *PLoS ONE*. 7:e34447.

Rink, J.C. (2013). Stem cell systems and regeneration in planaria. *Dev. Genes Evol*. 223: 67–84.

Robb, S., Ross, E., and Sanchez Alvarado, A. (2008). SmedGD: the Schmidtea mediterranea genome database. *Nucleic Acids Res*. 36: 599–606.

Roberts-Galbraith, R.H., and Newmark, P.A. (2013). Follistatin antagonizes Activin signaling and acts with Notum to direct planarian head regeneration. *PNAS*. 110 (4) 1363-1368.

Rossi, A., Ross, E.J., Jack, A., Sanchez Alvarado, A. (2014). Molecular cloning

and characterization of SL3: a stem cell-specific SL RNA from the planarian Schmidtea mediterranea. *Gene.* 533: 156–167.

Roten, V.A., Barakat, A.Z., Wuoters, A., Tran, A.T., Mouton, S., Noben, J.P., Gentile, L., Smeets, K. (2018). A carcinogenic trigger to study the function of tumor suppressor genes in Schmidtea mediterranea. *Disease Models & Mechanisms.*

Russell, W. M. S. and Burch, R. L. (1959). The principles of humane experimental technique. *Vol. London: T. Methuen.*

Salo, E., Abril, J.F., Adell, T., Cebria, F., Eckelt, K., Fernandez-Taboada, E., Handberg-Thorsager, M., Iglesias, M., Molina, M. D., Rodriguez-Esteban, G. (2009). Planarian regeneration: achievements and future directions after 20 years of research. *Int. J. Dev. Biol.* 53: 1317–1327.

Salvetti A, Rossi L, Lacopetti P, Li X, Nitti S, Pellegrino T, Mattoli V, Golberg D, Ciofani G. In vivo biocompatibility of boron nitride nanotubes: effects on stem cell biology and tissue regeneration in planarians. *Nanomedicine.* 2015, 10(12):1911-22. doi: 10.2217/nnm.15.46.

Salvetti, A., Rossi, L., Bonuccelli, L., Lena, A., Pugliesi, C., Rainaldi, G., Evangelista, M., Gremigni, V. (2009). Adult stem cell plasticity: Neoblast repopulation in non-lethally irradiated planarians. *Developmental Biology.* 328:2: 305–314.

Salvetti, A., Rossi, L., Lena, A., Batistoni, R., Deri, P., Rainaldi, G., Locci, M.T., Evangelista, M., Gremigni, V. (2005). DjPum, a homologue of Drosophila Pumilio, is essential to planarian stem cell maintenance. *Development.* 132: 1863–1874.

Sanchez Alvarado, A. (2000). Regeneration in the metazoans: why does it happens? *Bioessays* 22: 578–590.

Scholz, H. and Kirschner, K. M. (2011). Oxygen-Dependent Gene Expression in Development and Cancer: Lessons Learned from the Wilms' Tumor Gene, WT1. *Front Mol Neurosci* 4, 4.

Schulz, A., Katsen-Globa, A., Huber, E.J., Mueller, S.C., Kreiner, A., Pütz, N., Gepp, M.M., Fischer, B., Stracke, F., von Briesen, H., Neubauer, J.C., Zimmermann, H. (2018). Poly(amidoamine)-alginate hydrogels: directing the behavior of mesenchymal stem cells with charged hydrogel surfaces. *J. Mater. Sci. Mater. Med.* 29(105).

Schulz, A., Gepp, M.M., Stracke, F., von Briesen, H., Neubauer, J.C., Zimmermann, H. (2018). Tyramine-conjugated alginate hydrogels as a platform for bioactive scaffolds. *J. Biomed. Mater. Res.* 107(1): 114-121.

Scimone, L.M., Kravarik, K.M., Lapan, S.W., and Reddien, P.W. (2014). Neoblast Specialization in Regeneration of the Planarian Schmidtea mediterranea. *Stem Cell Reports.*12; 3(2): 339–352.

Scimone, M.L., Srivastava, M., Bell, G.W., Reddien, P.W. (2011). A regulatory program for excretory system regeneration in planarians. *Development.* 138: 4387–4398.

Shang, L., Nienhaus, K., Nienhaus, G.U. (2014). Engineered nanoparticles interacting with cells: size matters. *J Nanobiotechnology.* 2014, 12:5. doi: 10.1186/1477-3155-12-5.

Sharma, G., Kodali, V., Gaffrey, M., Wang, W., Minard, K.R., Karin, N., Teequarden, J.G., Thrall, B.D. (2014). Iron oxide nanoparticle agglomeration influences dose rates and modulates oxidative stress-mediated dose-response profiles in vitro. *Nanotoxicology.* 6, 663-675.

Shen, J.M., Guan, X.M., Liu, X.Y., Lan, J.F., Cheng, T., Zhang, H.X. (2012). Luminiscent/magnetic hybrid nanoparticles with folate-conjugated peptide composites for tumor-targeted drug delivery. *Bioconj. Chem.* 23, 1010–1021.

Shibata, N., Hayashi, T., Fukumura, R., Fujii J, Kudome-Takamatsu T, Nishimura O, Sano S, Son F, Suzuki N, Araki R, et al. (2012). Comprehensive gene expression analyses in pluripotent stem cells of a planarian, Dugesia japonica. *Int J Dev Biol.* 56: 93–102.

Shibata, N., Umesono, Y., Orii, H., Sakurai, T., Watanabe, K., Agata. K. (1999). Expression of vasa (vas)-related genes in germline cells and totipotent somatic stem cells of planarians. *Dev Biol.* 206:73–87.

Solana, J., Kao, D., Mihaylova, Y., Jaber-Hijazi, F., Malla, S., Wilson, R., Aboobaker, A. (2012). Defining the molecular profile of planarian pluripotent stem cells using a combinatorial RNAseq, RNA interference and irradiation approach. *Genome biology.* 13:R19.

Srivastava, M., et al. (2014). Whole-body acoel regeneration is controlled by Wnt and Bmp-Admp signaling. *Curr. Biol.* 24: 1107–1113.

Stevenson, C.G., and Beane, W.S. (2010). A low percent ethanol method for immobilizing planarians. *PLOS ONE.* 5, e15310.

Szalay, B., Tatrai, E., Nyiro, G., Vezer, T., Dura, G. (2012). Potential toxic effects of iron oxide nanoparticles in in vivo and in vitro experiments. *J. Appl. Toxicol.* 32, 446–453.

Talbot, J., and Schotz, E.M. (2011). Quantitative characterization of planarian wild-type behavior as a platform for screening locomotion phenotypes. *J Exp Biol.* 214: 1063–1067.

Tanaka, E.M., Reddien, P.W. (2011). The cellular basis for animal regeneration. *Dev. Cell.* 21: 172–185.

Thomas, C.R., Ferris, D.P., Lee, J.H., Choi, E., Cho, M.H., Kim, E.S., Stoddart, J.F., Shin, J.S., Cheon, J., Zink, J.I. (2010). Noninvasive remote-controlled release of drug molecules in vitro using magnetic actuation of mechanized nanoparticles. *J Am Chem Soc.* 132(31), 10623-5.

Tran, A.T., Gentile, L. (2018). A lineage CLOUD for neoblasts. *Seminar in Cells and Developmental Biology.*

Tran, A.T., Hesler, M., Moriones, O.H., Jimeno-Romero, A., Fisher, B., Bastus, N., Puntes, V., Wagner, S., Kohl, Y., Gentile, L. (2019). Assessment of iron oxide nanoparticle ecotoxicity on regeneration and homeostasis in the replacement model system Schmidtea mediterranea. *ALTEX.*

Tu, K.C., Cheng, L.C., Vu, H.T.K., Lange, J.J., McKinney, S.A., Seidel, C.W., and Sanchez Alvarado, A. (2015). Egr-5 is a post-mitotic regulator of planarian epidermal differentiation. *Elife.* 4, e10501.

van Wolfswinkel, J.C., Wagner, D.E., and Reddien, P.W. (2014). Single-cell analysis reveals functionally distinct classes within the planarian stem cell compartment. *Cell Stem Cells.*

Veiseh, O., Gunn, J.W., Zhang, M. (2010). Design and fabrication of magnetic nanoparticles for targeted drug delivery and imaging. *Adv Drug Deliv Rev.* 62(3):284–304.

Voronina, E., Seydoux, G., Sassone-Corsi, P., Nagamori, I. (2011). RNA granules in germ cells. *Cold Spring Harbor Perspectives in Biology.* 3.

Voura, E. B., Montalvo, M. J., Dela Roca, K. T., Fisher, J. M., Defamie, V., Narala, S. R., Khokha, R., Mulligan, M. E. and Evans, C. A. (2017). Planarians as models of cadmium-induced neoplasia provide measurable benchmarks for mechanistic studies. *Ecotoxicol Environ Saf* 142, 544-554.

Waalkes, M. P. (2003). Cadmium carcinogenesis. *Mutat Res* 533, 107-20.

Wagner, D.E., Ho, J.J., and Reddien, P.W. (2012). Genetic regulators of a pluripotent adult stem cell system in planarians identified by RNAi and clonal analysis. *Cell Stem Cell.* 10(3): 299–311.

Wagner, D.E., Wang, I.E., Reddien, P.W. (2011). Clonogenic Neoblasts Are Pluripotent Adult Stem Cells That Underlie Planarian Regeneration. *Science.* 332: 811–816.

Wang, D., Lin, Z., Wang, T., Yao, Z., Qin, M., Zheng, S., Lu, W. (2016). Where does the toxicity of metal oxide nanoparticles come from: Thenanoparticles, the ions, or a combination of both? *Journal of Hazardous Materials.* 308, 328–334.

Watanabe, M., Yoneda, M., Morohashi, A., Hori, Y., Okamoto, D., Sato, A., Kurioka, D., Nittami, T., Hirokawa, Y., Shiraishi, T., et al. (2013). Effects of Fe3O4 Magnetic Nanoparticles on A549 Cells. *Int. J. Mol. Sci.* 14, 15546–15560.

Wenemoser, D., Lapan, S.W., Wilkinson, A.W., Bell, G.W., Reddien, P.W. (2012). A molecular wound response program associated with regeneration initiation in planarians. *Genes Dev.* 26: 988–1002.

Wenemoser, D., Reddien, P.W. (2010). Planarian regeneration involves distinct stem cell responses to wounds and tissue absence. *Dev. Biol.* 344: 979–991.

Witchley, J.N., Mayer, M., Wagner, D.E., Owen, J.H., and Reddien, P.W. (2013). Muscle Cells Provide Instructions for Planarian Regeneration. *Cell Rep.* 2013, 4(4): 633–641.

Wurtzel, O., Oderberg, I.M., Reddien, P.W. (2017). Planarian Epidermal stem cells respond to Positional Cues to Promote Cell-Type Diversist. *Dev Cell.* 40, 491–504.

Xing, M., Zhang, Y., Zou, H., Quan, C., Chang, B., Tang, S., Zhang, M. (2015). Exposure characteristics of ferric oxide nanoparticles released during activities for manufacturing ferric oxide nanomaterials. *Inhal. Toxicol.* 27, 138–148.

Yamada, T., Oshima, T., Yoshihara, K., Tamura, S., Kanazawa, A., Inagaki, D., Yamamoto, N., Sato, T., Fujii, S., Numata, K. et al. (2010). Overexpression of MMP-13 gene in colorectal cancer with liver metastasis. *Anticancer Res* 30, 2693-9.

Zayas, R.M., Cebrià, F., Guo, T., Feng, J., and Newmark, P.A. (2010). The use of lectins as markers for differentiated secretory cells in planarians. *Dev Dyn.* 239(11): 2888–2897.

Zhang, Y. (2012). A study on the heterogeneity of planarian adult stem cells. Max Planck MPI, Münster, Germany.

Zhu, S.J., and Pearson, B.J. (2016). (Neo)blast from the past: new insights into planarian stem cell lineages. *Current Opinion in Genetics Development.* 40: 74–80.

Zhu, S.J., Hallow, S.E., Currie, K.W., Xu, C., Pearson, B.J. (2015). A mex3 homolog is required for differentiation during planarian stem cell lineage development. *Elife.* 4.